Lithological mapping by remote sensing using emittance information in the thermal infrared region

Peter Sean Kealy

LITHOLOGICAL MAPPING BY REMOTE SENSING USING EMITTANCE INFORMATION IN THE THERMAL INFRARED REGION.

A thesis presented for the degree of

Doctor of Philosophy

by

Peter Sean Kealy

University of Durham

Department of Geological Sciences

November 1990

DECLARATION

The work contained in this thesis has not been submitted elsewhere for any other degree or qualification and that unless stated otherwise is the author's own work.

Peter Sean Kealy

University of Durham

November 1990.

ABSTRACT

The aims of this study were to assess existing techniques, and develop new methods for extracting the geologically significant parameter spectral emittance from passive multispectral scanner data in the Thermal Infrared. Emittance cannot be extracted directly from the radiance data due to the underdetermined nature of the resultant equation set. Quantitative analysis of the Thermal Infrared data also requires the application of calibration and atmospheric correction algorithms. A calibrated and atmospherically corrected Thermal Infrared Multispectral Scanner (TIMS) scene from Halls Creek, Western Australia, was selected as a test area on which to apply the techniques. However, detailed mapping of the Halls Creek area was not an objective of this research.

Existing image enhancement techniques namely the Decorrelation-Stretch and Thermal Log Residuals (TLR) as well as the alpha coefficients calculation (a simplification of the TLR method developed during this research) were applied to the TIMS data and each created useful images for delineating boundaries.

A new emittance estimating technique, the Alpha Derived Emittance method, developed during this research was applied to the data for comparison with existing algorithms, the Model Emittance and Maximum Temperature methods. The Alpha Derived Emittance method utilised the Wien approximation to the Planck function and solved the underdetermined equation set by assuming the existence of a relationship between the mean and variation of emittance spectra.

A Thermal Infrared spectral library was created from a representative collection of Halls Creek lithologies in order to assess the applicability of each emittance estimating method. Analysis of these spectra indicated that each of the methods were equally accurate in estimating emittance for Halls Creek lithologies. Further, each technique estimated the emittance to within 0.02 of emittance for approximately 65% of the lithologies.

TIMS image statistics suggested that the Alpha Derived Emittance method most effectively separated the emittance and temperature from the radiance signal.

This research indicates that the variability within samples may hinder the ability to discriminate lithologies.

ACKNOWLEDGEMENTS

I would like to thank my supervisor, Tim "Wallaby Jones" Munday for initiating the project and reviewing this manuscript. I would also like to thank him and his family for putting up with me on the odd occasion. I wish to acknowledge the much appreciated continual encouragement and advise that was received from Simon "Captain Efficient" Hook. Tim's departure to Australia afforded the opportunity to work with Andy "Oberführer" Gabell at CSIRO which proved to be very useful. I would like to thank Dr B. J. J. Embleton, the Chief of the Division at CSIRO for the opportunity of working there for those many months. I would also like to thank Dr Anne Kahle of the Jet Propulsion Laboratory for the use of the facilities in Pasadena that allowed the collection of the Halls Creek data set.

I would like to thank the British Government for their various forms of financial support these last three years, especially the NERC studentship.

Finally I would like to thank the Officers, men, boys and girls of the various institutions with which I have been associated with over the course of the time at Durham. They are too numerous to mention, but they know who they are, especially Steve "Laughing Boy" Mackin, Seamus F. O'Hoolighan, and Clinton J. Thrust for being little rays of sunshine in the dark old days.

TABLE OF CONTENTS.

CHAPTER 3. VARIABLE REDUCTION METHODS FOR THE ESTIMATION OF EMITTANCE AND TEMPERATURE FROM MULTISPECTRAL THERMAL INFRARED DATA.

CHAPTER 5. A COMPARISON OF METHODS FOR ESTIMATING EMITTANCE AND TEMPERATURE USING TIMS DATA FROM HALLS CREEK W. A.

CHAPTER 1

INTRODUCTION

1.1 BACKGROUND

The Middle InfraRed (MIR) portion of the electromagnetic spectrum extends from 3 to 35 μm. However, the region that may be used for passive remote sensing is limited by the amount of energy radiated by the surface, and the proportion of that energy that is transmitted through the atmosphere. The source of the energy that can be measured remotely is thermal radiation from surface materials at ambient terrestrial temperatures (300K). At these temperatures, the spectral radiance of a blackbody is at a maximum at around 10-11μm (Figure 1.1). The 8-14 μm region, the Thermal InfraRed (TIR), has associated with it an atmospheric window that allows the thermal radiation emitted from the ground to be transmitted through the atmosphere. Figure 1.2 shows the transmittance expected through a U.S. standard atmosphere for wavelengths between 7 and 14μm. This is the best window in the Middle InfraRed with poorer windows found between 3 and 5μm and 17 and 25μm. Thus, sensing at these wavelengths benefits from being able to use the maximum emitted signal from materials at the Earth's surface and a region where transmission through the atmosphere is very good. Fortuitously, the 8-14μm wavelength region also contains diagnostic spectral information on commonly occurring minerals, especially the silicates which constitute a major component of surface lithologies.

1.2 THERMAL INFRARED SPECTRA OF ROCKS AND MINERALS BETWEEN 8-14μm

The potential for using multispectral remote sensing techniques in the thermal infrared for geological applications was recognised following some early laboratory spectroscopic studies by Lyon (Lyon (1962), (1965)). This has been substantiated by further laboratory based studies (for example Hunt and Salisbury (1974), (1975), (1976), and Salisbury *et al* (1988)).

The fundamental physical property upon which identification of lithologies can be made is emittance, the ratio of the radiance emitted by the body to that of the radiance

emitted by a blackbody at the same temperature.

$$\varepsilon_i = \frac{L_i}{L_{ibb}} \qquad [1.1]$$

where:

ε_i = Emittance at wavelength i.

L_i = Radiance of a sample at wavelength i, and temperature T.

L_{ibb} = Radiance of a blackbody at wavelength i, and temperature T.

The term emittance is used here as it is a more general term than emissivity, which is a term reserved for opaque targets (Swain and Davis (1981)). Equation 1.1 indicates that the emittance is a ratio of radiances such that emittance has no units and may take values from 0.0 to 1.0.

Many silicate, carbonate, and sulphate minerals are characterised by emittance variations in the 8 to 12μm wavelength region. The spectral features result from vibrational (bending and stretching) molecular motions with the most intense (known as the Reststrahlen band) resulting from the excitation of the fundamental modes (EOSAT 1986). The vibrational energy, and therefore the wavelength of these bands is diagnostic of both the composition and crystal structure. Thermal Infrared spectra provide a direct means for identifying the composition of many silicates, carbonates, and sulphates.

The strengths and positions of spectral features have a mineralogical significance that has been used in the laboratory environment to study a wide variety of geologic materials including silicates, carbonates, sulphates, oxides and hydroxides (for example Lyon (1962), Lazarev (1972), Farmer (1974), Hunt and Salisbury (1974), (1975), (1976)). Much theoretical work has also been conducted to interpret the observed spectral features on the basis of ion mass, bond strength and crystal structure (Lazarev (1972), Farmer (1974), Karr (1975)). These and other studies (Lyon (1965)) have shown that the location, strength and form of Thermal Infrared spectral features vary systematically with composition and crystal structure. Figure 1.3 demonstrates this for various lithologies. The combination of emittance responses from individual mineralogies will produce a characteristic emittance spectra for the lithologies from which they are composed. Of particular importance for geological applications is the observed systematic shift to longer wavelengths in the position of the emittance minima due to a variation in the Si-O bond strength between 8 and

12μm. This occurs as the type of silicate crystal lattice changes from a framework structure of silica tetrahedra to a sheet structure, then to a chain structure and finally to an isolated tetrahedra structure. This shift provides a means of identifying silicate bearing lithologies (Vickers and Lyon (1967), Hunt and Salisbury (1974), Hunt (1980), EOSAT (1986), Siegal and Gillespie (1980)).

Thus the position depth and form of the spectral emittance curve provide a direct means of identifying the composition and mineralogy of geologic material, and it is the extraction of this geologically significant parameter to which this research has been directed.

1.3 MULTISPECTRAL THERMAL INFRARED MAPPING FOR GEOLOGY

Historically, the measurement of thermal infrared radiance has been used to estimate the temperature of surfaces. Thermal infrared remote sensing has been used in the same way. Thermal radiance as measured by a remote sensing device is related to surface temperature and emittance. The temperature of a surface is controlled by its reflectivity at visible and near infrared wavelengths and also by its geometry with respect to the sun, the time of day, the atmosphere and other factors unrelated to composition (Gillespie (1986)). In contrast, the thermal emittance of a surface is controlled largely by it's composition (as discussed in the preceding section). Given that emittance varies systematically with wavelength in a manner that is diagnostic of many silicate and other rock forming minerals, the remote estimation of spectral emittance offers considerable potential as an aid in lithological mapping and other geological studies.

The possibility of exploiting the presence of diagnostic spectral features for the remote sensing of rock-type was suggested by numerous workers through the late 1960's and 70's (for example Vickers and Lyon (1967), Vincent and Thomson (1972), Vincent (1975)). However, owing to the lack of suitable instruments during this period, few tests of the technique were possible. Airborne experiments with non-imaging spectrometers (Hovis *et al* (1968), Lyon (1972)) indicted that the reststrahlen bands of silicate rocks were observable. This was substantiated by Vincent *et al* (1972) who flew a two channel Thermal Infrared scanner (bands from 8.2 - 10.9μm and 9.4 - 12.1μm) over a sand quarry in the USA. They produced band ratio images which distinguished between quartz sand, sandstone and non-silicate surface materials. A further study with the same instrument (Vincent and Thomson (1972)) demonstrated that it was possible to separate dacite from basalt, and rhyolitic tuff

from surrounding alluvium. The lack of adequate imaging devices prevented the further validation of the use of spectral emittance data until the late 1970's and early 1980's.

In 1979 Kahle and Rowan (1980) analysed 6-channel (between 8.27 and 13μm) multispectral data from the Bendix 24-band scanner and showed that it was possible to separate several rock and ground-cover types as a function of spectral emittance differences. On the basis of this and other studies, NASA funded the development of the Thermal Infrared Multispectral Scanner (TIMS) in the early 1980's.

The TIMS is a six-channel airborne scanner that measures spectral radiance in the 8.2-12.2μm part of the electromagnetic spectrum. The spectral bands covered by the scanner are given in Table 1.1. The scanner is characterised by a high radiometric sensitivity ranging between 0.1K and 0.3K noise-equivalent temperature change (NEΔT) at 300K. This translates to a noise-equivalent change in spectral emittance of 0.002 to 0.006. Further details concerning the TIMS are given in Palluconi and Meeks (1985).

The first flights of the TIMS scanner over Death Valley in California and Cuprite, Nevada, USA (Kahle and Goetz (1983); Gillespie *et al* (1984)), provided further demonstration of the potential of multispectral remote sensing in the Thermal Infrared for geological compositional mapping. Since that time TIMS data have been acquired over sites throughout the USA, Europe and Australia. Results from their analysis have indicated broad-band multispectral thermal infrared data from the 8-12μm data to be of value in a variety of geological and geomorphological applications including the detection of silicification in altered areas (Kahle and Goetz (1983), Watson *et al* (1990)); the relative dating of lava flows in young volcanic terrains (Kahle *et al* (1988)); geological mapping in accreted terrains (Lahren *et al* (1988)); lithological mapping in heavily weathered terrain (Drury and Hunt (1989), Hook (1989)); and mapping alluvial fan systems (Gillespie *et al* (1984)).

A key to the successful application of TIMS data in the studies mentioned above, has been the development of appropriate image processing algorithms which enhance the often subtle information they contain. Simple contrast enhancement and colour compositing of the various spectral bands is not sufficient to reveal the spectral emittance variations that form the basis for lithological discrimination. The measured radiance has a strong dependence on the temperature of the surface. When combined with characteristically small variations in thermal emittance, the radiance data are found to be very highly correlated from one spectral band to the next.

Several techniques have been developed to enhance and by definition, to separate emittance from temperature in multispectral thermal infrared data. These include the Decorrelation Stretch (Gillespie *et al* (1986)), based upon the principal component transformation, which causes the spectral emittance differences between surface units to be displayed as colour differences, while most of the temperature information is displayed as intensity differences. This algorithm has seen widespread use in geological applications of TIMS data in large part because it is easy to apply and it generates a colourful image which can be interpreted qualitatively with an underlying physical basis. The main drawback to the approach is that the decorrelated composites still contain both temperature and emissivity information. As a result they cannot be related directly to laboratory measurements of emittance, nor can they be interpreted in a truly quantitative manner (although a recent attempt has been made to quantitatively link the chromacity in a decorrelated image to spectral variation in emittance, Kahle *et al* (1988)).

In order to generate images which could be interpreted with a reliable underlying physical basis (i.e. pixel spectra could be related directly to laboratory or field estimates of spectral emittance and in turn can be related to composition - mineralogical or otherwise) and which could be subject to quantitative analyses, several alternative methods have been developed for TIMS data. The principal objective to all these is the effective separation of spectral emittance from temperature. They include the Model Emittance calculation (Kahle *et al* (1980)), the Maximum Temperature method (Gillespie (1986)), and the Thermal Log Residuals technique (Hook (1989)). Of these, the most commonly used is the Model Emittance calculation (e.g. Kahle (1987); Kahle *et al* (1988); Gillespie (1986)).

The relative merits of each of these methods has been the subject of very little research despite the importance attached to their common goal. Hook and Kahle (1990) and this author along with others (Hook *et al* (1990)), describe some recent attempts at making an objective comparison between several of the available techniques.

Each technique adopts certain basic assumptions to achieve the separation of emittance and temperature from a measure of spectral radiance. The validity of these assumptions and the significance of their violation in spectral terms, particularly as it relates to compositional mapping, has not been examined in detail. Alternative approaches to the estimation of emittance are continually being sought, not least to

circumvent some of the inherent limitations of existing methodologies.

1.4 STATEMENT OF THE PRINCIPAL AIMS

The principal aims of this thesis are to examine existing, and develop new techniques for extracting emittance information from spectral radiance data in the Thermal Infrared, in order to develop the best processing methodology for thermal infrared data.

1.5 FACTORS PREVENTING THE EXTRACTION OF EMITTANCE IN THE THERMAL INFRARED

There are several factors that preclude the direct extraction of emittance information from radiance measured in the Thermal Infrared by a remote sensing device. The atmosphere interacts with the ground emitted radiance such that the radiance received at the scanner is not solely a result of the radiance emitted from a sensed area but also has components due to the transmissivity and emittance of the atmosphere (reviewed in Wolfe and Zissis (1979)). The effects of selective, wavelength dependent atmospheric absorptions change the radiance values received by the scanner. To correct for these effects an atmospheric correction must be applied to compensate for these factors.

Another problem that prevents the direct calculation of emittance from radiance is the nature of the Planck function (Equation 1.2). This function which describes the spectral distribution of radiation from a body with temperature relates the desired parameter emittance to the radiance measured by the scanner.

$$L_i = \frac{\varepsilon_i C_1}{\lambda_i^5 \left[e^{(C_2/\lambda_i T)} - 1 \right]} \qquad [1.2]$$

where:

L_i = spectral radiance in band i. (measured in units of $mW.m^{-2}.\mu m^{-1}.sr^{-1}$)

ε_i = spectral emittance in band i.

C_i = first radiation constant/π.

λ_i = wavelength in band i. (measured in μm)

C_2 = second radiation constant.

T = temperature. (measured in K)

For each band there is a known value L_i, and two unknowns, ε_i and T. Thus the equation is underdetermined. The TIMS measures radiance in six bands from 8.2μm to 11.8μm, (Palluconi and Meeks 1985). For six TIMS bands there will be six known L_i from the scanner but seven unknowns: six ε_i and a temperature, T. The equation set is thus not directly solvable as there will always be one more unknown than there are equations.

1.6 SPECIFIC OBJECTIVES

Until recently the TIMS represented the only widely applied multispectral Thermal Infrared instrument and so the following objectives will be considered with respect to their application to the TIMS data. The techniques that are investigated however will be applicable to any passive Thermal Infrared multispectral instrument such as the Geoscan Mark II and the GER MK II scanner provided that they are calibrated. At present neither of these instruments are calibrated and as a result the quantitative extraction of emittance and temperature are not possible.

The specific objectives are;

1. The evaluation of existing image processing techniques for enhancing emittance variations in multispectral Thermal Infrared data.

2. The development of algorithms for the extraction of quantitative estimations of spectral emittance from radiance in the Thermal Infrared. These algorithms will again be applied specifically with regard to the TIMS.

3. The creation of a library of Thermal Infrared emittance spectra that contain measurements of the weathered surface of rocks. To assess the accuracy of emittance information extracted from the TIMS it is necessary to compare this information to laboratory emittance spectra obtained from the surfaces of the rock types found within the TIMS scene itself.

4. Correction of TIMS data to ground radiance. In order to apply quantitative emittance estimation algorithms it is necessary to correct the raw data for effects that are not related to the emittance signal emitted from the ground. These corrections are:
A) Calibration of the TIMS to remove instrument related effects.
B) The atmospheric correction of the TIMS data.

5. An evaluation and comparison of the techniques for enhancing emittance variations applied to a particular test area. To assess the relative merits of each processing technique it is necessary to apply each to Thermal Infrared data of a particular area. The data to which the techniques are applied is a TIMS scene obtained from Halls Creek in the Kimberley district of Western Australia.

1.7 THESIS STRUCTURE

The thesis is divided into 6 chapters. Chapters 2 to 4 explain the methodologies behind each Thermal Infrared technique for enhancing the TIMS data. Each Chapter contains methods that are similar in the approach taken to solve the problem. For each type of solution, there are commonly several variations. The description of each method will state the background to its development, the aim of the method, indicating what each is intended to achieve, the methodology, and there will follow a discussion of the theoretical strengths and weaknesses of each technique.

Chapter 2 is concerned with the type of solution that attempts to enhance emittance variations without assigning quantitative values to the data. The Decorrelation Stretch method described by Soha and Schwartz (1978), and its variants are discussed. Chapter 3 describes a set of solutions that all involve simple assumptions that reduce the number of variables in the underdetermined equation set. These solutions include the Model Emittance method, the Maximum Temperature method, and the Universal Temperature method. Chapter 4 is concerned with techniques that utilise the Wien approximation to the Planck function in order to calculate temperature independent coefficients. Firstly the Thermal Log Residual (TLR) technique is discussed. This was described by Hook (1989), and enhances the emittance information within TIMS data. This is followed by a description of a new method, the Alpha method, which was developed during the course of this research. This method extracts quantitative emittance information from the TIMS using a knowledge of the behaviour of thermal infrared emittance spectra derived from laboratory studies.

Chapter 5 is concerned with the application and evaluation of the image processing algorithms to the Halls Creek test site in the Kimberley region of W.A. Firstly the calibration of the TIMS instrument and the atmospheric correction of the data is discussed. The LOWTRAN6 atmospheric modelling algorithm (Kneizys *et al* (1983)) was used for this correction. This is followed by a review of the geological setting of the test area which is situated 20km NE of Halls Creek, Western Australia. The calibrated and atmospherically corrected TIMS data from this area may be used

to test the algorithms described in the methodologies chapters. The results are presented in terms of the analysis of Thermal Infrared laboratory spectra collected in the course of this study and the interpretation of the TIMS data in the spatial, image sense, and in terms of the spectral information contained within each technique.

Chapter 6 presents a summary of the work conducted, and the conclusions that may be drawn from the study.

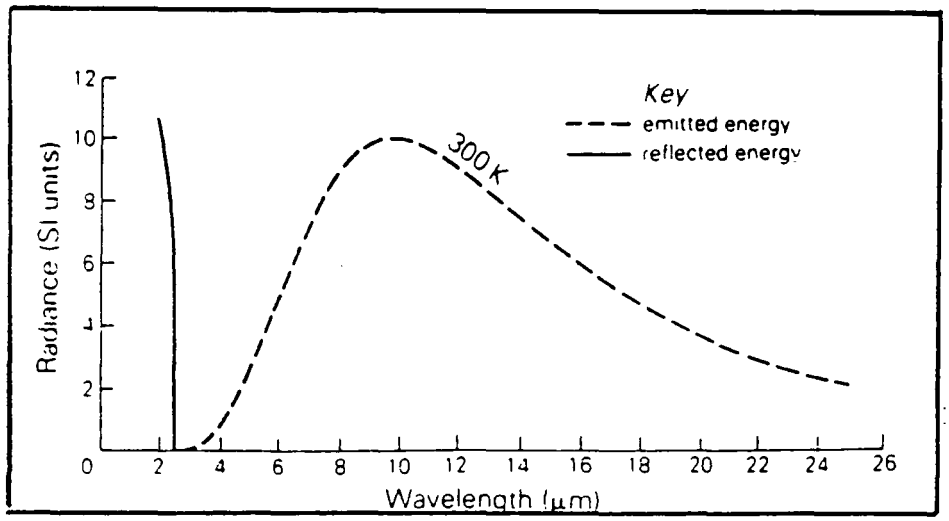

Figure 1.1 Energy received from the Earth's surface in the 2 to 26μm wavelength region, showing a blackbody curve at 300K (from Drury 1987).

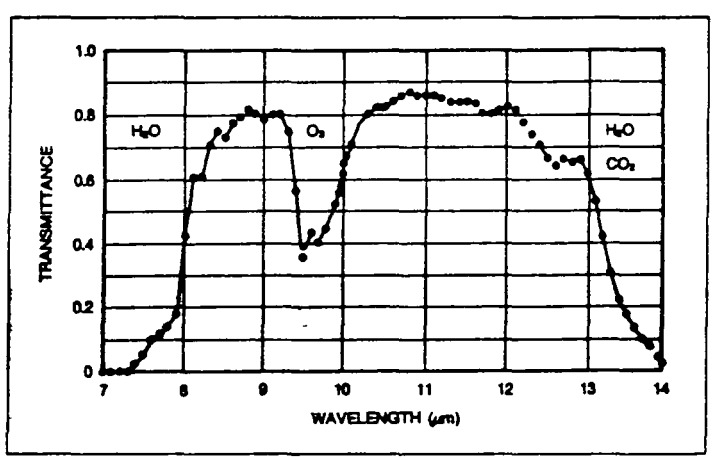

Figure 1.2 Atmospheric transmittance in the 7 to 14μm wavelength region for the U.S. Standard Atmosphere, from LOWTRAN5 (from EOSAT 1986).

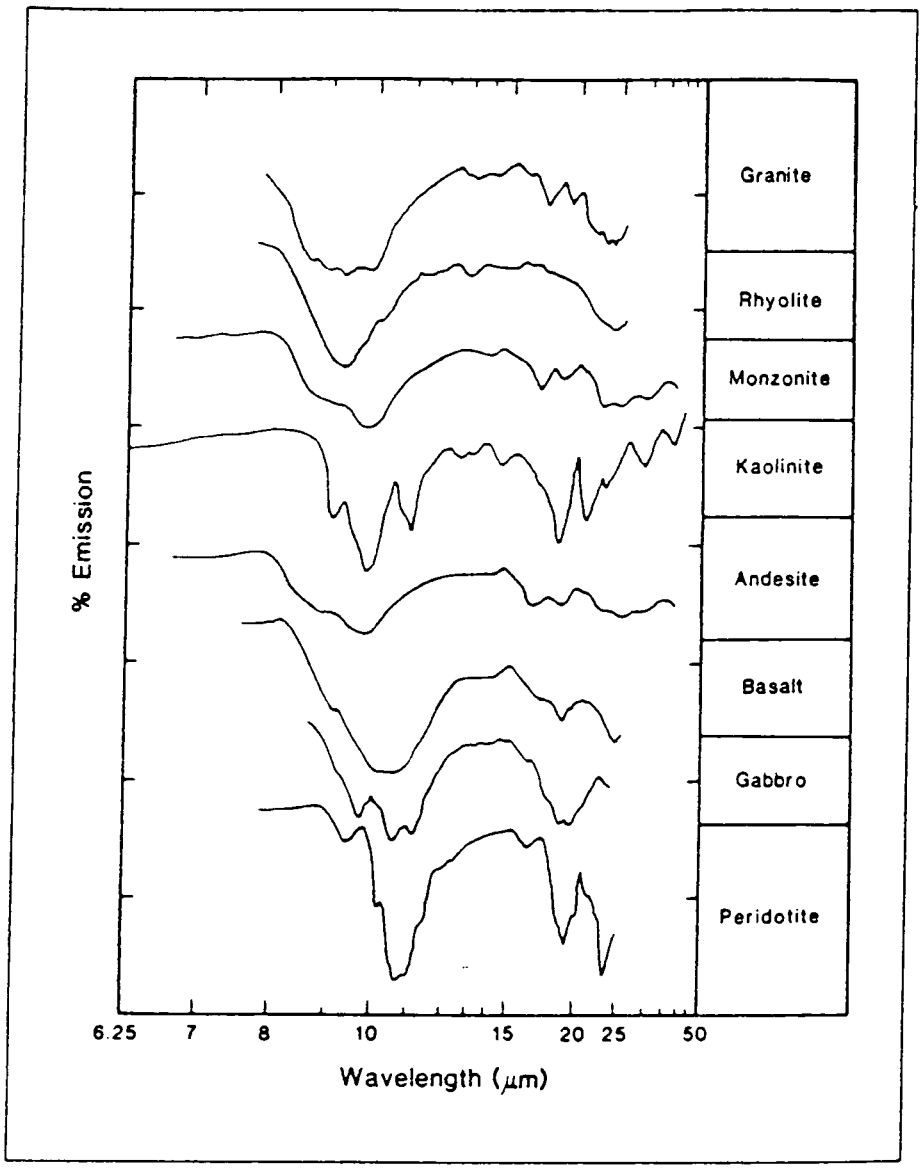

Figure 1.3 Emittance spectra for various lithologies (from EOSAT 1986).

BAND	WAVELENGTH RANGE	CENTRAL WAVELENGTH
1	8.2 - 8.6	8.512
2	8.6 - 9.0	8.864
3	9.0 - 9.4	9.152
4	9.4 - 10.2	9.952
5	10.2 - 11.2	10.432
6	11.2 - 12.2	11.424

Table 1.1 Wavelength ranges and central wavelength values for the TIMS for the U.S./Australia Joint Scanner Campaign.

CHAPTER 2

THE DECORRELATION-STRETCH METHODS

2.1 BACKGROUND

The Decorrelation stretch (D-stretch) was developed by Soha and Schwartz (1978) and has been widely applied to TIMS data since that time. Numerous studies involving this technique and minor variations on it have been published: for example, Kahle *et al* (1980), Kahle and Goetz (1983), Gillespie *et al* (1984), Gillespie *et al* (1986), Macias *et al* (1987), Rothery and Hunt (1990).

2.2 AIM OF METHOD

The Decorrelation-Stretch method (D-stretch), when applied to multispectral TIR data, is designed to enhance the emittance variations and suppress temperature variations in any given band combination of data.

2.3 METHODOLOGY

The theory behind this method is given in Gillespie *et al* (1986), and a review of the mathematical expression of this method is outlined in Rothery and Hunt (1990). The method is generally applicable to TIR scanner data, but since the TIMS represents the only widely applied multispectral thermal scanner it is with regard to this instrument that this method has been applied in the literature.

Colour images are usually made by selecting three channels of data and displaying each in red, green, blue to display a colour additive image. The TIMS measures emitted thermal infrared radiation that is the product of blackbody radiation and the emittance of the radiating surface, Equation 2.1.

$$L_i = \frac{\varepsilon_i C_1}{\lambda_i 5\left[e^{C_2/\lambda_i T} - 1\right]} \qquad [2.1]$$

where:

L_i = Radiance emitted by the surface in band i.

ε_i = Emittance of the body in band i.

C_1 = First radiation constant/π

λ_i = wavelength in band i.

C_2 = Second radiation constant.

T = Temperature.

The resulting radiance data are highly correlated, Table 2.1 shows the correlation coefficients for the TIMS scene from Halls Creek, Western Australia. When any three bands of TIMS radiance data are displayed as an image the high correlation of the bands creates an image that is generally grey and does not show a great deal of variation in colour. The emittance components of the signal are not effectively displayed due to the dominant effect of temperature. The D-stretch, using principal component analysis (Gonzales and Wintz (1977)), exaggerates the variations due to emittance changes. The highly correlated temperature information is displayed as brightness variations whilst the uncorrelated emittance information is displayed as colour (or hue) variations (Kahle *et al* (1980)). This enhancement is achieved by contrast stretching along the principal component axes such that the variances of each principal component are equalised, and then rotating back to the original axes. Figure 2.1 illustrates the process of calculating D-stretch images for a two dimensional case (from Gillespie *et al* (1986)) and is outlined below.

Stage A. Orthogonal principal component axes P1 and P2 are calculated.
Stage B. The data are rotated to P1 and P2 axes.
Stage C. A linear contrast stretch is applied to the data. These stretches are applied such that the variances in each principal component are made equal to the greatest variance in any of the bands.
Stage D. The data are rotated back to their original axes.

The D-stretch, as illustrated above for the two dimensional case is generally applied using three selected bands. The resulting colour composite of any three chosen bands thus produces a colourful image that enhances the poorly correlated emittance component of the data rather than the highly correlated temperature information. Several variations to the method have been published. Drury and Hunt (1989), have produced a variant of this method by calculating Principal Components (PC's) for all six TIMS bands, omitting noisy PC's, median filtering the remaining PC's and reassembling the decorrelated bands. Hunt (1990) calculates PC's for four selected TIMS bands and discards the first PC assuming this to contain the temperature variations. This is defined as the Colour-stretch (C-stretch). Hook (1989) applies the

D-stretch method to six TIMS bands and displays bands 1, 3, 5. The commonest three-band combination used in the literature for maximising discrimination was found to be bands 1, 3, and 5 (Kahle *et al* (1988)). However other band combinations such as 1, 4, 6 also prove highly discriminatory.

2.4 DISCUSSION

The D-stretch method increases discrimination of lithological units by enhancing the emittance variations within TIMS data. No attempt is made to assign quantitative emittance values to the data. This is achieved by statistical manipulation. For the two dimensional case, the position of a data point, x, y is changed to x', y' depending upon its relative position to other data points (Figure 2.2). Thus the transformation is scene dependent. The final value attributed to a point after the transformation is not consistent in all scenes. Thus a D-stretch of one scene would assign a set of coordinates x, y to data values x', y', whereas a D-stretch of a subscene containing that value would assign other values x", y" to it, (Figure 2.2). The scene dependant characteristic of this technique means that any value assigned to a pixel is due in part to lithologies present elsewhere in the scene. The colour that a lithology displays in one D-stretch image will not be the same as the colour that same lithology would display if it were present in another scene where adjacent rock types were different. In general however, if a D-stretch scene contains many different lithologies such that a scene may be considered typical, i.e. containing a wide variety of rock types, then the colours displayed will be similar from scene to scene. For instance, for the 5, 3, 1 band combination displayed in red, green and blue it is generally found that quartz rich material is displayed as red (Kahle and Goetz (1983), Drury and Hunt (1989)). This is because quartz has low values in bands 1 and 3 and comparatively higher values in band 5, resulting in a high value in the red channel. If one considers, however, a scene entirely composed of quartzose materials; quartz lag, quartzites and sandstones, then these materials would not all display red colours but would, utilising the whole colour space, exhibit various colours. For a TIMS scene containing a variety of lithologies, the D-stretch provides a means of assigning relative emittance values which can be used to group lithological types into general generic classes, but the non-uniqueness of an assigned colour prevents the colours displayed in one scene being indicative of the lithologies in another. This feature of the D-stretch highlights the weakness of this and any scene dependent technique.

Since the technique enhances emittance differences without assigning quantitative emittance values, the atmospheric correction of the data is not of critical importance.

Only relative differences between pixel values are important, and not the absolute values of the pixels. The relative distribution of data points along a histogram will not change if a multiplicative or additive atmospheric effect is present uniformly across a scene. If, however, an atmospheric effect is not uniform across a scene, then the data will be affected by different amounts and the relative distribution of values may change. The change in scan angle as the TIMS collects data along a flightline causes an increase in the length of the atmospheric column through which the emitted radiance travels. For atmospherically uncorrected data, pixels will have values due to variable amounts of atmospheric components which may affect the relative distribution of the data. It is for this reason that data should be atmospherically corrected before the D-stretch is applied. Whilst it is desirable to model out atmospheric affects present in the data, the method will produce highly discriminating images for delineating lithological boundaries if these effects remain, Hook (1989).

2.5 CONCLUSIONS

1. The D-stretch will provide a useful means of enhancing highly correlated thermal data for the discrimination of surface lithologies.

2. The application of an atmospheric correction is not critical to the successful application of this technique.

3. This is a scene dependent technique: the association of a colour with a particular lithology in one scene cannot necessarily be used to infer the lithology in another scene.

4. Quantitative interpretation of the data is not possible.

5. The D-stretch method is an image enhancement technique that does not produce spectra.

6. Temperature information is present in the D-stretch image.

Figure 2.1 Schematic representation of the Decorrelation stretch method for a two dimensional case, (from Gillespie *et al*1986).

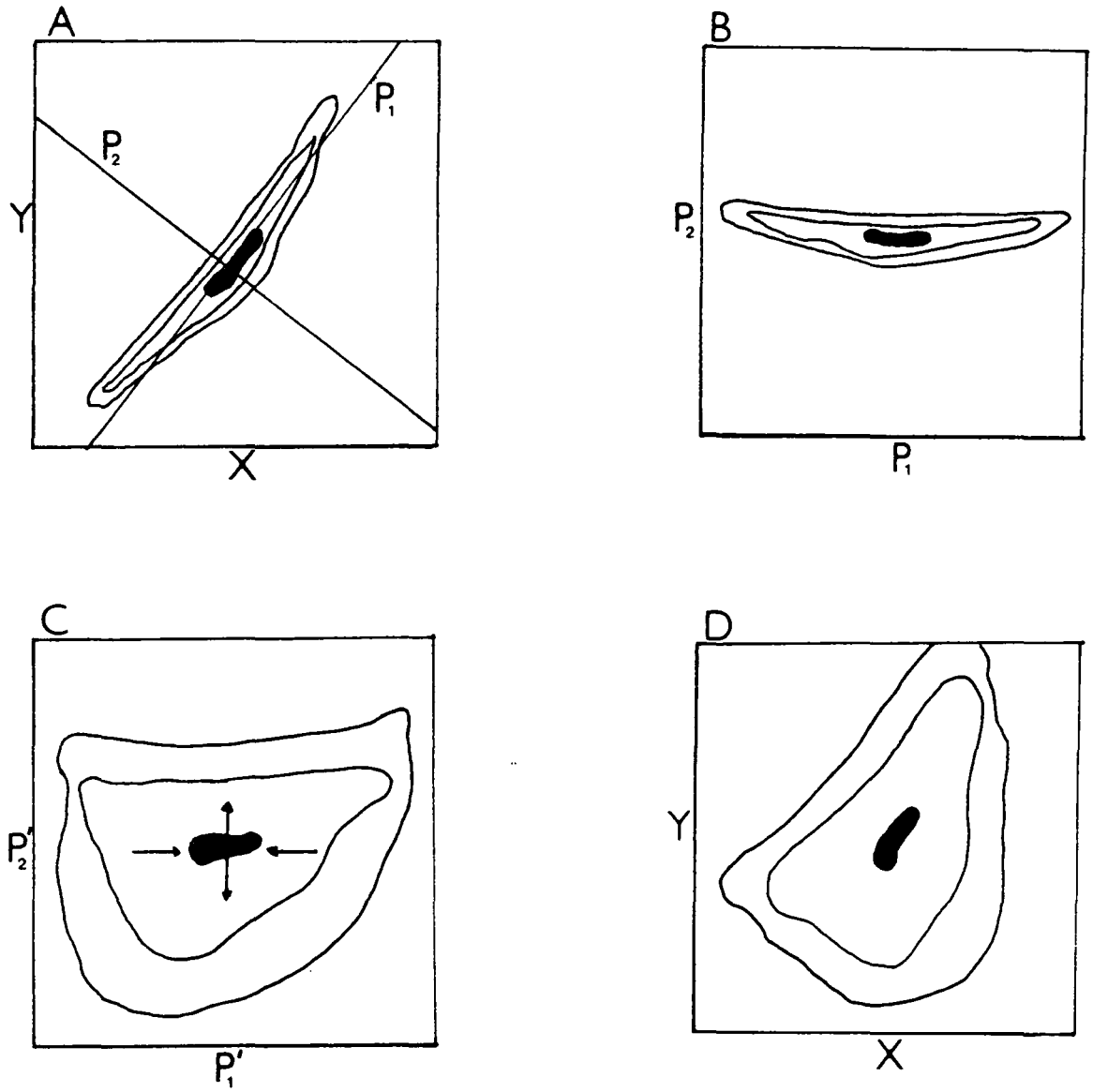

A. Variation of data X,Y showing orthogonal axes P_1, P_2.

B. Data after principal component transformation and translation.

C. Equalisation of variances along P_1, P_2 axes.

D. Return to original axes by the inverse principal component transformation.

Figure 2.2 Schematic representation illustrating the scene dependancy of the Decorrelation stretch method.

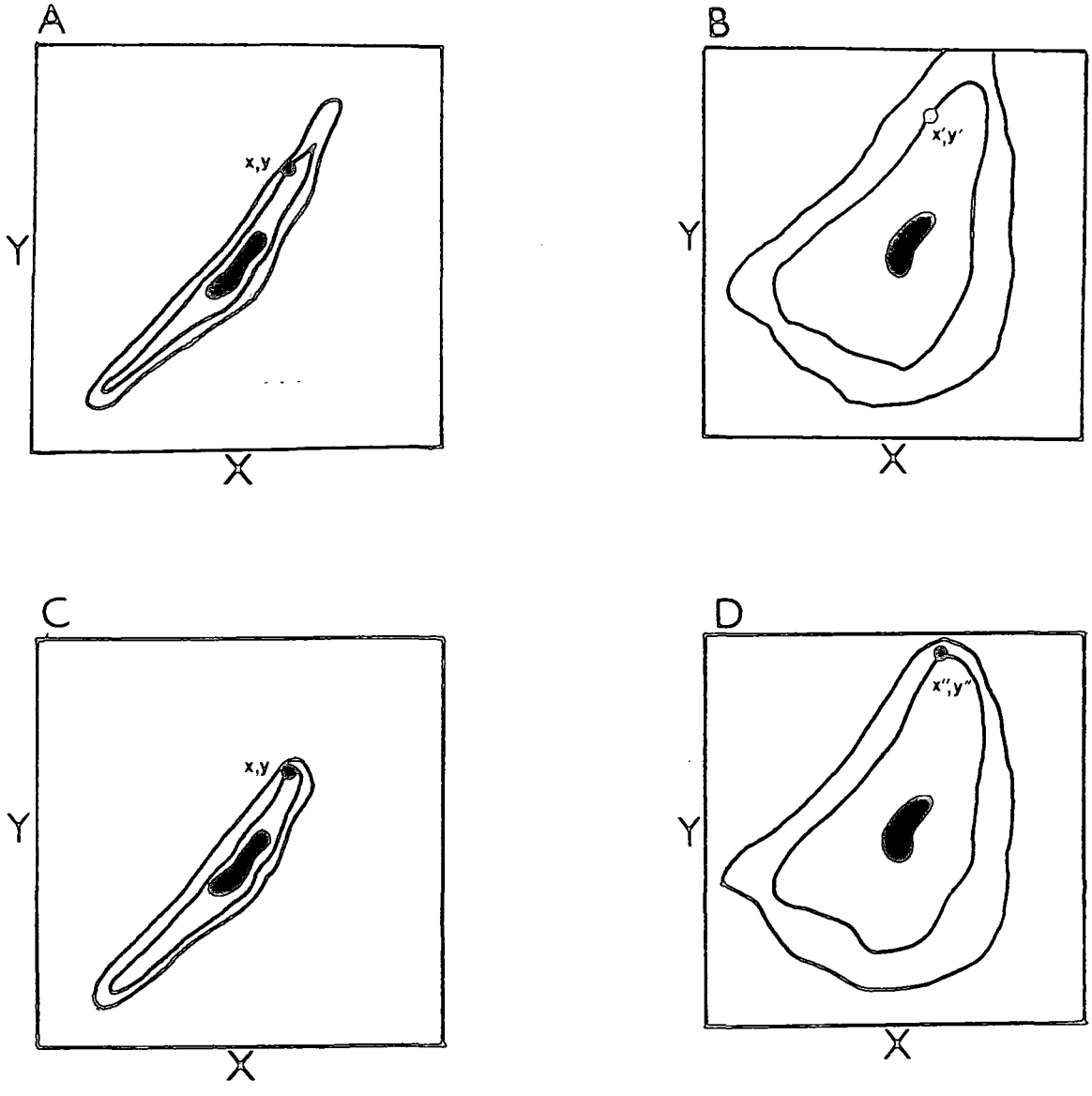

A. Original data set.

B.Data after Decorrelation stretch transformation, showing change in position of point x, y to x', y'.

C. Data set subscene containing less high values than in A.

D. Data distribution after Decorrelation stretch transformation showing point x, y has been tranformed to x", y".

	CORRELATION		MATRIX	FOR	6 BANDS	
	1	2	3	4	5	6
1	1	0.99	0.981	0.97	0.995	0.945
2		1	0.996	0.96	0.931	0.917
3			1	0.951	0.915	0.899
4				1	0.988	0.977
5					1	0.994
6						1

Table 2.1 Correlation matrix for radiance data for the TIMS from Halls Creek W.A.

CHAPTER 3

VARIABLE REDUCTION METHODS FOR THE ESTIMATION OF EMITTANCE AND TEMPERATURE FROM MULTISPECTRAL THERMAL INFRARED DATA

3.1 BACKGROUND

The variable reduction methods seek to calculate values of emittance by the introduction of an assumption, thus reducing the number of variables in the equation set such that the equation set is no longer underdetermined.

As has been discussed in Chapter 1, the Planck function relates the geologically significant parameter emissivity, to the scanner derived radiance, L_i;

$$L_i = \frac{\varepsilon_i C_1}{\lambda_i 5\left[e^{C_2/\lambda_i T} - 1\right]} \qquad [3.1]$$

where:

L_i = spectral radiance at wavelength i.

ε_i = spectral emittance in band i.

λ_i = wavelength in band i.

C_1 = first radiation constant/π.

C_2 = second radiation constant.

T = temperature.

This equation cannot be directly solved because there are two unknowns, the emittance and the temperature. A line of solution, with different values of emittance and temperature that together will calculate the same radiance value, is possible (see Figure 3.1). For the TIMS there are six of these equations such that there are six radiance measurements and seven unknowns: six emittances and a single temperature. The resulting equation set is underdetermined and cannot be simply solved for emittance. Figure 3.2 shows that for one set of radiance values emittance values may be calculated for increments of temperature. These emittance spectra have similar shape, varying most significantly in their mean values. It should be noted that the shape also changes slightly, the values in the lower bands changing more rapidly than the values in the higher bands. It is the position and depth of emittance minima that are critical for identifying lithologies (Lyon (1965)), and these are generally

preserved in successive estimations of spectra in Figure 3.2, such that small errors in the temperature, and consequently the emittance calculated, do not destroy the spectral information present.

The following methods attempt to calculate emittance by the application of various assumptions. Each method will select one of the potentially correct suite of emittance spectra that may be generated from a set of radiances. The best method will be that which most accurately estimates the emittance for most lithologies present in a scene.

These methods are all described with reference to the Thermal Infrared Multispectral Scanner (TIMS) instrument, but are applicable with some modification to data acquired by other passive multispectral scanners sensing in the Thermal Infrared which have different configurations.

3.2 THE MODEL EMITTANCE METHOD

This method was developed by Kahle *et al* (1980) and has been used to estimate emittance for several TIMS scenes; for example Kahle *et al* (1989), Hook (1989), Realmuto (1990).

3.2.1 ASSUMPTIONS

1. It is assumed that the data have been calibrated and atmospherically corrected.

2. The emittance in a band is constant. For example, band 6 = 0.93

3.2.2 METHODOLOGY

Planck's function is:

$$L_i = \frac{\varepsilon_i C_1}{\lambda_i 5\left[e^{C_2/\lambda_i T} - 1\right]}$$

which can be rearranged such that:

$$T = \frac{C_2}{\lambda_i \ln\left[\frac{L_i \lambda_i^5}{\varepsilon_i C_1} + 1\right]} \qquad [3.2]$$

If $\varepsilon_6 = 0.93$ the temperature can be calculated directly from Equation [3.2]

$$T(6) = \frac{C_2}{\lambda_i \ln\left[\frac{L_i \lambda_i^5}{0.93\, C_1} + 1\right]} \qquad [3.3]$$

By rearranging Equation [3.1]

$$\varepsilon_i = \frac{L_i \lambda_i^5 \left(e^{(C_2/\lambda_i T)} - 1\right)}{C_1} \qquad [3.4]$$

Using the value of temperature T(6), calculated in Equation [3.3], and the values L_i from the TIMS, an estimate of ε_i for i = 1, 5 can be found.

This method produces six emittance values (the value of the emittance in band six is always 0.93) and a temperature (derived by using the radiance and emittance in band 6). Results of the application of this method on TIMS data from Halls Creek, Western Australia, are discussed in Chapter 5.

3.2.3 DISCUSSION

In order to calculate emittance from the TIMS, using the ME method, two assumptions are necessary. These assumptions are a source of error.

Assumption 1. The data is calibrated and atmospherically corrected. The TIMS data must be calibrated to account for scanner derived effects that are not due to variations within the scene. The method for calibrating TIMS data is given in Palluconi and Meeks (1985) and outlined in Chapter 5. The TIMS data must also be corrected for the effects of the interaction of the emitted radiation received by the scanner with the atmosphere. Assuming the atmospheric correction of the data is perfect, there will be no error. However, perfect correction of the data will not, in general, be possible because the atmospheric parameters needed will not be precisely known. Thus an

error associated with residual atmospheric effects will be present. The magnitude of this error will be entirely dependant on the accuracy of the correction applied. The problems associated with the atmospheric correction is discussed in detail in Chapter 5 where the LOWTRAN6 atmospheric correction algorithm has been applied to TIMS data from Halls Creek W.A..

Assumption 2. Emittance in band 6 = 0.93. This method reduces the number of unknowns by setting one of the variables to a constant value. The variable to be made constant was chosen, according to Kahle *et al* (1980) because, for common silicate rock types the assumption of $\varepsilon 6 = 0.93$ is not drastically in error for commonly occurring lithologies. However Lyon (1965) shows that mafic and ultramafic rocks do not have $\varepsilon 6 = 0.93$ and for these terrains a better assumption would be that $\varepsilon 1 = 0.93$. A study of example emittance spectra given in Figures 5.16 to 5.22 show that the assumption of a constant emittance in any single band will not be satisfactory for a wide variety of rock types, and that the choice of band number and emittance value will depend upon the particular lithologies that may be expected within the scene.

A solution can be found for any band and any set emittance value. Some studies (Kahle (1987)) assumed $\varepsilon 6 = 0.93$, whilst in other terrains the assumption utilised is $\varepsilon 6 = 0.95$, (Kahle *et al* (1988)). Figure 3.3 indicates the magnitude of error that may be expected if such an assumption is made for a laboratory emittance spectrum of quartz at 300K.

The Model Emittance method, in assigning a constant emittance value in a constant band, ($\varepsilon = 0.93$), destroys any variation that in reality exists in that band. The effect on emittance spectra of assigning $\varepsilon 6 = 0.93$ is illustrated in Figure 3.4 using schematic spectra. It shows that individual spectra will have their emittance values increased or decreased in order to make $\varepsilon 6 = 0.93$. It also shows that the relative difference in emittance between the spectra will be altered. In Figure 3.4a the difference in emittance values for band 1 is reduced, in 3.4b the difference in band 1 is increased, and in 3.4c the emittance values have been changed such that the emittance in spectrum F is now greater than the emittance for spectrum E in band 1. In an image, the assumption will cause, in some cases, the reordering of emittance

values in a band. Figure 3.5 demonstrates the effect on four library spectra. The relative emittance values in Figure 3.5a are;

Band 1 $\varepsilon_A > \varepsilon_B > \varepsilon_C > \varepsilon_D$
Band 5 $\varepsilon_A > \varepsilon_B > \varepsilon_C > \varepsilon_D$
Band 6 $\varepsilon_A > \varepsilon_C > \varepsilon_D > \varepsilon_B$

When the assumption is applied, Figure 3.5b, the relative values have been reordered thus;

Band 1 $\varepsilon_B > \varepsilon_A > \varepsilon_C > \varepsilon_D$
Band 5 $\varepsilon_B > \varepsilon_A > \varepsilon_D > \varepsilon_C$
Band 6 $\varepsilon_A = \varepsilon_B = \varepsilon_C = \varepsilon_D$

This reordering of emittance values will be manifest in the resultant emittance images.

A further problem that occurs with the implementation of this assumption is that the magnitudes of emittance variations will be changed. Assigning a constant value to a band (for example, $\varepsilon 6 = 0.93$), for all pixels, will tend to reduce the range of emittance values that the adjacent band takes. This is also illustrated in Figure 3.4. In 3.4a it is clear that for all bands the differences are reduced. For 3.4b, the emittance for bands 1 and 2 have been separated further while the values in band 5 have been reordered and their differences reduced. In 3.4c the emittance values in each band have been reordered and the difference between the emittance values has been increased in bands 1 and 2, and decreased for band 5. These schematic spectra show that setting a particular band to a constant emittance will tend to reduce relative differences in the adjacent band and reorder the emittance values in the other bands.

In Figure 3.5, the variation in band 5 for laboratory derived example emittance spectra has been reduced as has the band furthest removed from the constantly held band which has shown a decrease in separation. For the TIMS, where $\varepsilon 6 = 0.93$, this results in the band 5 image displaying little variation in emittance, and thus being dominated by noise. Thus only bands 1, 2, 3 and 4 will show any great variation within the scene and meaningful emittance images are effectively lost in 5 and 6. The effect of fixing the emittance value in a band can be seen in the TIMS data set from Halls Creek W.A., which is described in Chapter 5.

A temperature image may be created in place of band 6 which should highlight the topographic features of the scene. This would indicate that this method has gone some way to separate the temperature information from the emittance information.

3.2.4 CONCLUSIONS

1. Atmospheric corrections must be attempted to prevent artifacts appearing in the emittance spectra.

2. The Model Emittance method allows a quantitative estimate of emittance and temperature to be made with multispectral Thermal Infrared data.

3. Any one choice of an emittance value in a band is not valid for most lithologies and will thus produce errors in emittance estimation, the magnitude of which will depend on the difference in emittance of the estimated value to the actual value in that band.

4. The error due to inaccuracies in the estimation will cause the mean of the spectrum to increase or decrease. The principal difference between the correct emittance values and the emittance values estimated by this method will be in mean value and not in the shape of the spectrum.

5. Images from bands adjacent to the constant band will tend to exhibit reduced variations and reordering of emittance values. For $\varepsilon 6 = 0.93$, images in bands 5 and 6 will not show useful variations. Band 5 will contain much noise and band 6 will be uni-valued.

3.3 THE MAXIMUM TEMPERATURE METHOD

This method was originally suggested by Gillespie (1986) as a possible improvement over the Model Emittance technique. It has been applied to TIMS data from Hawaii, Realmuto (1990).

3.3.1 ASSUMPTIONS

1. The data have been calibrated and atmospherically corrected.

2. It is assumed that the greatest emittance value in the spectrum will be a constant, but the band in which this occurs is not specified, for example, $\varepsilon max = 0.94$.

3.3.2 METHODOLOGY

The Maximum Temperature method represents an alternative to the assumption used in the Model Emittance algorithm. If it was found that the highest value of emittance in a band was 0.94 and that the value in band 6 was 0.93, then the predicted emittances from both these methods would be the same. In order to obtain the band in which the emittance is highest the Planck function is rearranged to make temperature the subject;

$$T = \frac{C_2}{\lambda_i \ln\left(\frac{L_i \lambda_i^5}{\varepsilon_i C_1} + 1\right)}$$

Using the value $\varepsilon = 0.94$, six temperatures are calculated from the equation set. The highest value of temperature will correspond to the maximum emittance in the spectrum. This temperature is then used in Equation [3.4] to calculate six emittances. The highest emittance value in the spectrum will be 0.94. This method yields 6 emittance images and a temperature image.

3.3.3 DISCUSSION

The assumptions used in the Maximum Temperature calculation are a source of error.

Assumption 1. The magnitude of errors due to inaccuracies in the calibration of the TIMS and the atmospheric correction are discussed in Chapter 5. If there are errors in the correction, the resultant emittance values will contain atmospheric artifacts.

Assumption 2. This method, in contrast to the Model Emittance method, assumes that the maximum emittance value in the spectrum is 0.94. However if there is no band where $\varepsilon max = 0.94$, an error will occur in the emittance estimation. Setting a maximum emittance value to 0.94, does not allow maximum emittance values greater

than or less than this value. Many emittance spectra do in fact have values over 0.94, and indeed many spectra have maximum emittance values below 0.94. Figure 3.6 illustrates the magnitude of error that may occur for several example spectra. The magnitude of the error that may be present if the maximum emittance is not 0.94 will tend to create spectra whose mean will be under- or over-estimated (Figure 3.6). The spectral shape, important for lithological identification, will be preserved.

In creating six emittance images and a temperature image, it at first appears that more useful bands have been created than in the Model Emittance calculation. The Model Emittance calculation assumes that one band has a constant emittance, and so that band is not displayed as it contains no variation and therefore no useful information. In the Maximum Temperature method, the band in which the assumption is made may vary on a per pixel basis and so there is no single band that is uni-valued over the whole scene. Any band combination used to display the variation in emittance may contain areas of pixels within the scene that show no variation. In effect this method potentially mixes the grey toned image (band 6 of the Model Emittance calculation) amongst all six bands.

Another problem that exists with this method is similar to the problem discussed with regard to the Model Emittance method, namely that the differences between values in bands adjacent to the εmax band will be reduced. If for example, $\varepsilon 3 = 0.94$ for a particular group of pixels then the variations in $\varepsilon 2$ and $\varepsilon 4$ values will tend to be reduced.

Consider an artificial scene where 6 fields, all of different materials, have their highest emittance values in successive bands. In the Model Emittance method (for $\varepsilon 6 = 0.93$), band 5 would be noisy and band 6 would be a single grey tone. Using the Maximum Temperature method, the fields containing the highest emittance in a band would create a noisy image in the adjacent bands (for similar reasons as the noise produced with the Model Emittance method). Thus for pixels where $\varepsilon 1$ was a maximum, the variation of the estimated emittance in band 2, would be reduced. If $\varepsilon 3$ was a maximum, then the variation of the estimated emittance in bands either side (bands 2 and 4) would also tend to decrease. If εmax was in band 2, then those areas in band 2 would be uni-valued; a grey tone. Band 2 would consequently show little variation in areas where $\varepsilon 1$ or $\varepsilon 3$ where maximum, and no variation where $\varepsilon 2$ were a maximum. If a scene were a complex mix of lithologies where εmax varied from band to band, then parts of the scene would contain little useful information where

values could be attributable to the nature of the assumption of the Maximum Temperature method.

In consequence, adjacent pixels may have emittance values in a particular band that have the same value but the assumption used to produce those two values may be different. It would be difficult to decide which, if any, of the two values would be due to genuine variations in emittance or due to inaccuracies in the original assumption. The resulting images could have areas that were a grey tone, (where it was found that the pixels in that band provided the highest temperature) and areas that were noisy (where the band is adjacent to the εmax band). In contrast to the Model Emittance method, noise would be potentially spread amongst all bands rather than a single band being a grey tone and its adjacent band containing noise. In a spectral sense the resulting emittance spectra will all share the characteristic imposed upon them that they all have a maximum emittance value of 0.94. The accuracy of this assumption is discussed with regard to laboratory Thermal Infrared spectra collected from Halls Creek in Chapter 5.

3.3.4 CONCLUSIONS

1. The Maximum Temperature method relies on an accurate atmospheric correction being applied to the data.

2. The method allows an estimation of emittance and temperature to be made by assigning the maximum emittance in an unspecified band to a constant value.

3. Individual emittance spectra will be in error if the maximum emittance in one of the bands is not equal to the assumed maximum emittance value.

4. Errors in the assumption will cause the resultant emittance spectra to have higher or lower mean emittance values, rather than effecting the shape of the emittance spectra.

5. Due to the nature of the assumption made, some areas of an image will show little variation and thus appear noisy.

3.4 THE UNIVERSAL TEMPERATURE METHOD

This method reduces the number of variables by setting the temperature across the scene to a constant value in order to calculate emittance images.

3.4.1 ASSUMPTIONS

1. The data have been calibrated and atmospherically corrected.

2. Temperature is constant over the scene.

3.4.2 METHODOLOGY

A simple solution to relieve the underdetermined system is to assign the temperature in all pixels to an arbitrary value (eg. 300K). Using Planck's function (Equation [3.1]), six emittances may be calculated.

The resultant emittance spectra will generally be in error, the magnitude of which will be determined by the difference between the correct temperature in comparison to that assigned to it. Examples of the effect of changes of estimates of temperature is given in Figure 3.2, Slater (1980) has shown that for the 8-12μm region, and with emittance of 0.9, a 1K change in temperature will cause a 0.02 change in emittance.

3.4.3 DISCUSSION

The Universal Temperature method suffers from the obvious handicap of assigning one value of temperature to an area where temperature variations may be as much as 20K (pers. comm. A. Gabell (1989)). Variations in radiance within the scene will be assigned to emittance differences rather than temperature changes. An over estimate of the emittance variations will result causing the emittance images to display residual temperature effects. The interpretation of an image calculated in this way will be difficult because pixels may be assigned the same values of emittance as a result of the assumption, whereas in fact the variation in observed radiance is due to a temperature difference. Scenes of low topographic variation will provide smaller temperature ranges and so this technique will be more useful over these areas.

When assessing the spectral information contained within a pixel it is possible to generate the suite of curves that are potentially correct by assigning a temperature and

calculating emittance for increments of temperature. The resulting spectra are all of similar shape, as can be seen in Figure 3.2b. In this case no assumption has been made, except for the range of likely temperatures for the pixel. This method, in making no assumption to reduce the number of variables, creates a suite of spectra from which the user makes the decision of which spectrum is responsible for the radiance received. This has the advantage of not selecting the spectrum for the user based on an arbitrary assumption, as is the case in the Model Emittance calculation or Maximum Temperature method, but allows selection based upon the user's experience. The disadvantage of this method is that a suite of spectra must be produced for each sample of radiances under investigation and there is no absolute criterion to select which of the spectra is the correct one as they are all potentially correct.

3.4.4 CONCLUSIONS

1. This method requires accurately calibrated and atmospherically corrected data.

2. An emittance image calculated assuming a constant temperature throughout the scene will attribute values of emittance that are in error as they contain components due to errors in temperature estimation.

3. A suite of emittance curves calculated from a pixel's radiance by assuming a range of temperatures presents the user with a set of potential spectra one of which may represent the true estimate of emittance. However the user has no objective means of determining which one is correct.

4. Scenes of low topographic expression would provide more accurate estimates of emittance because the variation in temperature, which is related to topography, will be reduced.

3.5 ESTIMATION OF EMITTANCE BY PARAMETRISATION

These methods are intended to model the emittance component of the Planck function as various functions, such that the number of unknowns is reduced to relieve the underdetermined system of equations. Two approximations have been investigated.

3.5.1 POLYNOMIAL APPROXIMATION

3.5.1.1 ASSUMPTIONS

1. The data have been calibrated and atmospherically corrected.

2. The emittance component of the Planck function may be described as a function of λ_i, and is approximated by the polynomial

$$\varepsilon = f(\lambda) = A + B\lambda + C\lambda^2 + D\lambda^3 + E\lambda^4 \qquad [3.5]$$

3. The best fitting polynomial will provide an estimate of the emittance values.

3.5.1.2 METHODOLOGY

A study of common emittance spectra reveals that most spectra have a simple shape. This shape is further simplified when a spectrum is measured over a broad bandwidth as is the case when a spectrum is convolved to six points with the TIMS response functions to create a TIMS equivalent spectrum, Realmuto (1989). It is generally possible to approximate an emittance spectrum to a quartic polynomial. This creates an Equation set of 6 unknowns, (A,B,C,D,E,T) and six equations:

$$L_i = \frac{\left(A_i + B\lambda_i + C\lambda_i^2 + D\lambda_i^3 + E\lambda_i^4\right) C_1}{\lambda_i^5 \left[e^{C_2/\lambda_i T} - 1\right]} \qquad [3.6]$$

By varying these parameters, a set of polynomial coefficients may be found that produce values of the emittance component of the signal which, when combined with the Planck function, will closely fit the observed radiance values. Using Powell's technique for N-dimensional minimisation (Press (1986)) a best fit solution was sought where the parameters (A,B,C,D,E,T) would minimise the difference between the observed radiance values and the calculated radiance values. This minimisation technique was chosen as it is considered a robust method of minimisation.

3.5.1.3 DISCUSSION

The best fitting polynomial should approximate most closely to the emittance spectrum. Test pixels were calculated using six emittance values taken from laboratory spectra and a temperature to produce radiance data values. There were two set boundary conditions in the minimisation technique. Firstly, there was a maximum temperature beyond which a solution was not allowed, (to a maximum reasonable allowable temperature). The second condition was the tolerance. When the magnitude of error was less than a certain value (the tolerance), then the minimisation was deemed to have been satisfactorily completed to desired degree of accuracy. The tolerance was set at 0.15 $mW.m^{-2}.\mu m^{-1}.sr^{-1}$ as this value is far below the change in radiance value due to the noise equivalent change in temperature (NEΔT) of the TIMS instrument. The minimisation continued until a maximum temperature was achieved. It was found that two possible situations would occur.

Where the original emittance spectrum did not behave as an exact quartic equation, the temperature would increase as far as the boundary conditions would allow. This occurs because as the temperature increases, each of the emittance values decreases. This will reduce the amplitude of variation within the emittance spectrum. As the curve flattens, and thus exhibits less variation, the polynomial can more easily approximate to it with less error than if the curve contained large variations: a polynomial can more accurately approximate to a curve if that curve exhibits little variation. Figure 3.7 shows the behaviour of an emittance spectrum with changing temperature. It indicates that a polynomial may best fit the emittance curve if it exhibits small variations.

Test pixels were also created whose emittance component could be described exactly by a quartic equation. In these situations a solution would be found to within the set tolerance level. However the solution in these cases was dependant upon the initial starting values for the minimisation and so different solutions were achieved for the same radiance values.

For pixels where there is no exact solution, as is generally the case, the magnitude of error at the correct temperature will be small. As the temperature increases, the magnitude of error will decease as the contrast in emittance values between the bands is reduced. For an exact solution, the error will be zero at the correct temperature, but will remain so as the temperature rises. Thus there is no local minimum in error at a particular temperature, but a trend in the reduction of the magnitude of error with

increasing temperature. No stable solution can be found because there is no local minimum.

Realmuto (1989) has also investigated the possibility of parametrising the emittance component using polynomials. He considered the behaviour of the system of equations that this parametrisation creates for a quartic polynomial on the emittance component alone, without considering the effect of the temperature variable. He concludes that the ill-conditioned power series parametrisation would require a degree of accuracy in radiance measurements that is beyond the capacity of the TIMS.

In addition Realmuto (1989) has also shown that it is possible to reduce the required accuracy in radiance values at the expense of the number of terms in the power series. However, reducing the power series to a parabola containing three elements would not, in general, be a good representation of an emittance curve. When considering the emittance component alone, the parametrisation will fail because the ill-conditioning of the equation set necessitates an accuracy in radiance measurements beyond the capability of the TIMS. When considering the temperature component, as well as the emittance component, the parametrisation will fail because there is no local minimum in error.

The polynomial parametrisation of the emittance function is not considered a useful technique for use with TIMS data, or indeed with other passive Thermal Infrared scanners.

3.5.2 GAUSSIAN APPROXIMATION

Realmuto (1989) also suggested an alternative parametrisation of an emittance spectrum, that of a Gaussian approximation may be possible. This takes the form:

$$\varepsilon_i = M_0 + M_1\lambda - M_2 \exp\left(-\pi\left[\frac{(\lambda - M_3)}{M_4}\right]^2\right) \qquad [3.7]$$

However Realmuto (pers. comm. (1990)) finds that this alternative parametrisation suffers from the same problems of ill-conditioning and lack of a local minimum as was found for the polynomial parametrisation.

3.5.3 CONCLUSION

1.Parametrisations using polynomial and Gaussian approximations do not provide stable solutions.

3.6 SUMMARY

Each one of the above mentioned methods seeks to reduce the number of variables in the underdetermined system. Each assumption will be correct over some portion of the scene but will create errors in other parts of the scene where the pixels depart from the assumed behaviour. The best technique will be that which produces the least significant error over a large portion of a scene.

Each method has a major failing, the Model Emittance method destroys useful image information in the constant band and the adjacent band. If $\varepsilon 6 = 0.93$ Bands 5 and 6 will show no useful variation in the emittance images. The Maximum Temperature method destroys image information in those bands adjacent to the εmax band (for similar reasons as the Model Emittance method does). The Constant Temperature method assigns all the variation of radiance to emittance changes, ignoring the effect of temperature.

Figures 3.5 and 3.6 illustrate the differences between the Model Emittance and Maximum Temperature methods for example spectra at 300K. Two separate estimates of emittance for each spectrum are calculated by applying each method described above. The 'best' solution will be that which is not significantly in error for most of the scene. Each method will be more accurate in some cases than the others depending upon the individual pixels within the scene.

Other assumptions may be made that reduce the number of variables. For instance, it is sufficient to relieve the underdetermined equation set for the TIMS by the assumption:

$\varepsilon 5 = \varepsilon 6$.

This creates five different emittance values and a temperature, which can be solved for six equations. This assumption would not in general be true for most lithologies. Figure 3.8 shows the variation of emittance with temperature for a quartz spectrum at 300K. If $\varepsilon 5 = \varepsilon 6$ the estimated temperature is 289K whereas the true temperature is

300K. To find the best method it is necessary to study the characteristic behaviour of Thermal Infrared emittance spectra from the scene under investigation to determine which method would yield an accurate result for a large proportion of the scene. These features of Thermal Infrared spectra are discussed in Chapter 5 using the spectra obtained from Halls Creek W.A..

Although the Model Emittance method is the commonly described method in the literature, these other methods provide alternative approximations to calculate emittance that will, for certain spectra, be as accurate as the Model Emittance method but do not provide a significant improvement in the ability to extract emittance. A more complex set of assumptions based on pixel characteristics would be necessary to extract emittance to a greater degree of accuracy. The Model Emittance and Maximum Temperature methods have been described in detail with regard to Halls Creek TIMS data in Chapter 5.

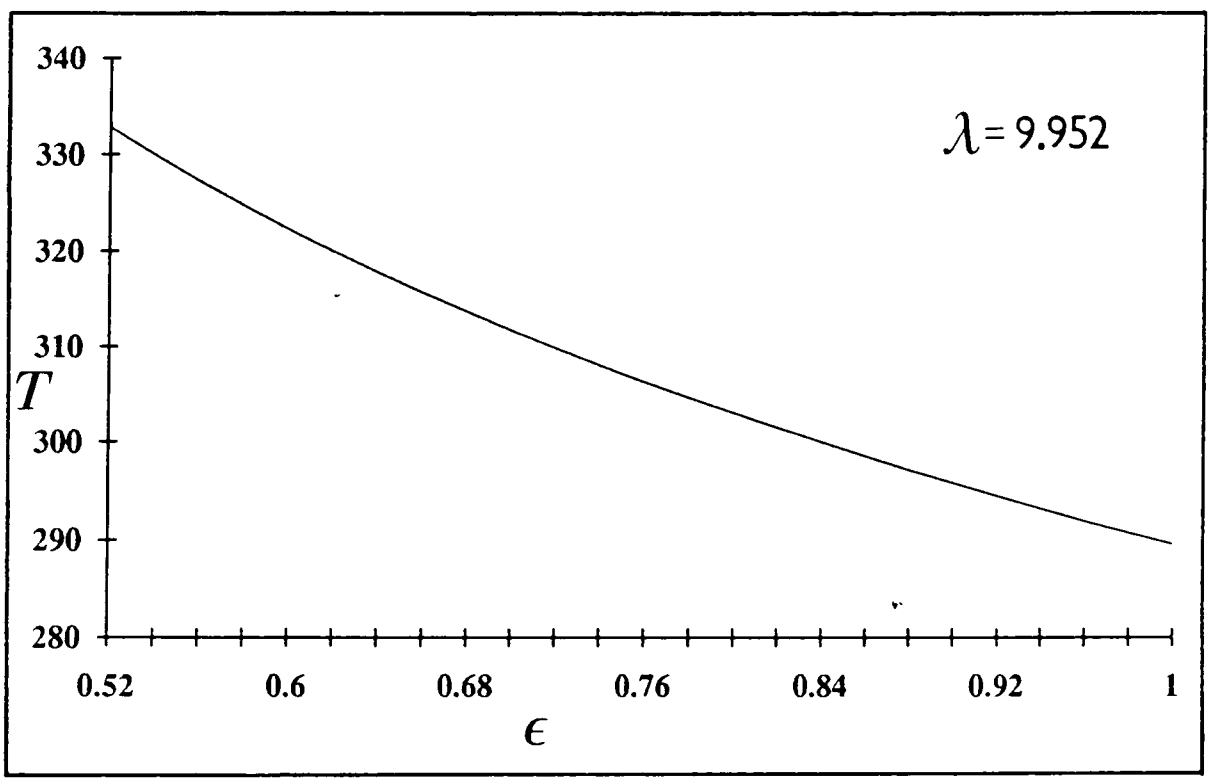

Figure 3.1 Constant radiance graph. The line of solution represents temperature and emittance pairs that, using the Planck function, will calculate one radiance value.

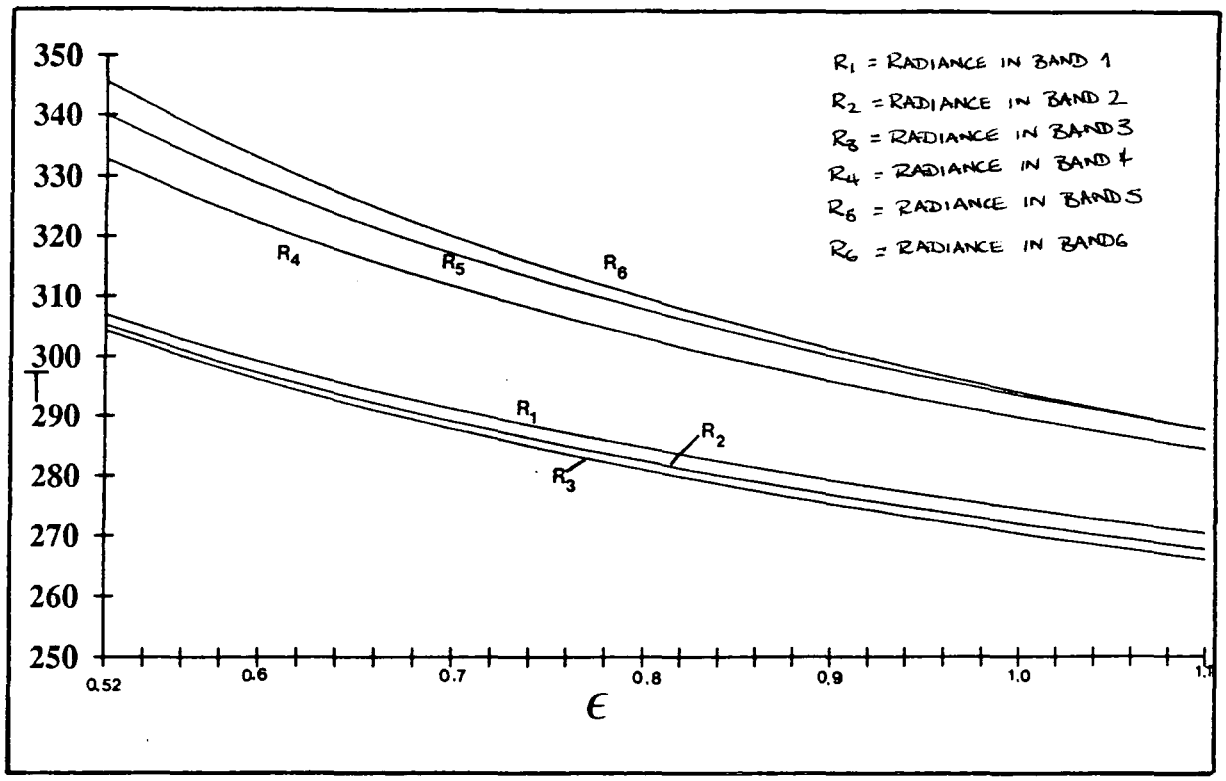

Figure 3.2a Constant radiance graph for quartz.

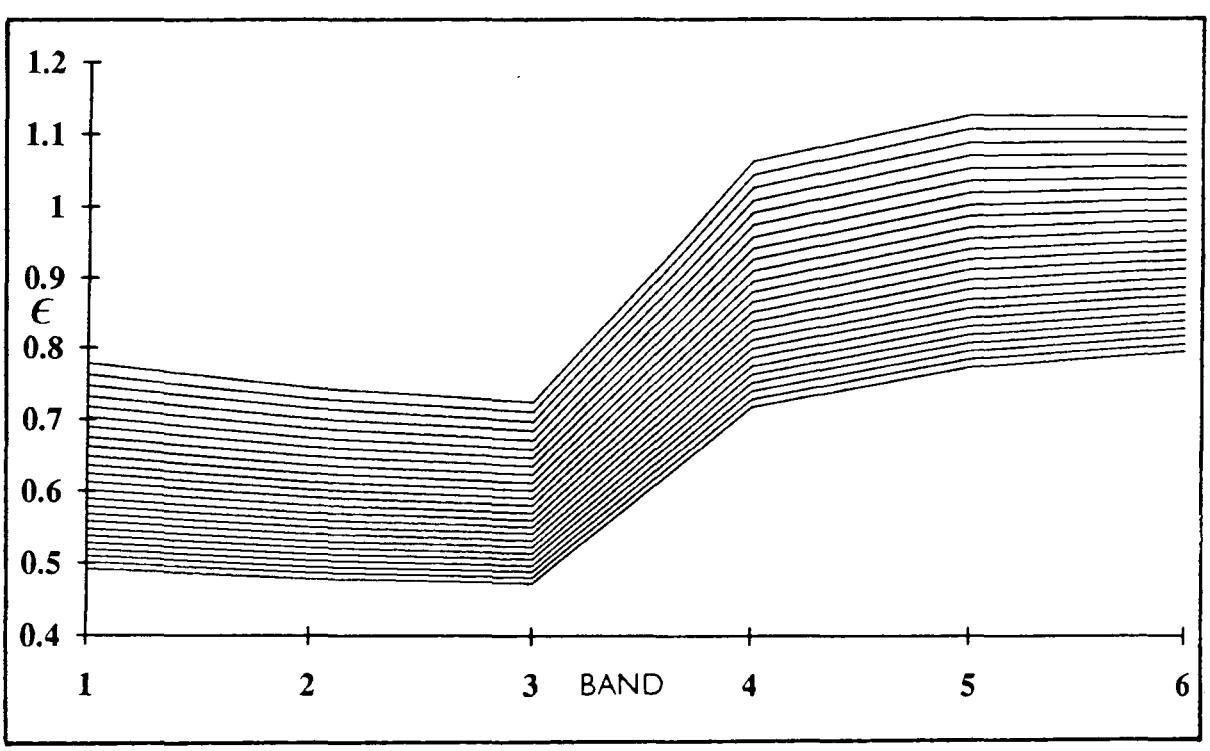

Figure 3.2b Suite of emittance spectra which will be calculated from graph 3.2a for single values of temperature.

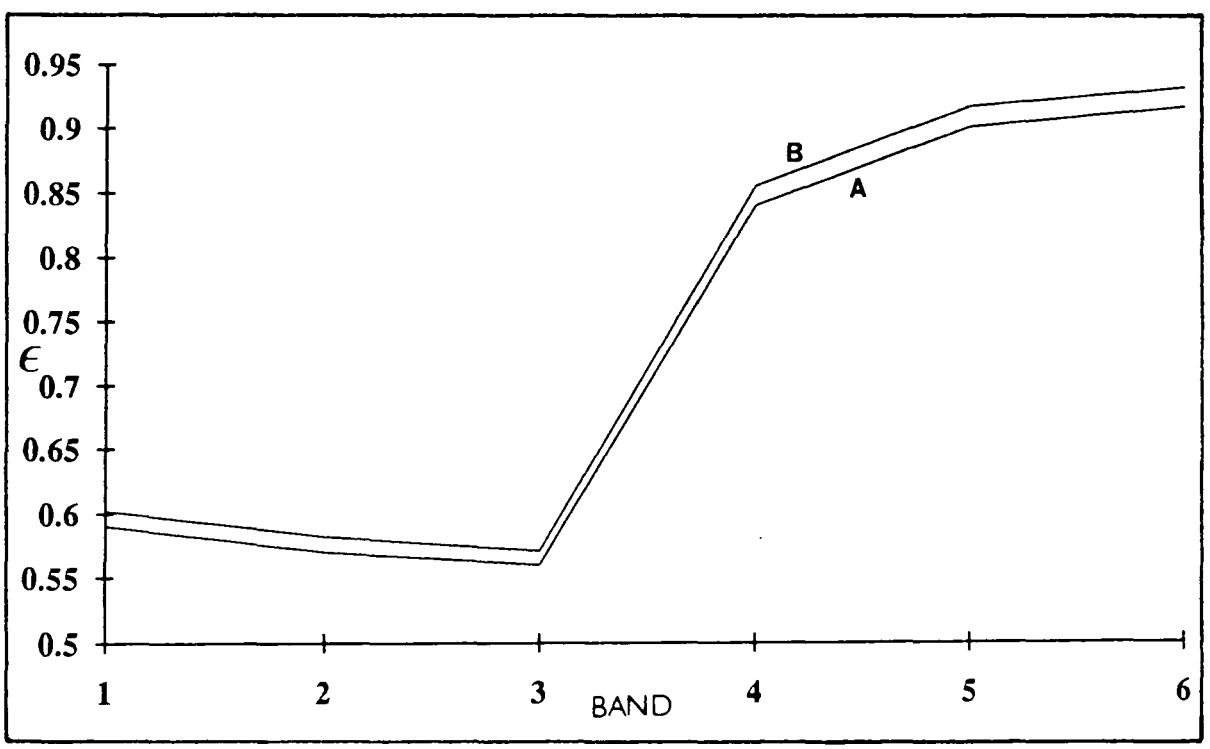

Figure 3.3 Magnitude of error in emittance for an example quartz spectrum using the Model Emittance method.

Spectrum A. Quartz spectrum (assumed to be at 300K).
Spectrum B. Quartz spectrum with $\varepsilon_6 = 0.93$.

Figure 3.4 Diagram to illustrate the change in emittance values resulting from the application of the Model Emittance assumption for schematic spectra.

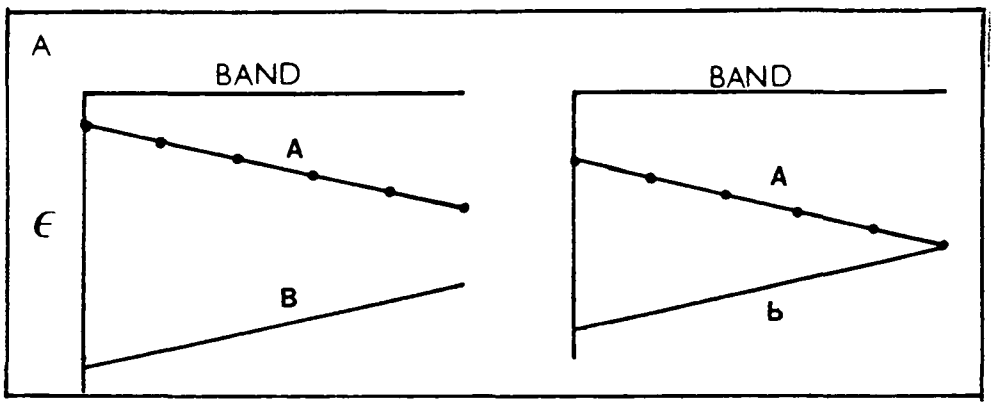

A. Differences in emittance values in each band are reduced.

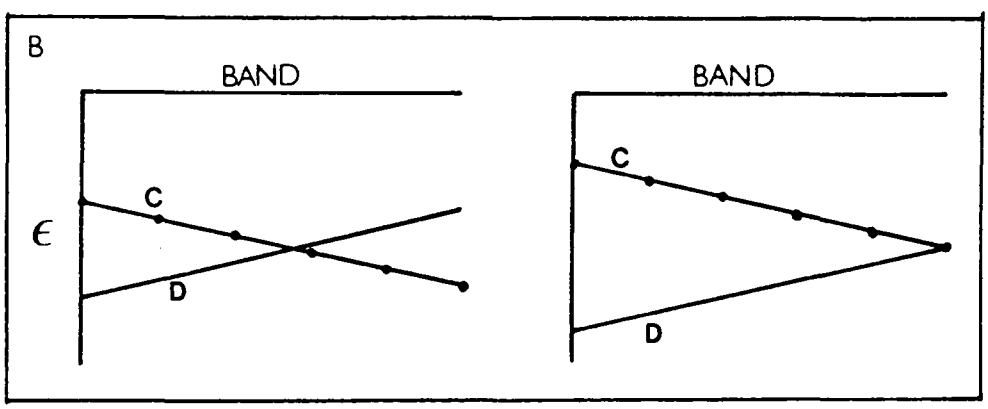

B. Differences in emittance values in bands 1,2 and 3 are increased, relative values in 4, and 5 are reversed.

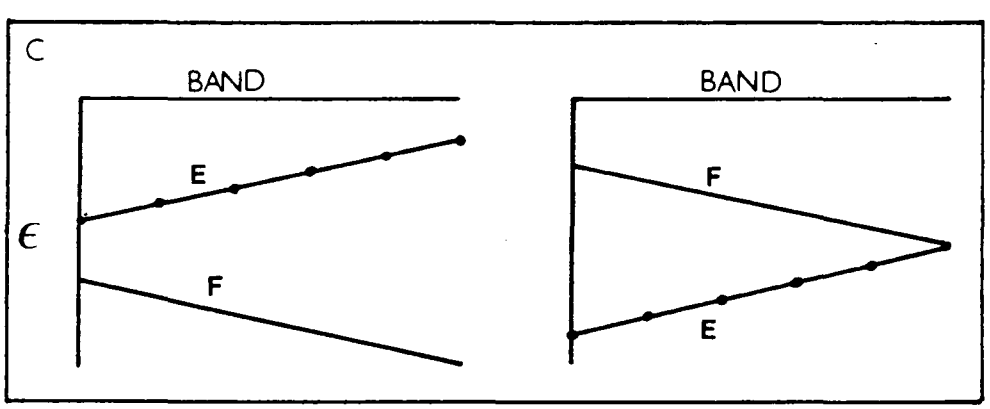

C. Relative emittance values in each band are reversed. The differences in emittance values in bands 1 and 2 are increased and relative values reversed. For bands 3,4 and 5 differences are decreased and relative emittance values are reversed.

Figure 3.5 Graphs to show the effect on laboratory spectra of the implementation of the Model Emittance assumption, for lithologies at 300K.

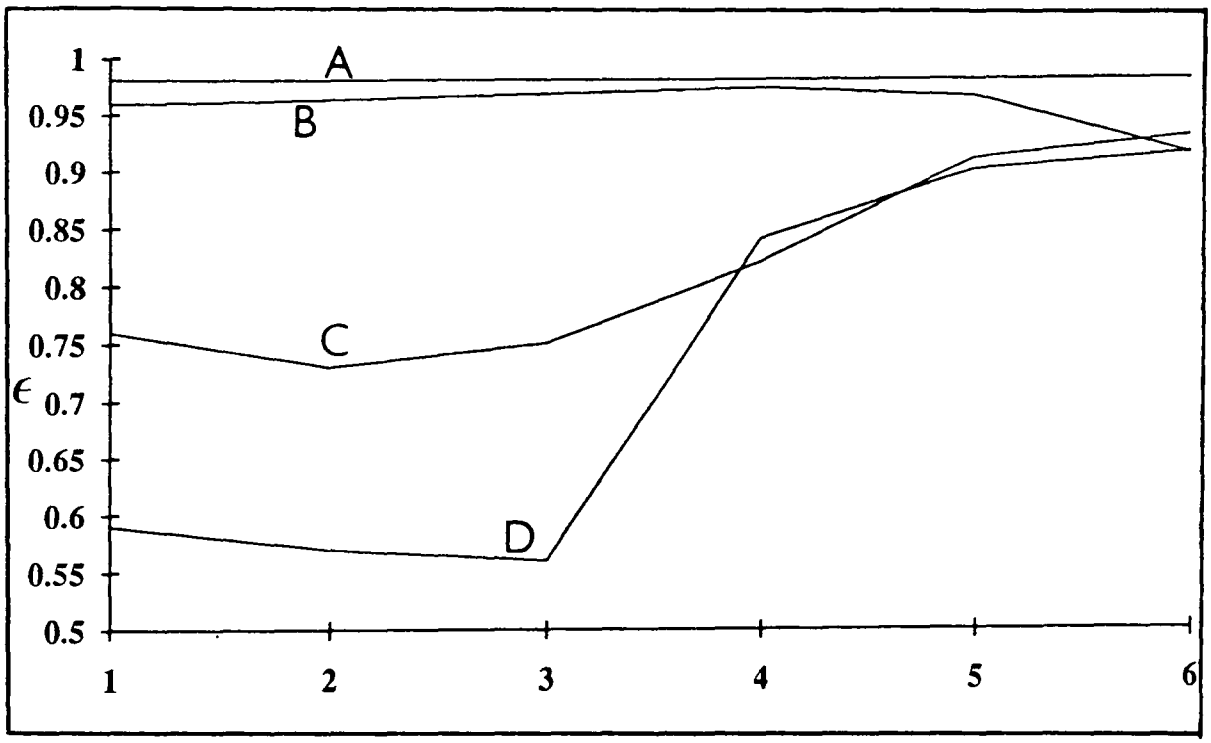

3.5a. Emittance spectra of A. Vegetation. B. Dolomite. C. Granite. D. Quartz.

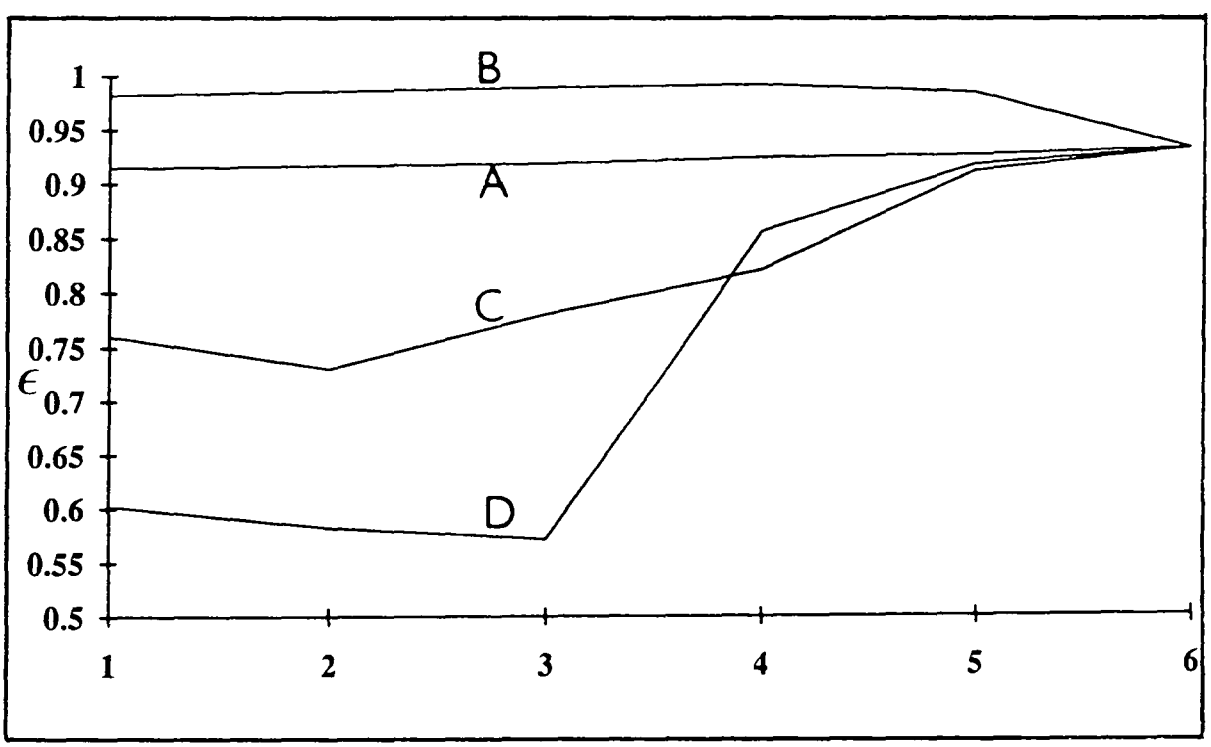

3.5b. Emittance spectra after $\varepsilon_6 = 0.93$ criterion has been imposed upon them.

Figure 3.6 Graphs to show the effect on lab spectra of the implementation of the Maximum Temperature assumption, for lithologies at 300K.

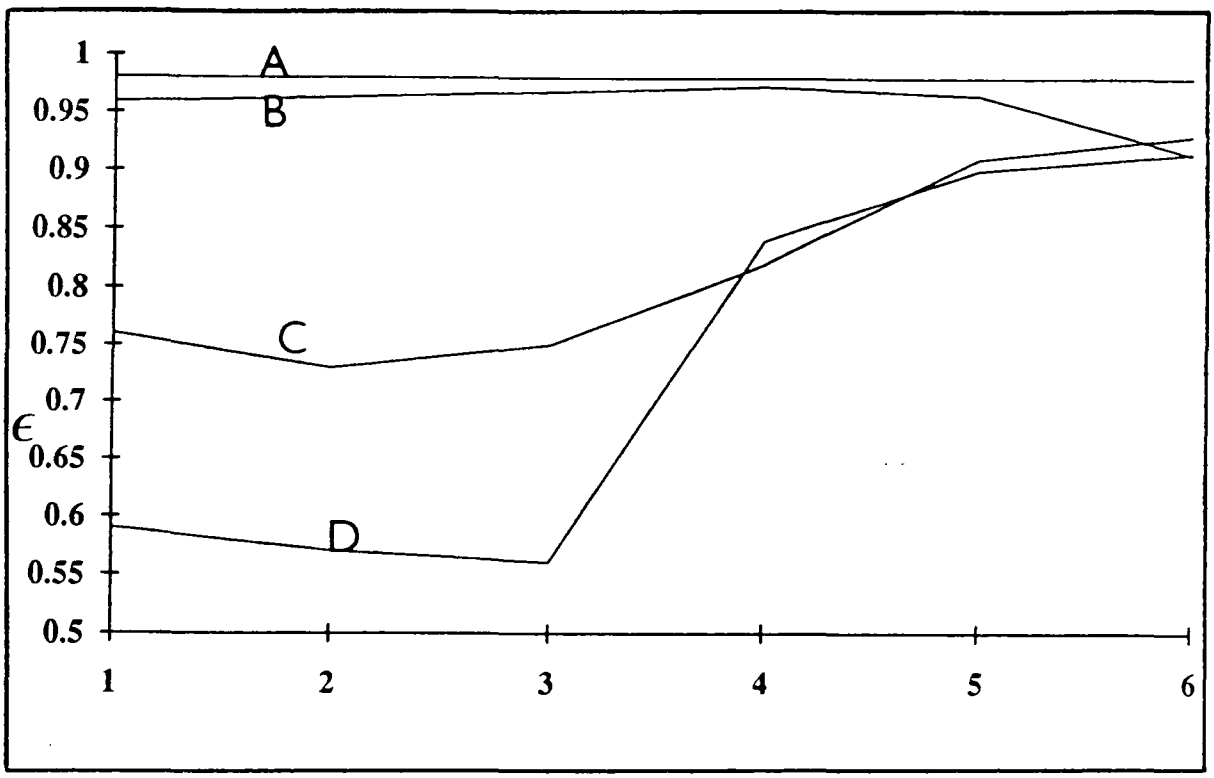

3.6a. Emittance spectra of A. Vegetation. B.Dolomite. C. Granite. D. Quartz.

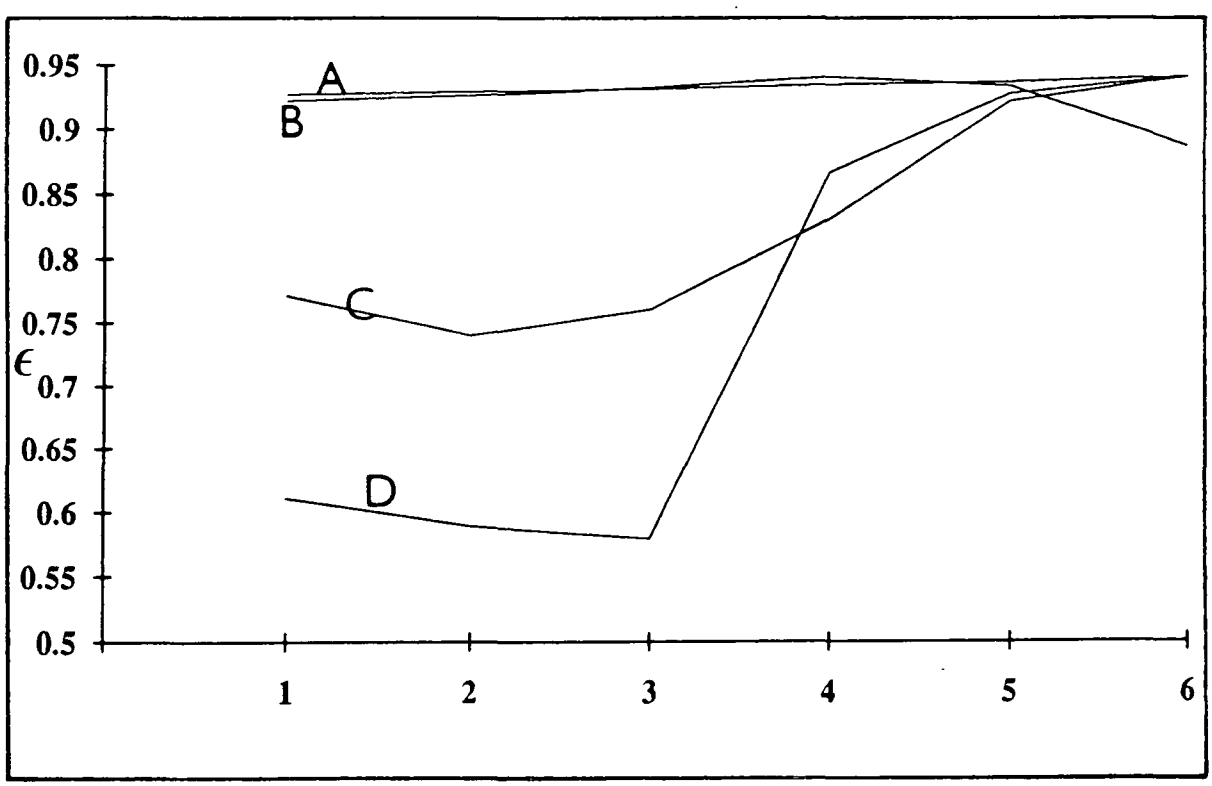

3.6b. Emittance spectra after $\varepsilon_{max} = 0.94$ criterion has been imposed upon them.

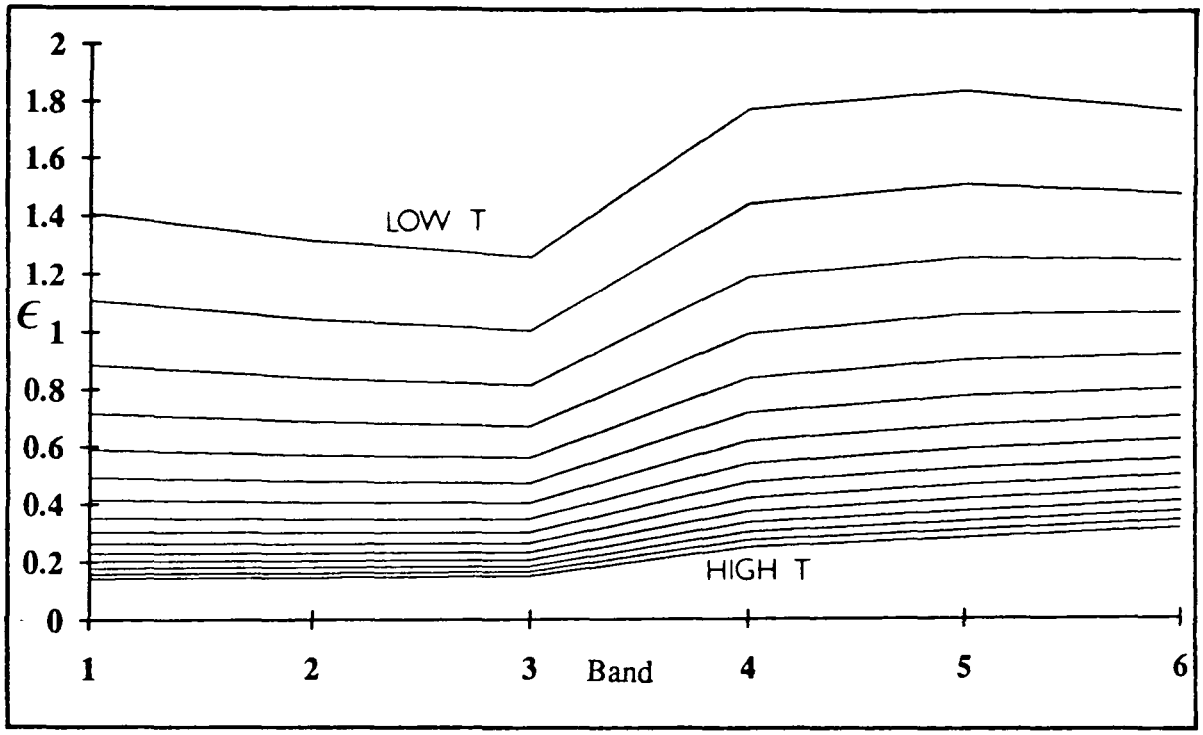

Figure 3.7 Graph to show the decrease in variation within an emittance spectrum with increase in temperature.

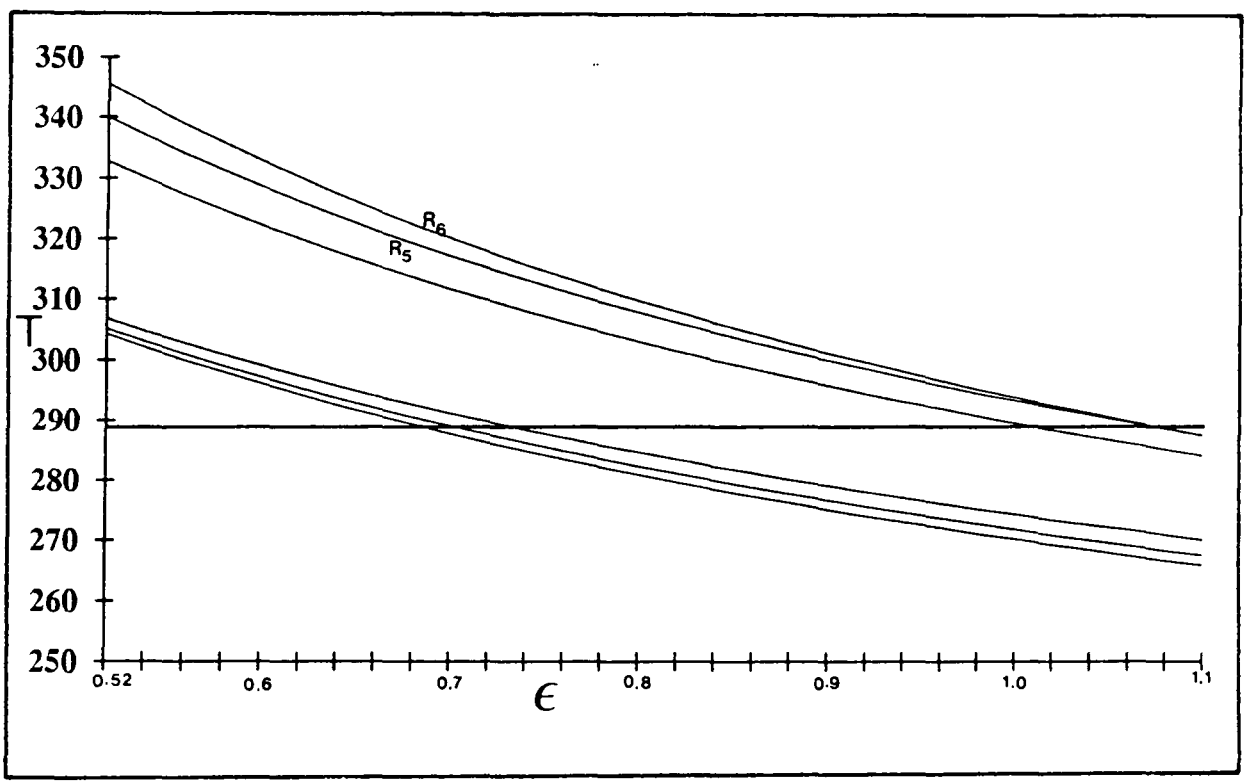

Figure 3.8 Constant radiance plot for quartz at 300K. The temperature where $\varepsilon_5 = \varepsilon_6$ is 289K. This assumption predicts a difference in temperature of 11K from the original emittance spectrum at 300K.

CHAPTER 4

ENHANCEMENT AND CALCULATION OF SPECTRAL EMITTANCE USING THE WIEN APPROXIMATION

4.1 BACKGROUND

This Chapter deals with the processing techniques that enhance and calculate spectral emittance information by the use of the Wien approximation to the Planck function.

The Planck function was developed from quantum theory whereas Wien's approximation was derived from classical physics (Swain and Davis 1981). Wien's law is a valid approximation when the product of wavelength and temperature is less than 3000 μm.K. For typical terrestrial temperatures (300K), and for the thermal infrared wavelength region, we may therefore use Wien's law. An indication of the magnitude of error that may be expected is given in Table 4.1.

Thus the Planck function;

$$L_{ij} = \frac{\varepsilon_{ij} C_1}{\lambda_i^5 \left[e^{(C_2/\lambda_i T_j)} - 1 \right]} \qquad [4.1]$$

may be approximated to Wien's law;

$$L_{ij} = \frac{\varepsilon_{ij} C_1}{\lambda_i^5 \left[e^{(C_2/\lambda_i T_j)} \right]} \qquad [4.2]$$

where:

i = band number (from 1 to 6 for TIMS).

j = pixel number.

L_{ij} = radiance in j^{th} pixel, and i^{th} band.

ε_{ij} = emittance in j^{th} pixel, and i^{th} band.

λ_i = wavelength value in i^{th} band.

C_1 = first radiation constant/π

C_2 = second radiation constant

T_j = temperature in j^{th} pixel.

Three techniques are examined, firstly the Thermal Log Residual (TLR) technique is described. It creates scene-dependant-temperature-independent coefficients related to the emittance. Secondly a new method, the calculation of alpha coefficients is given. This is a simplification of the TLR method and creates scene and temperature independent values related to the emittance component of the radiance received by the scanner. Finally, it is possible to calculate emittance and temperature from the Thermal InfraRed (TIR) data using the alpha coefficients and a knowledge of the characteristic behaviour of TIR laboratory spectra. The latter two methods were developed during the course of this study.

As with the techniques used to estimate emittance and temperature described in Chapter 3, these methods are all discussed with reference to the Thermal Infrared Multispectral Scanner (TIMS) instrument, but can be modified and applied for use with other passive multispectral scanners sensing in the TIR which have different configurations.

4.2 THE THERMAL LOG RESIDUALS METHOD

The Thermal Log Residual (TLR) method, Hook (1989), was developed from log residuals, (Green and Craig (1985)), a technique used in the Visible Near InfraRed (VNIR) region which extends from 0.4 to 2.5μm.

This method intends to create temperature independent coefficients whose values are dependent only upon emittance variations.

4.2.1 ASSUMPTIONS

1. The data have been calibrated and atmospherically corrected.

2. Wien's law is a valid approximation to the Planck function.

4.2.2 METHODOLOGY

To calculate Thermal Log Residuals, (TLR) for the TIMS data the following steps are taken:

1. Take the natural logs of the Wien Equation [4.2]:

$$\ln L_{ij} = \ln \varepsilon_{ij} + \ln C_1 - 5\ln \lambda_i - \frac{C_2}{\lambda_i T_j} \qquad [4.3]$$

2. Multiply each Equation [4.3] by λ_i:

$$\lambda_i \ln L_{ij} = \lambda_i \ln \varepsilon_{ij} + \lambda_i \ln C_1 - 5\lambda_i \ln \lambda_i - \frac{C_2}{T_j} \qquad [4.4]$$

3. Calculate different means:

Let $X_{ij} = \lambda_i \ln L_{ij}$

and

X_{ij} =value in band i of pixel j.
X_{6j} = mean of pixel values for a pixel j.
X_{iN} = mean of pixel values in band i.
X_{6N} = mean of pixel values in all pixels in all bands.

$$X_{ij} = \lambda_i \ln \varepsilon_{ij} + \lambda_i \ln C_1 - 5\lambda_i \ln \lambda_i - \frac{C_2}{T_j}$$

$$X_{6j} = \frac{1}{6} \sum_{i}^{6} \lambda_i \ln \varepsilon_{ij} + \frac{\ln C_1}{6} \sum_{i}^{6} \lambda_i - \frac{5}{6} \sum_{i}^{6} \lambda_i \ln \lambda_i - \frac{C_2}{T_j}$$

$$X_{iN} = \frac{1}{N} \sum_{j}^{N} \lambda_i \ln \varepsilon_{ij} + \lambda_i \ln C_1 - 5\,\lambda_i \ln \lambda_i - \sum_{j}^{N} \frac{C_2}{T_j}$$

$$X_{6N} = \frac{1}{6N} \sum_{i\,j}^{6\,N} \lambda_i \ln \varepsilon_{ij} + \frac{\ln C_1}{6} \sum_{i}^{6} \lambda_i - \frac{5}{6} \sum_{i}^{6} \lambda_i \ln \lambda_i - \sum_{j}^{N} \frac{C_2}{T_j}$$

Let $Y_{ij} = X_{ij} - X_{6j} - X_{iN} + X_{6N}$ [4.5]

$$Y_{ij} = \lambda_i \ln \varepsilon_{ij} - \frac{1}{6} \sum_{i}^{6} \lambda_i \ln \varepsilon_{ij} - \frac{1}{N} \sum_{j}^{N} \lambda_i \ln \varepsilon_{ij} + \frac{1}{6N} \sum_{i\,j}^{6\,N} \lambda_i \ln \varepsilon_{ij} \qquad [4.6]$$

Many of the terms (including those elements containing T) have been cancelled out, leaving only elements containing emittance.

Now let:

$$l_i = \lambda_i / \sum_{i}^{6} \lambda_i \qquad [4.7]$$

and

$$e_{ij} = (\varepsilon_{ij})^{\,l_i} \qquad [4.8]$$

then

$$\frac{Y_{ij}}{\sum_{i}^{6} \lambda_i} = \ln e_{ij} - \frac{1}{6} \sum_{i}^{6} \ln e_{ij} - \frac{1}{N} \sum_{j}^{N} \ln e_{ij} + \frac{1}{6N} \sum_{i\,j}^{6\,N} \ln e_{ij} \qquad [4.9]$$

and so

$$\frac{Y_{ij}}{\sum_i^6 \lambda_i} = \ln\left[\frac{e_{ij} \cdot e_{6N}}{e_{iN} \cdot e_{6j}}\right] \qquad [4.10]$$

$$\exp\left[\frac{Y_{ij}}{\sum_i^6 \lambda_i}\right] = \frac{e_{ij} \cdot e_{6N}}{e_{iN} \cdot e_{6j}} = \text{Thermal Log Residual in band i and pixel j.} \qquad [4.11]$$

Thus an individual TLR contains some combination of emittance that is independent of the temperature component associated with the Wien equation. The calculated value of a TLR is due to emittance in an individual pixel at an individual wavelength, (eij), but also has components of emittance from the average emittance from the pixel, (e6j), the average emittance from an individual band, (eiN), and the average emittance over the whole scene, (e6N). This results in each TLR value not being purely a measure of emittance in that particular pixel and at a particular wavelength, but also containing contributions from other wavelengths and other pixels. The TLR method is therefore a scene dependent technique.

4.2.3 DISCUSSION

This method creates six bands of temperature independent coefficients, any 3 band combination of which provides a highly discriminatory image (Hook (1989), Hook *et al* (1990)). If TLR bands 1, 3 and 5 are displayed (in comparison to Decorrelation-stretch 1,3,5) the image provides an increment of discriminatory power over the D-stretch as has been noted by other workers, Hook *et al* (1990). This is because the temperature information has been eliminated from the TLR image whereas the D-stretch still contains residual, subdued temperature effects. The variation in the image is entirely due to emittance differences.

Interpretation of TLR in a spectral sense is possible despite the fact that a TLR spectrum has unwanted emittance components from other pixels present. This scene dependency creates an image spectrum that is not directly related to a laboratory emittance spectrum. However, a laboratory emittance spectrum may be transformed to a TLR spectrum. For a particular scene, the band mean (eiN), and the scene mean (e6N), are known, and using an individual laboratory spectrum one may calculate the pixel mean (e6j). Applying these means to the laboratory spectrum, using Equations

4.5 to 4.11, one may transform an emittance spectrum to an equivalent laboratory derived TLR spectrum. In this way it is possible to directly compare emittance information from both the scanner and the laboratory.

A disadvantage of this method of changing laboratory spectra to TLR spectra is that for each scene the factors used are derived from the scene itself and will therefore be different for each scene. Transforming a laboratory spectrum to a scene dependant TLR spectrum allows direct comparison of emittance information, but the exact transformation will be different for each case. This does not ease the task of interpreting the resulting spectra.

An evaluation and comparison of the TLR technique with other methods is discussed below with regard to a similar technique; the calculation of alpha coefficients.

4.2.4 CONCLUSIONS

1. The TLR method calculates temperature independent estimates of emittance.

2. A colour composite of TLR produces a highly discriminating image.

3. A TLR contains emittance information chiefly from the emittance of an individual pixel at a particular wavelength but also contains emittance information from adjacent pixels and adjacent bands.

4. Laboratory emittance spectra can be transformed to TLR spectra to allow direct comparison of emittance information derived from the scanner and the laboratory.

5. The transformation of laboratory emittance spectra to TLR will be scene dependant. Therefore, for each scene examined a new set of laboratory derived TLR spectra will have to be calculated if comparisons between the two data sets are to be made.

4.3 CALCULATION OF ALPHA COEFFICIENTS

The alpha method for calculating temperature independant spectra (alpha coefficients) was developed from the TLR method described in the previous section.

The alpha method calculates temperature independant spectra from multispectral TIR data that may be directly compared to laboratory data. The alpha coefficients may further be used to calculate emittance and temperature using information based on the characteristic behavior of laboratory thermal infrared emittance spectra.

The method for calculating alpha coefficients is given below. This method, developed during this research by the author, is a simplification of the TLR technique, as detailed in section 4.3.3.4.

It was originally intended to calculate the fundamental physical parameter emittance from the radiance received by the scanner. This technique is a compromise, where it is possible to calculate a new parameter alpha, α, from both scanner radiance measurements and from laboratory emittance measurements. Direct comparison of emittance information may then be made by the investigation of alpha spectra derived from both scanner and laboratory instruments.

4.3.1 ASSUMPTIONS

1. The data have been calibrated and atmospherically corrected.

2. It is assumed that Wien's law is a valid approximation to the Planck function.

4.3.2 METHODOLOGY FOR THE CALCULATION OF ALPHA COEFFICIENTS.

As stated above, it is valid to assume that Wien's law is a valid approximation to the Planck function for typical terrestrial temperatures and thermal infrared wavelengths. The following method is given specifically with respect to the TIMS but may be modified to other scanner configurations. Initially the methodology follows the TLR method given in section 4.2.

The Planck function for a single pixel is;

$$L_i = \frac{\varepsilon_i C_1}{\lambda_i 5\left[e^{(C_2/\lambda_i T)} - 1\right]} \qquad [4.12]$$

which may be approximated to Wien's law;

$$L_i = \frac{\varepsilon_i C_1}{\lambda_i 5\left[e^{(C_2/\lambda_i T)}\right]} \qquad [4.13]$$

where:

i = band number (from 1 to 6 for TIMS).

L_i = radiance in the i^{th} band.

ε_i = emittance in the i^{th} band.

λ_i = wavelength value in i^{th} band.

C_1 = first radiation constant/π

C_2 = second radiation constant

T = temperature of the pixel.

Taking natural logarithms of the Wien approximation;

$$\ln L_i = \ln \varepsilon_i + \ln C_1 - 5\ln \lambda_i - \frac{C_2}{\lambda_i T} \qquad [4.14]$$

and multiplying each equation by λ_i.

$$\lambda_i \ln L_i = \lambda_i \ln \varepsilon_i + \lambda_i \ln C_1 - 5\lambda_i \ln \lambda_i - \frac{C_2}{T} \qquad [4.15]$$

isolates the element of the equation that contains the temperature term from the variables in the equation.

Calculate the mean of the equation set for i = 1,6.

$$\frac{1}{6}\sum_{1}^{6} \lambda_i \ln L_i = \frac{1}{6}\sum_{i}^{6} \lambda_i \ln \varepsilon_i + \frac{\ln C_1}{6}\sum_{i}^{6} \lambda_i - \frac{5}{6}\sum_{i}^{6} \lambda_i \ln \lambda_i - \frac{C_2}{T} \qquad [4.16]$$

The element containing the temperature term has no summation sign associated with it because it is invariant over the six equations.
Now take [4.15] - [4.16]

$$\lambda_i \ln L_i - \frac{1}{6}\sum_{i}^{6} \lambda_i \ln L_i = \lambda_i \ln \varepsilon_i + \lambda_i \ln C_1 - 5\lambda_i \ln \lambda_i$$

$$- \frac{1}{6}\sum_{i}^{6} \lambda_i \ln \varepsilon_i - \frac{\ln C_1}{6}\sum_{i}^{6} \lambda_i + \frac{5}{6}\sum_{i}^{6} \lambda_i \ln \lambda_i \quad . \qquad [4.17]$$

Equation [4.17] now has no T term, as it has been cancelled out.

For six TIMS bands there will be six similar equations.

Rearrange the equation set of [4.17] so that elements containing unknowns are put to the LHS:

$$\lambda_i \ln \varepsilon_i - \frac{1}{6}\sum_{i}^{6} \lambda_i \ln \varepsilon_i = \lambda_i \ln L_i - \frac{1}{6}\sum_{i}^{6} \lambda_i \ln L_i + C_i \qquad [4.18]$$

where;

$$C_i = - \lambda_i \ln C_1 + 5\lambda_i \ln \lambda_i + \frac{\ln C_1}{6}\sum_{i}^{6} \lambda_i - \frac{5}{6}\sum_{i}^{6} \lambda_i \ln \lambda_i$$

C_i contains values that are related to wavelength and constants only, and are independent of pixel values. C_i may thus be calculated and assigned six values.
Defining a new parameter, α_i,

$$\lambda_i \ln \varepsilon_i - \frac{1}{6}\sum_{i}^{6} \lambda_i \ln \varepsilon_i = \alpha_i = \lambda_i \ln L_i - \frac{1}{6}\sum_{i}^{6} \lambda_i \ln L_i + C_i \qquad [4.19]$$

The set of six values of alpha can be calculated, using the RHS of Equation [4.19] from the scanner radiance. These alpha spectra are temperature independent, (containing no T term).

Using laboratory derived emittance spectra, it is possible, using the LHS of Equation [4.19] to calculate αi. Thus direct comparison of scanner alpha spectra to laboratory alpha spectra is possible.

4.3.3 DISCUSSION

4.3.3.1 CHARACTERISTICS OF ALPHA SPECTRA

An alpha spectrum, Figure 4.1, will provide information on the shape of the emittance spectrum but, since an alpha spectrum will have values about zero, no information is present on the mean.

Figure 4.1 shows an emittance spectrum and its corresponding alpha spectrum. Although their absolute values are different, the shape is qualitatively the same. The similarity of shape is due to the values of wavelength and emittance that are under consideration;

for $8 < \lambda_i < 12 \qquad \lambda_i \equiv \lambda_{10}$

and

for $0.7 < \varepsilon_i < 1.0, \quad \ln\varepsilon_i \sim \varepsilon_i - 1$

thus

$$\lambda_i \ln\varepsilon_i \sim \varepsilon_i - 1 \qquad [4.20]$$

The general shape of the spectral curve displayed by an emittance spectrum will be reproduced in the alpha spectrum. As has been previously stated, the solution of the Planck function to emittance is impossible without simplification, or addition of extra information to solve the underdetermined problem. This transformation has not solved the problem but transformed the unknown element of information to a least significant parameter; the mean. The main difference between emittance spectra and alpha spectra is not in shape displayed but in the lack of information on the mean of alpha spectra since all alpha spectra will have a mean value of zero.

The transform still leaves the equation set underdetermined. This is illustrated in Figure 4.2 where it can be seen that whilst one emittance spectrum will produce a unique alpha spectrum, the converse is not true. One alpha spectrum can generate a suite of emittance spectra all of similar shape but varying in mean value. These emittance curves vary in their mean values and also are slightly different in their shape. A subtle change in signature is evident due to the fact that the approximations of [4.20] are not exact.

The alpha coefficients make it possible to obtain temperature independent spectra whose shapes can be compared directly to equivalent laboratory data. The position and depth of minima of an emittance curve at the spectral resolution of the TIMS are diagnostic of particular lithological groupings. Although no mean value is known (and so emittance cannot be calculated), it is believed that alpha spectra contain sufficient spectral information to discriminate surface lithologies. This method has confined the unknown element of information in the underdetermined data set (the mean) to the least important parameter for lithological discrimination.

The calculation of alpha coefficients for a TIMS data set from Halls Creek are used in Chapter 5 in order to calculate emittance from the radiance data.

4.3.3.2 ERRORS DUE TO ASSUMPTIONS

The errors involved in calculating alpha coefficients result from the initial assumptions used.

1. Assuming atmospheric correction of the data set is perfect, there will be no error. However the exact modelling of the atmospheric profile for the majority of data sets will not be possible, thus an error associated with residual atmospheric artifacts will, in general, exist. The magnitude of the error is entirely dependent upon the accuracy of atmospheric correction used. The problems associated with atmospheric correction is discussed in Chapter 5 with regard to the correction of Halls Creek data.

2. Assuming Wien's law to be valid will produce an error of approximately 1% for typical terrestrial temperatures and TIR wavelengths (Swain and Davis 1978). This error has been discussed earlier with regard to the TLR method, and is illustrated in Table 4.1. The magnitude of the error for alpha coefficients associated with the use of the Wien law is illustrated in Table 4.2. For a quartz spectrum at 300K, radiances were calculated using the Planck function and the Wien approximation. Using these

radiances, the alpha coefficients in Table 4.2 were calculated. The difference is greater at longer wavelengths as the Wien approximation diverges more significantly from the Planck function as the product of wavelength and temperature is greater.

4.3.3.3 THE NEED FOR A MEAN VALUE

The alpha coefficients provide a direct means of comparing the shape of spectra derived from scanner and laboratory data. However they do not provide information on mean values of the basic physical parameter emittance. A study of emittance spectra for rocks and minerals reveals that the diagnostic information useful for lithological identification is contained within curve shape (EOSAT 1986).

Theoretically, there may be cases where two surface types have similar shaped emittance spectra but different means. For instance, greybodies of $\varepsilon = 0.98$ (for vegetation, Figure 5.16) and $\varepsilon = 0.5$ (for a tin roof) would produce similar alpha coefficients and would thus be indistinguishable. Such a situation is not a common occurrence for the vast majority of surface cover types found in the exploration environment. Although information on the absolute value of emittance is desired it is not of critical importance for identification.

4.3.3.4 COMPARISON TO THERMAL LOG RESIDUALS.

From the preceding text it can be seen that Equation [4.11] is

$$\exp\left[\frac{Y_{ij}}{\sum_i^6 \lambda_i}\right] = \frac{e_{ij} \cdot e_{6N}}{e_{iN} \cdot e_{6j}}$$

and from the derivation of alpha coefficients [4.19] that;

$$\lambda_i \ln \varepsilon_i - \frac{1}{6}\sum_i^6 \lambda_i \ln \varepsilon_i = \alpha_i = \lambda_i \ln L_i - \frac{1}{6}\sum_i^6 \lambda_i \ln L_i + C_i$$

Essentially the difference in methods stems from the subtraction of band means (eiN), and the addition of a scene mean (e6N), in the derivation of TLR. Alpha coefficients are thus a simplification of the TLR method containing only information from a single pixel rather than pixels from the scene. This simplification means that the alpha coefficient method is scene independent. The TLR has factors relating to

band mean and scene mean and so emittance in other areas effects the values in a particular pixel, making the TLR scene dependent. A further advantage that alpha coefficients have over TLR is that in the transformation of laboratory emittance spectra to alpha spectra the qualitative shape of the spectra is maintained and is scene independent, whereas the transformation to TLR will change from scene to scene, and the shape of the TLR spectrum may not approximate that of the original emittance spectra.

Upon scaling to byte data (range 0-255 for common data display systems) the TLR data look qualitatively similar to alpha coefficients. This is because the difference between the two techniques is the change in values due to the multiplicative factors e6N and eiN. The effect of scaling to byte for display is to impose new factors on the data from both techniques. This causes the data to have the same values. Thus alpha coefficients when scaled for display become equivalent to scaled TLR. The similarity between TLR and alpha images has been shown in Hook *et al* (1990).

4.3.4 CONCLUSIONS

1. The alpha technique allows the calculation of temperature independent spectra from scanner data that may be directly compared to laboratory data.

2. Alpha coefficients contain information on the shape of an emittance spectrum without providing information on the absolute values.

3. Alpha coefficients are scene independent.

4. The alpha method is a simplification of the TLR method.

5. When scaling alpha coefficients for display, the images produced will be similar to a TLR image.

6. The errors associated with this technique are due to two factors, the accuracy of the atmospheric correction, and also the use of the Wien law.

7. The alpha coefficients provide no estimate of temperature.

4.4 METHODOLOGY FOR THE CALCULATION OF EMITTANCE AND TEMPERATURE USING ALPHA COEFFICIENTS

This method utilises the alpha spectra calculation described in the previous Section (Section 4.3) and a knowledge of the behaviour of thermal infrared spectra to derive estimates of emittance and temperature.

Emittance and temperature are calculated using the alpha spectral values and an empirically derived relationship between means and variances of laboratory emittance spectra.

4.4.1 ASSUMPTIONS

1. The data have been calibrated and atmospherically corrected.

2. Wien's approximation is valid.

3. A relation exists between the mean and the variability of emittance spectra.

4.4.2 METHODOLOGY

Initially the method follows the derivation of alpha spectra:

$$\lambda_i \ln \varepsilon_i - \frac{1}{6}\sum_{i}^{6} \lambda_i \ln \varepsilon_i = \alpha_i = \lambda_i \ln L_i - \frac{1}{6}\sum_{i}^{6} \lambda_i \ln L_i + C_i \qquad [4.21]$$

rearranging the LHS of Equation 4.21 such that;

$$\varepsilon_i = \exp\left[\frac{\alpha_i + \frac{1}{6}\sum_{i}^{6} \lambda_i \ln \varepsilon_i}{\lambda_i}\right] \qquad [4.22]$$

does not allow the emittance to be calculated because the value of the mean (the mean of the wavelength weighted log emittance in Equation 4.22) is not known. It is the lack of an estimate of this mean value which indicates that the equation set remains underdetermined.

An estimate of this mean value may be made by considering the behaviour of Thermal Infrared spectra for commonly occurring rocks and minerals. Observation of emittance spectra shows that in general, emittance spectra with high mean values exhibit little variation, while those spectra that exhibit a greater variation have lower means. Figure 3.5a shows the spectral characteristics of several different materials.

The TIR spectra of a suite of igneous rocks from Salisbury *et al* (1988), were transformed to TIMS equivalent spectra. This was achieved by convolution of laboratory emittance spectra with the appropriate response functions for the TIMS similar to the method used for the calibration of TIMS described in Chapter 5 (Section 5.1.2) and described with respect to Halls Creek TIMS data). Once a 6-pointed TIMS-equivalent emittance spectrum has been calculated, as for example in Figure 4.1, the alpha spectrum can be calculated using the LHS of Equation [4.21]. The variance of alpha coefficients and the mean (in Equation [4.22]), are then calculated. Figure 4.3 shows a plot of mean and variance for rocks taken from Salisbury *et al* (1988). A best fit curve for this data was obtained by a least squares solution applied by the Applied Statistics Group at CSIRO in Perth.

The calibration curve is used to obtain a relationship between mean and variance. For Salisbury *et al* (1988) data the best fitting curve was found to be of the form;

$$\frac{1}{6}\sum_{i}^{6} \lambda_i \ln \varepsilon_i = \frac{-1}{0.3145} + \frac{1}{0.3145 + \sigma^2_{\alpha_i}} \qquad [4.23]$$

where;

$\frac{1}{6}\sum_{i}^{6} \lambda_i \ln \varepsilon_i$ = mean term in Equations 4.22 and 4.23

$\sigma^2_{\alpha_i}$ = variance of α_i

The variance calculated from individual TIMS pixels can, using Equation 4.23, estimate a value of the mean which in turn is used to calculate emittance using Equation 4.22. Once emittance is known, a single temperature may be calculated by rearranging the Wien law to solve for temperature.

The estimated emittance in conjunction with the radiance from each band can be used to calculate a temperature. This will be the same for all bands using the Wien approximation. The estimated emittances are a set of emittances that may all be calculated from one value of temperature, and so there will be no variance in temperature values over the six TIMS bands.

It is the assumption that all lithologies will behave according to the relationship in Equation 4.23 that allows the underdetermined system of equations to be solved. Where lithologies have variances and means that do not conform to this equation, the predicted mean will be in error. This error causes the emittance spectra to be under or over estimated by a similar amount in each band. Whilst the absolute values, in some cases, will be in error the shape of the emittance spectra will be preserved.

This method allows emittance and temperature to be calculated. Its application to Halls Creek TIMS data is discussed in Chapter 5.

4.4.3 DISCUSSION

4.4.3.1 ERROR DUE TO ASSUMPTIONS.

The assumptions used will be a possible source of error.

1. The atmospheric correction. Any residual effects that are present in the scanner data will be evident in the alpha coefficients. Thus any calculation of variance will be in error if atmospheric artifacts remain in data. The resulting estimate of mean from the variance will be incorrect as will subsequently derived emittance and temperature values. It is imperative therefore, that this method is only applied to corrected data that contains no atmospheric artifacts if the results are to be generally applicable.

2. The Wien approximation. As stated above, this approximation creates a small error of approximately 1% in the alpha coefficients which will not cause significant error in mean estimation. The temperature is calculated using the approximation to estimate a "Wien temperature". This "Wien temperature" will have error associated with it due to the approximation but the temperature is not of primary importance for geological applications.

3. The use of the calibration curve. Where lithologies do not behave according to the relationship expressed in Equation 4.23 there will be an error in the emittance estimation. The magnitude of the error is discussed below.

4.4.3.2 CHARACTERISTICS OF THE MEAN VARIANCE CURVE

Figure 4.3 shows the curve fitted to Salisbury *et al* (1988) data for a suite of igneous rocks. The curve goes through 0,0 (a blackbody). The mean calculated is the mean of the wavelength weighted log emittance which is the desired quantity in Equation [4.22]. The variance is the variance of the alpha coefficients, which is directly obtainable from the scanner data. Thus the equation provides a direct link between the desired quantity and a readily obtainable parameter. Both of these expressions are independent of the temperature variable.

The values of mean and variance are derived from each 6 pointed TIMS equivalent laboratory emittance spectrum, thus the values are specific to the TIMS scanner, different values of mean and variance are possible if these values were calculated for a continuous spectrum rather than 6 points. Since TIMS scanner response functions change slightly with flight campaign (Palluconi and Meeks 1985) the exact value of variance and mean may vary slightly. The calibration curve produced here is specific to the TIMS for the Salisbury *et al* (1988) data and for the US/Australia Joint Scanner Campaign of 1985.

There are several factors involved in calculating the equation of the curve that in turn may affect the coefficients of the equation.

1. The accuracy of individual variance and mean measurements.

Each spectra is the average of 255 individual measurements, such that the emittance values calculated for each wavelength are very precise. The precision of the emittance values is increased further when the continuous lab spectra are convolved to 6 discrete values for comparison to the TIMS data.

2. Rock types used.

The curve is calculated using Salisbury's data for the fresh sawn surface of an igneous rock suite. Such surfaces are not representative of the surfaces encountered in the natural environment. If TIR laboratory spectra were available that were representative

of the spectra from a particular scene it would be possible to calculate the mean and variance for these spectra, and to fit a curve to that data set. In this way terrain specific curves for particular flight campaigns can be calculated. Using the weathered surface for a suite of representative lithologies collected from Halls Creek, the curve still fits the data well (see Section 5.2.2.6 and Figure 5.11). This suggests that the curve calculated using Salisbury's data is generally applicable.

3. The variability about the curve.

With any curve fitting technique there will be data points that plot away from the curve. In Figure 4.4 for example, if the rock whose spectrum produces the point X, Y is found within the scene, the curve would predict a mean of -3.0 whereas the correct value would be mean = -2. The resulting emittance spectrum is shown in Figure 4.6b. The magnitude of error that may commonly be expected for lithologies representative of Halls Creek are discussed in Section 5.2.2.6. Temperature values calculated from the data will be in error when a lithology does not conform to the relationship of Equation 4.23. Analysis of the temperature image may indicate areas which exhibit anomalous temperature values. These areas may reflect genuine variations within the scene or may indicate areas where the lithologies do not behave according to the assumption.

The purpose of the curve is to use extra information on individual pixel characteristics to provide a variable estimate of the unknown property, namely the mean. This is required for the direct solution of the equation set. Any mean will create a set of emittance which will produce one value of temperature. There will be no variance in temperature calculated over each band since these sets of emittance are from a possible correct set.

The error in emittance values resulting from a rock type plotting away from the curve does not render the resulting spectrum uninterpretable, as the spectra will maintain the shape critical for interpretation in a physical sense with respect to composition.

4.4.3.3 COMPARISON OF ALPHA COEFFICIENTS TO ALPHA DERIVED EMITTANCE METHODS

The alpha coefficients calculate temperature independent spectra but do not estimate emittance. The Alpha Derived Emittance method uses a curve to estimate a parameter (the mean) and thus calculates the emittance. The advantage in using alpha coefficients is that the coefficients do not use assumptions that may result in errors. They are calculated assuming that the data is corrected and that Wien's approximation is true. In contrast the emittance calculated using the curve is potentially in error if a particular lithology does not have a mean and variance that lies on the curve. The disadvantage of alpha coefficients is that emittance is not calculated, nor is a measure of temperature. Using the curve to calculate emittance provides the user with the basic physical parameter of geological significance and a quantitative measure of temperature which may be used to indicate errors in emittance estimates.

4.4.4 CONCLUSIONS

1. Emittance and temperature can be calculated using the alpha coefficients and TIR laboratory spectra.

2. Errors in the mean calculated from the equation of the curve will principally affect the mean value of emittance spectra which is a least significant factor for lithological identification.

3. Variations in the temperature image may indicate areas where the calculated emittance may be wrong.

4. The equation of the calibration curve is terrain specific.

5. The atmospheric correction is of critical importance for this method.

4.5 SUMMARY

The Thermal Log Residual (TLR) technique was developed to produce temperature independent indices relating to emittance variations in the radiance signal. The algorithm is an overly complicated method for cancelling the temperature component of the radiance. In addition the TLR method creates scene dependant residuals. The calculation of alpha coefficients is similar to the approach used to calculate TLR but is simpler and produces scene independent coefficients. The TLR technique is therefore made redundant by the alpha calculation.

The alpha coefficients, whilst generating temperature independent estimates of the variation in emittance, do not calculate emittance itself. Combining the alpha coefficients with the use of the mean variance curve allows emittance to be estimated. This method produces six emittance images free from the obvious noise problems inherent in the calculation of the Model Emittance and Maximum Temperature images. The emittance estimation technique using alpha coefficients is discussed in relation to other emittance estimating methods for a data set from Halls Creek TIMS data in Chapter 5.

Figure 4.1 Plots of the emittance spectrum of quartz and its corresponding alpha coefficients.

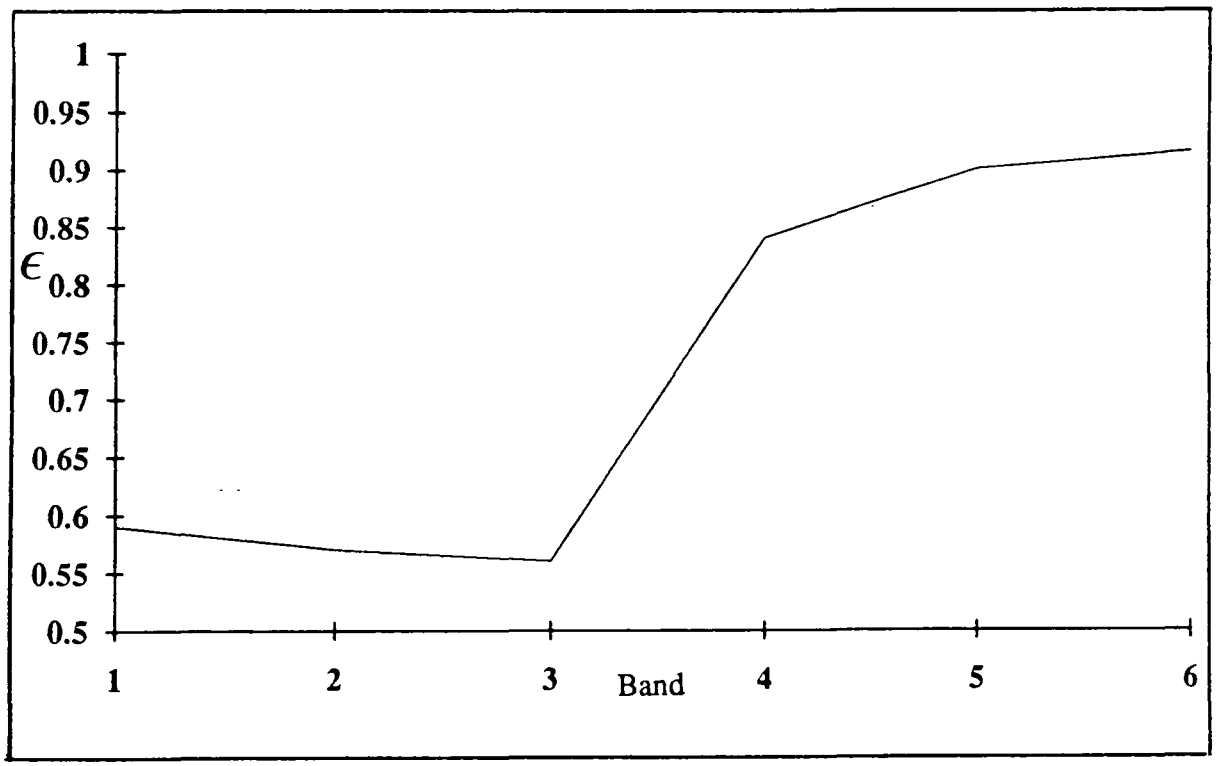

4.1a Emittance spectrum.

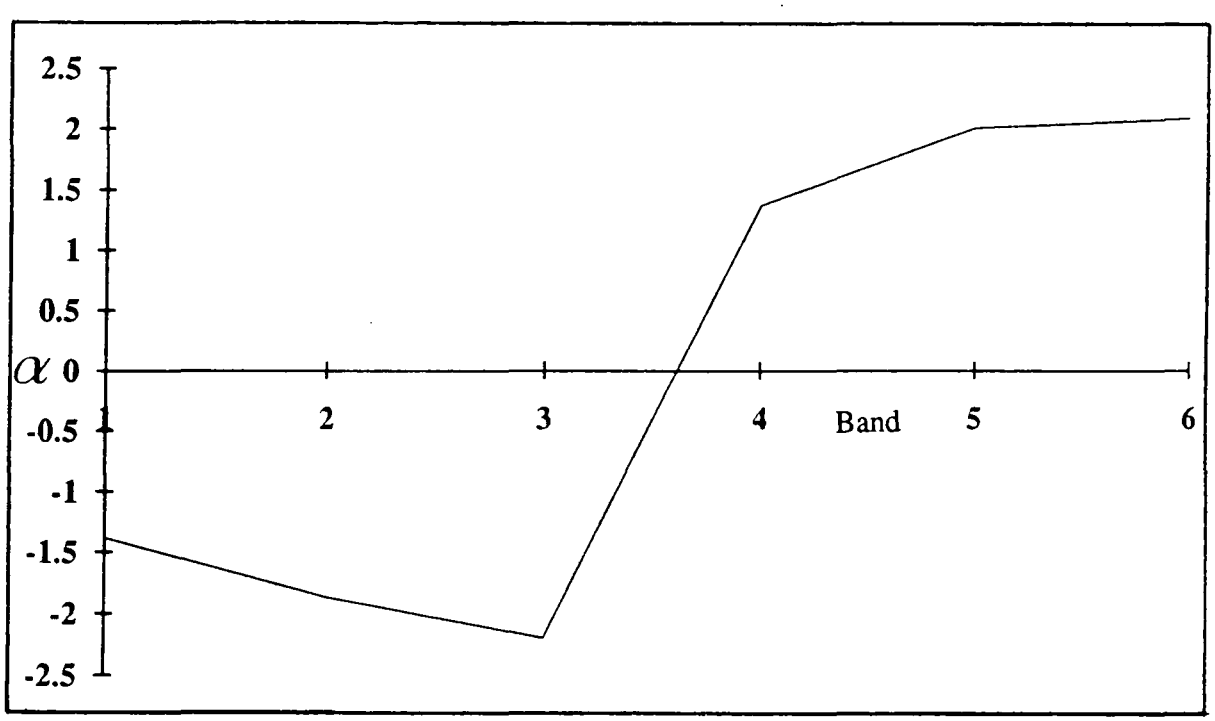

4.1b Alpha coefficient spectrum for quartz.

Figure 4.2 Plot of alpha coefficient spectrum for quartz and the suite of emittance spectra that may be generated from them.

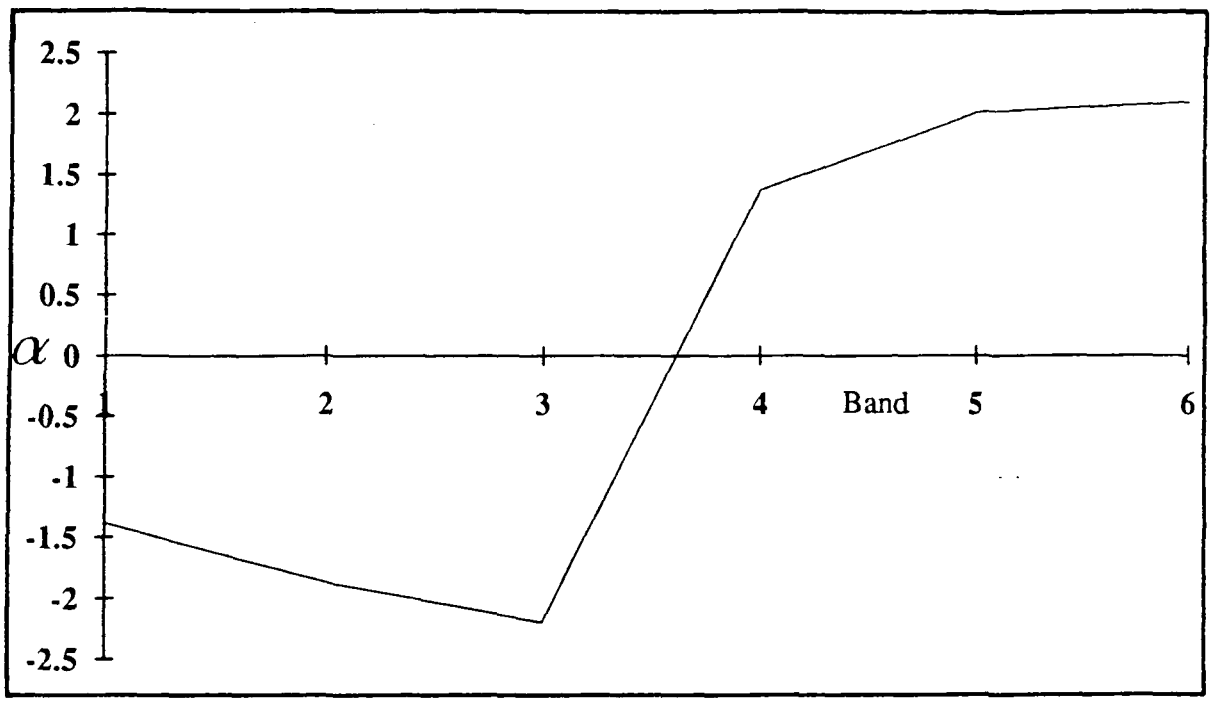

4.2a Alpha coefficients for quartz.

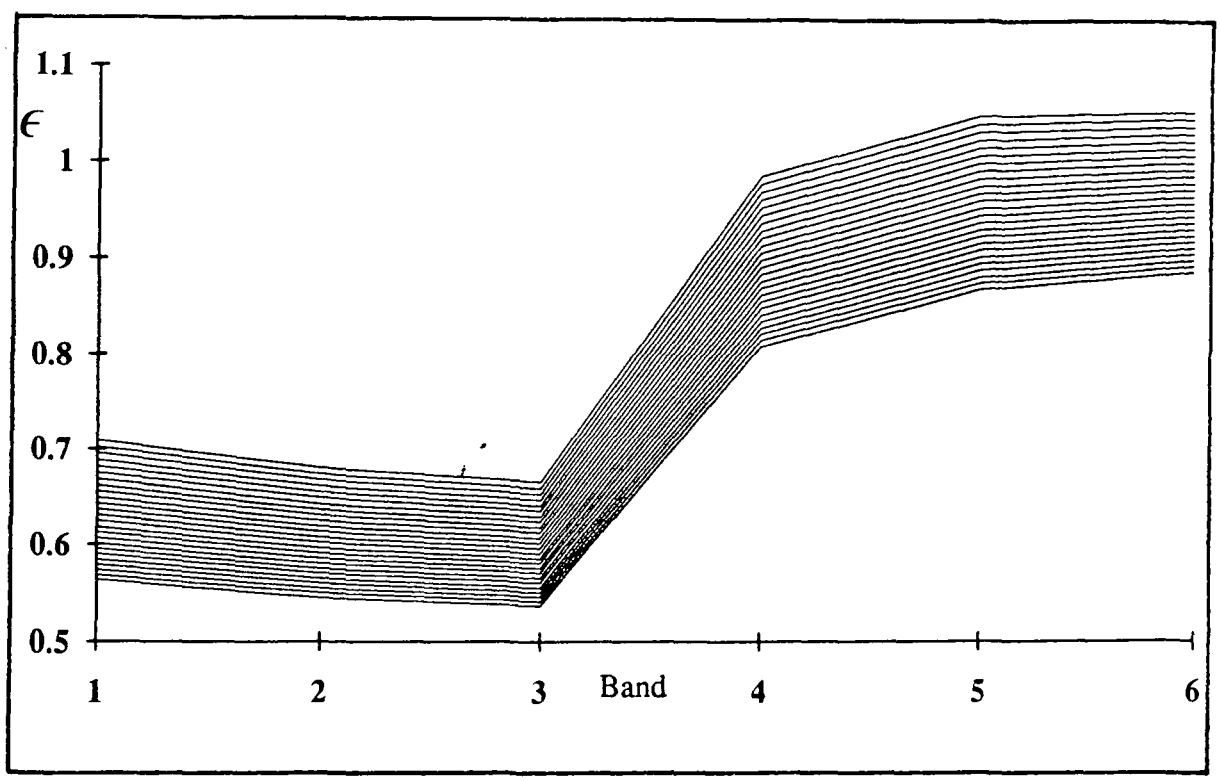

4.2b Emittance spectra generated from alpha coefficients in 4.2a.

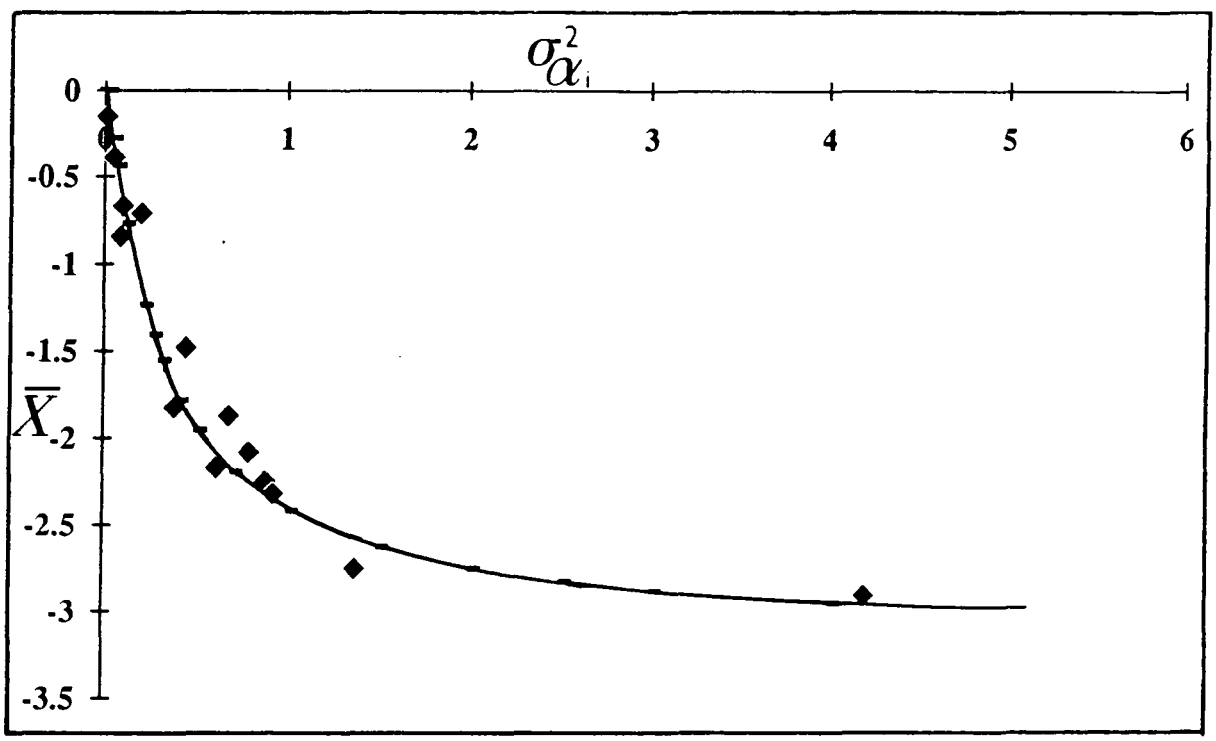

Figure 4.3 Mean variance plot calculated for Salisbury *et al*(1988) data, showing the best fit curve.

Figure 4.4 Graphs to show the magnitude of error due to differences in the estimated mean value.

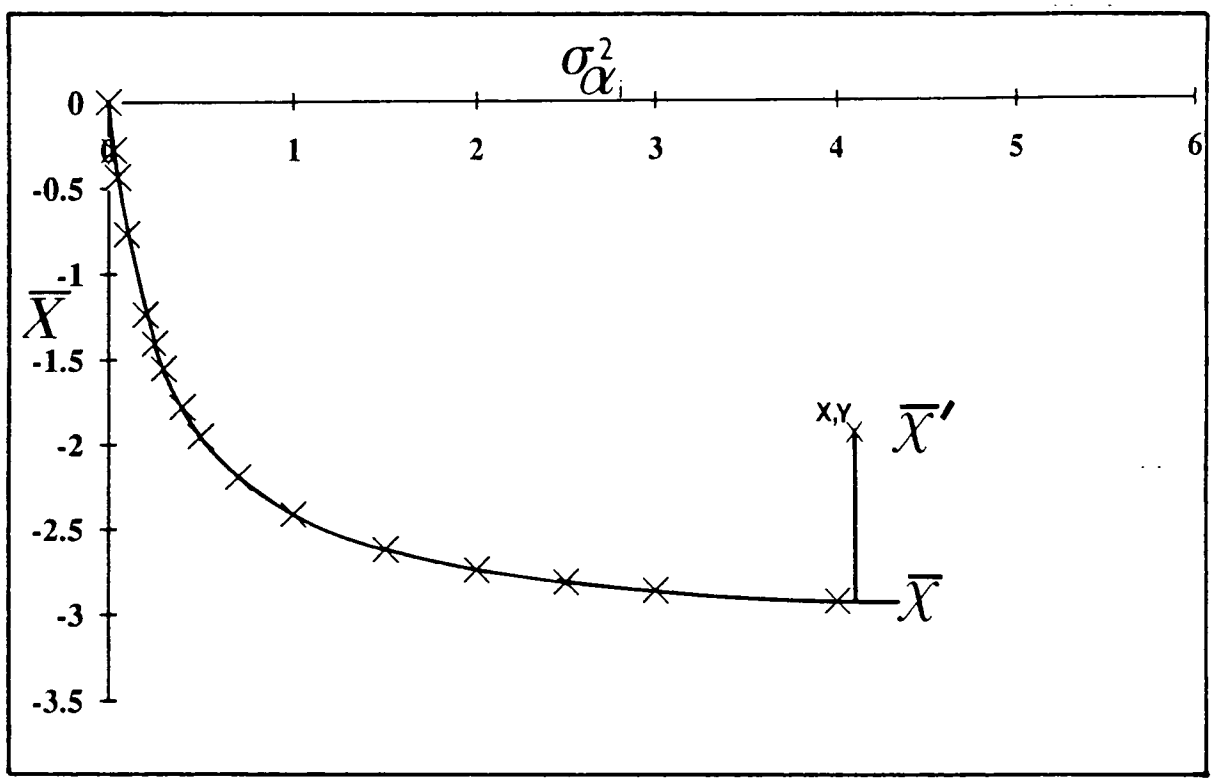

4.4a Best fit curve from Figure 4.3 showing a change in mean from -3 to -2.

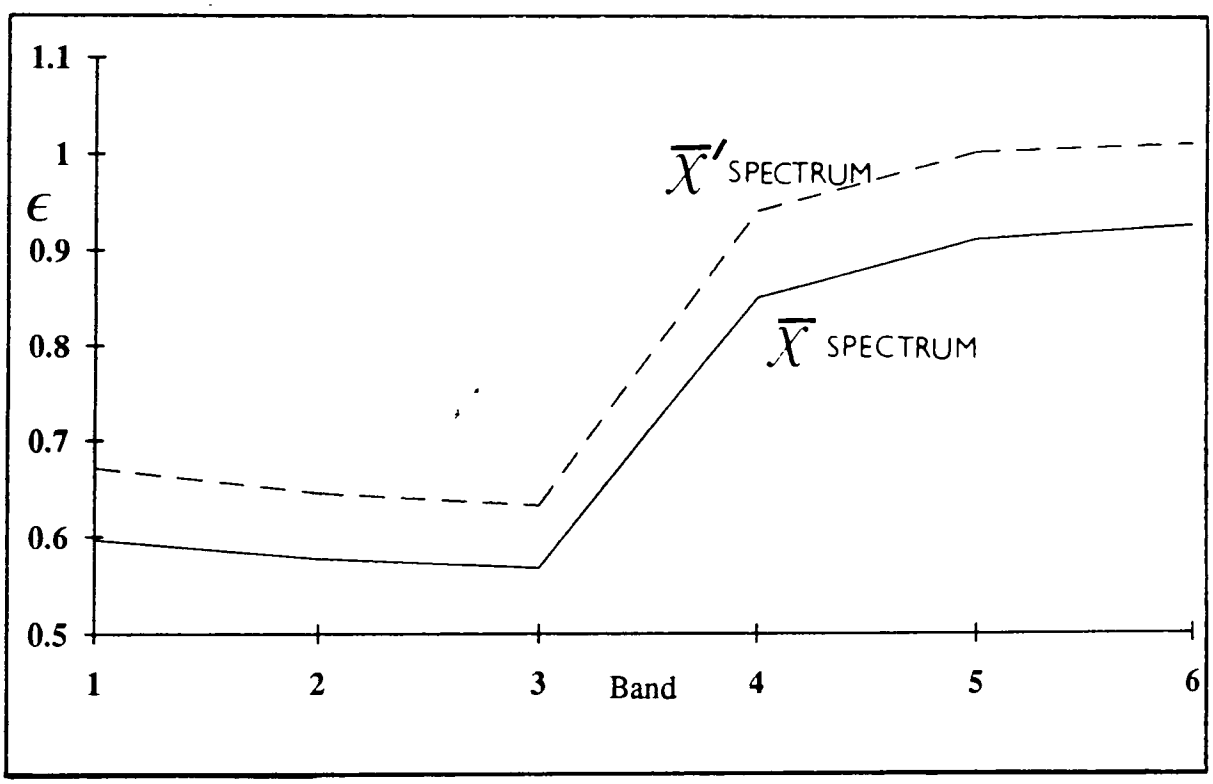

4.4b Resultant emittance spectra showing similar shape but exhibiting a change in mean value.

BAND NUMBER	RADIANCE OF QUARTZ USING WIEN APPROXIMATION	RADIANCE OF QUARTZ USING PLANCK FUNCTION
1	5617.9	5638.1
2	5543.5	5568.4
3	5503.1	5532.4
4	8273.3	8340.6
5	8742.9	8831.9
6	8413.1	8541.4

Table 4.1 Table showing the change in radiance values resulting from calculating radiance from the emittance and temperature of a quartz spectrum at 300K using the Planck function and the Wien approximation.
Radiances are in mW m^{-2} μm^{-1} sr^{-1}.

BAND NUMBER	ALPHA COEFFICIENTS USING WIEN APPROXIMATION	ALPHA COEFFICIENTS USING PLANCK FUNCTION
1	-1.38	-1.34
2	-1.87	-1.84
3	-2.2	-2.17
4	1.37	1.37
5	2.01	1.98
6	2.09	2

Table 4.2 Table to show the change in alpha coefficient values caused by using the Planck function and the Wien approximation. Emittances were calculated from radiances equivalent to quartz at 300K using the Planck function and the Wien approximation. Alpha coefficients were calculated from these emittances.

CHAPTER 5

A COMPARISON OF METHODS FOR ESTIMATING EMITTANCE AND TEMPERATURE USING TIMS DATA FROM HALLS CREEK, W.A.

This Chapter describes the methodology for the calibration and atmospheric correction of data collected by the TIMS scanner. The application of this methodology to a TIMS data set acquired as part of the US/Australia Joint Scanner Project conducted in October 1985 is then discussed. The TIMS data covered an area 20 km NE of Halls Creek, a township in the Kimberley region of Western Australia. A summary of the physiographic and geologic setting of the Halls Creek study area is given. This is followed by an analysis of the laboratory Thermal InfraRed (TIR) emittance spectra obtained from lithologies collected from Halls Creek. The application of each of the emittance estimating algorithms with respect to the TIMS data for Halls Creek is given. A detailed analysis to delineate boundaries within the test area is not made, rather emphasis is placed on the quantitative analysis of spectra from each of the Model Emittance, Maximum Temperature, and Alpha Derived Emittance techniques.

5.1 CORRECTION TO GROUND RADIANCE

5.1.1 AIM

The aim of this Section is to describe the methodology used to correct the raw TIMS data to the radiance emitted from the a pixel on the ground.

The calibration of the TIMS to radiance units is discussed and then the problem of atmospheric correction, as it relates to the TIMS scene from Halls Creek in Western Australia is addressed.

5.1.2 CALIBRATION TO PHYSICAL UNITS

The TIMS is a six channel thermal infrared spectrometer that measures the spectral radiance ($mW.m^{-2}.\mu m^{-1}.sr^{-1}$) of whatever is within its field of view. Internal reference sources enable the calibration of the spectral response to be independent of the instrument's characteristics. The method employed to calibrate the data is given below and is taken from Palluconi and Meeks (1985).

Calibration of the TIMS data to spectral radiance requires the derivation of calibration values for each scanline. These values are determined using the blackbody temperature and blackbody reference source values. Prior to recording the radiation from the surface of each scanline, the TIMS looks at two inbuilt blackbodies set at the minimum and maximum temperature thought to be encountered on the ground surface. These are referred to as the blackbody 1 and 2 reference source values and are recorded in the header information for the appropriate scanline together with the actual temperature of the blackbodies. These values are used to derive the calibration values to convert the digital numbers to spectral radiance.

5.1.2.1 DEFINITIONS

T_1 = Low reference source temperature (K)
T_2 = High reference source temperature (K)
DN_1= Low reference source data number
DN_2= High reference source data number
R_1 = Low reference source spectral radiance
R_2 = High reference source spectral radiance
DN_x,R_x = Data number and spectral radiance values respectively for any sample x on the same scanline as the reference source values.
$s(\lambda)_i$ = relative response of band i
$P(\lambda,T)$ = Plank function for a blackbody.

The TIMS is designed such that the output Data Number (DN) values are linearly related to the input radiance;

$$R_x = A + B(DN_x) \qquad [5.1]$$

The two internal reference sources can be used to determine the constants A and B relating spectral radiance to DN values for any given scanline by ;

$$R_1 = \frac{\int_\lambda P(\lambda,T_1) \,.\, S(\lambda)_i \, d\lambda}{\int_\lambda S(\lambda)_i \, d\lambda} \qquad [5.2]$$

$$R_2 = \frac{\int_\lambda P(\lambda,T_2) \,.\, S(\lambda)_i \, d\lambda}{\int_\lambda S(\lambda)_i \, d\lambda} \qquad [5.3]$$

where;

$$P(\lambda,T_j)=\frac{\varepsilon_i C_1}{\lambda_i^5\left[e^{(C_2/\lambda_i T_j)}-1\right]}$$

and

i = Band number (from 1 to 6 for TIMS).

L_i = Radiance in the i^{th} band in pixel j.

ε_i = Emittance in the i^{th} band.

λ_i = wavelength value in i^{th} band.

C_1 = first radiation constant/π.

C_2 = second radiation constant.

T_j = temperature of the j^{th} pixel.

for each of the six spectral bands. Given R_1 and R_2, R_x in Equation [5.1] can be solved using A and B where;

$$A = \frac{R_2D_1 - R_1D_2}{D_1 - D_2} \qquad [5.4]$$

$$B = \frac{R_1 - R_2}{D_1 - D_2} \qquad [5.5]$$

Equation 5.1 can be applied band by band and scan line by scan line to solve R_x from DN_x. R_x is then in physical units $mW.m^{-2}.\mu m^{-1}.sr^{-1}$ and is to first order independent of the TIMS at the time of measurement, Palluconi and Meeks (1985).

5.1.3 ATMOSPHERIC CORRECTION

Calibrated TIMS radiance data is a result of the radiance emitted by the ground and the interaction of the emitted energy with the atmosphere. The causes and effects of the atmosphere in the thermal infrared are reviewed in Wolfe and Zissis (1987). These effects are considered to include additive, atmospheric emission and scattering terms, and a multiplicative, transmittance term, Kahle *et al* (1980). Figure 5.1 illustrates the sources of these contributions to the total signal received by the scanner. Kahle *et al* (1980) gives a simplified model for these interactions;

$$L_i = [\varepsilon_i \, . \, P(\lambda,T) + (1 - \varepsilon_i) L_{skyi}] \, \tau_{Ai} + L_{vi} \qquad [5.6]$$

where:

L_i = Radiance received by the scanner in band i

ε_i = Spectral emittance.

$P(\lambda,T)$ = Planck function for a blackbody.

L_{skyi} = Spectral radiance incident upon the surface from the atmosphere in band i.

τ_{Ai} = Spectral atmospheric transmissivity for band i.

L_{vi} = Spectral radiance from atmospheric emission and scattering that reaches the sensor in band i.

The emittance and blackbody radiance term is the element we wish to solve for.

To obtain the necessary atmospheric factors the atmospheric modelling program LOWTRAN6 (Kneizys *et al* (1983)) developed by the U.S. Air Force Geophysics Laboratory was used.

5.1.3.1 THE LOWTRAN MODEL

The LOWTRAN model calculates atmospheric transmittance and radiance averaged over $20cm^{-1}$ intervals in steps of $5cm^{-1}$ from 0.25 to 28.5μm. The code contains representative standard atmospheric and aerosol models, but has the capability to use specific user defined atmospheric models from radiosonde data (Kneizys *et al* 1983). Using the LOWTRAN6 model installed on Jet Propulsion Laboratory, (JPL) VICAR software a user defined atmospheric profile, in conjunction with the U.S. standard midlatitude summer model was created. Ground measurements of pressure, temperature and humidity were available from Halls Creek on the flight date.

However the atmospheric profile used was obtained from Port Hedland, W.A., some 950km away from Halls Creek as this was the nearest available station. Figure 5.2 indicates the locations of the two townships. After consultation with Dr. A Scott from the W.A. Bureau of Meteorology, a complete profile was produced using all the available information. The atmospheric profile was interpolated from ground measurements at Halls Creek to the radiosonde data from Port Hedland, assuming an adiabatic atmosphere. This profile was then input into the LOWTRAN6 program.

The program "TIMSCAL2" on JPL VICAR software has been developed to use the LOWTRAN code specifically with TIMS data. This program calibrates the data using the TIMS response functions for the specified flight date and calculates the necessary atmospheric components with regard to the specifications of the TIMS band passes. The input parameters for the LOWTRAN code consist of radiosonde atmospheric data and other specific flight parameters. Annex A is an example of the input and output from the TIMSCAL2 program using the LOWTRAN model on the VICAR system. The output from LOWTRAN is in the form of nadir and off-nadir correction factors for transmittance, radiance and sky radiance that account for the variable amount of atmospheric component due to changes in scan angle of the instrument. Annex A shows the difference in correction factors with scan angle.

The LOWTRAN model, using the midlatitude summer ozone profile contains residual atmospheric effects due to errors in the default estimates of atmospheric ozone and water vapour. These residual artifacts are highlighted when one considers a vegetated area whose response should be a greybody where $\varepsilon = 0.98$. For the Halls Creek scene a vegetated areas response was found not to be that of a greybody. By varying the parameters responsible for the overestimation of the default values of water and ozone, the atmospheric correction may be adjusted such that the vegetated area's response is a greybody. This correction may then be applied to the whole scene.

The method of correcting for residual atmospheric effects by assuming a greybody response for a vegetated area has been used by Kahle *et al* (1988) for TIMS data over Hawaii following the method of R. S. Walker and A. R. Gabell (unpublished manuscript 1988). For Halls Creek, a site at the bend of a river was chosen as likely to offer a large area of vegetation with 100% cover. Subsequent fieldwork has shown this area to be a large dense stand of eucalyptus with an understorey of shrubs and leaf litter.

5.1.3.2 ERRORS IN THE ATMOSPHERIC CORRECTION OF THE TIMS DATA.

The Halls Creek data were atmospherically corrected using radiosonde data from Port Hedland and ground measurements at Halls Creek. The atmospheric profile from Port Hedland may not be valid for Halls Creek which is situated some 950km away inland. However, climatic conditions at the time suggest that the profile created would in general be valid (pers. comm., A. Scott 1989).

Residual effects due to incorrect default values in the LOWTRAN model were used as these values were not available from the radiosonde data. These residual effects were eliminated by "flat field correction" to a vegetated area of known spectral response. If this area were not 100% vegetated, the residual correction would be wrong. However fieldwork suggests the pixels used were effectively 100% vegetation.

The LOWTRAN atmospheric correction was applied to the data and subsequently modified to remove any observed structure in the TIMS emittance spectra of vegetation. This correction was made by varying the default values for ozone and water vapour in the LOWTRAN model. Assuming that the vegetation area is spectrally flat and that the user defined atmospheric profile parameters are correct, the application of this correction to the remainder of the scene should remove any residual artifacts.

If there are any errors in either of these assumptions then it is possible to introduce artifacts into the remainder of the scene.

5.1.4 CONCLUSIONS

1. A user defined atmospheric profile, when used in conjunction with the midlatitude summer ozone profile, from the LOWTRAN model contains residual atmospheric artifacts.

2. By applying a "flat field correction" such that a known vegetated area within these scene exhibits the expected response of a greybody, these residual effects can be removed from the data.

5.2 THE APPLICATION OF ALGORITHMS TO HALLS CREEK W. A.

This Section summarises the geological setting of Halls Creek W.A. and is followed by an analysis of the characteristics of the laboratory Thermal InfraRed (TIR) emittance spectra obtained from lithologies collected from Halls Creek. The application of each of the aforementioned algorithms with respect to Halls Creek is given firstly in a spatial, image sense and then on the basis of the spectral information contained within each technique.

5.2.1 THE PHYSIOGRAPHY AND GEOLOGY OF HALLS CREEK

The following description of the geology of the Halls Creek area is taken from the Gordon Downs 1:250,000 geological series compiled by I. Gemuts (1968). Additional information has also been compiled using the PNC Exploration Pty Ltd Sophie Downs Uranium Report (1986) and information gained during the course of fieldwork undertaken in October and November 1989.

5.2.1.1 SITUATION

TIMS data was collected for a flightline situated 20km NE of Halls Creek, which is in the East Kimberley District of Western Australia, (Figure 5.2). The Kimberley region is dominated by the Central Kimberley Basin and the Halls Creek Province flanking the basin.

5.2.1.2 GROUND

The physiography of the area of the flightline consists of rough irregular hills up to 300' high, or closely spaced dissected hogbacks which are rarely over 100' high. The drainage is closely spaced and structurally controlled. Steep sided ridges follow the regional N-N-E strike of the underlying rocks and are cut by small dendritic streams, controlled by joints and faults. Run-off is very fast, and there is little soil cover; the hills are covered by spinifex grass and stunted eucalyptus. Temperatures at the time of the November fieldwork were approximately 40-45°C.

5.2.1.3 STRATIGRAPHY

The stratigraphy is summarised below and a geological map of the area under the flightline is given in Figure 5.3 (redrawn from Gemuts 1968). The oldest rocks are Archean, consisting of tightly folded and regionally metamorphosed geosynclinal sediments, volcanic rocks, and igneous intrusives. They are intruded by Proterozoic gabbros and granites and overlain by gently folded Proterozoic sediments and volcanics.

5.2.1.3.1 ARCHAEAN OR PROTEROZOIC.

The Halls Creek Group.

The Halls Creek Group crops out in a NNE belt. The oldest rocks within the group, the Ding Dong Downs Volcanics, form the core of the Saunders Creek Dome. Quartz conglomerates and sandstones of the Saunders Creek Formation overlie these volcanics. A thin indurated remnant of the Saunders Creek Formation also occurs around the northern margin of the Sophie Downs Granite. The Biscay Formation consists of marine sediments and basic volcanics, intruded by sills and dykes of the Woodward Dolerite. Dolomite and carbonatised basalts define the top of the Biscay Formation. The Olympio Formation is composed of rhythmically-bedded greywacke and shale.

5.2.1.3.2 PROTEROZOIC.

The Lamboo Complex.

The Lamboo Complex consists of metamorphic and igneous intrusive rocks. The Woodward Dolerite consists of uralitised dolerite and pyroxenite sills and dykes, and was intruded into the Halls Creek Group before or during its deformation. The Sophie Downs Granite was intruded during or after the folding of the Halls Creek Group. The main mass is fine to coarse-grained granophyric granite. Dykes range in composition from doleritic, dacitic, microgranitic, to rhyolitic.

Adelaidean or Carpentarian.

Adelaidean or Carpentarian sandstone, shale, and dolomite crop out along the western margin of the Albert Edward Range. The Mount Parker sandstone rests on the Halls Creek Group with a strong angular unconformity. It is conformably overlain by the Bungle Bungle Dolomite, partly an algal dolomite which is eroded and overlain by glacial sediments of the Adelaidean.

5.2.1.3.3 CAINOZOIC

Tertiary sands and soils, and Quaternary alluvium are confined to stream channels and areas adjacent to major rivers.

5.2.1.4 STRUCTURE OF THE HALLS CREEK AREA

Folding.

East of the Halls Creek Fault, the Halls Creek Group has been tightly folded into the Biscay Anticlinorium, which trends NNE. The Saunders Creek Dome and the Sophie Downs Dome form the nuclei of this structure. The tightly folded Biscay Formation also outcrops marginally to the Lamboo Complex. Folding in the sediments of the Albert Edward Range is gentle and bedding generally becomes shallower.

Faulting.

The major fault is the NNE trending Halls Creek fault that extends to Wyndham 250 miles away. The fault affects both the Halls Creek Group and the Adelaidean rocks with many associated minor faults reflecting the movement of the major fault.

5.2.1.5 SUPPORTING FIELDWORK

Fieldwork was carried out in Oct-Nov, 1989, the chief purpose of which was to collect samples for later use with the Fourier Transform InfraRed (FTIR) spectrometer at JPL in California in order to gain TIR spectra for comparison with TIMS derived spectra. The experimental method used to create TIMS equivalent spectra from laboratory measurements is given below.

5.2.2 ANALYSIS OF THERMAL INFRARED LABORATORY SPECTRA

107 TIR laboratory spectra were collected from rock samples from the Halls Creek test site. The surfaces measured were from the weathered surface, as this is more representative of the surface that would be sensed by the scanner in the exploration environment.

5.2.2.1 EXPERIMENTAL METHOD.

The instrument used was the Fourier Transform InfraRed (FTIR) Analect Instrument's spectrometer (Doyle *et al* 1980, Carroll and Doyle 1981, Bartholomew *et al* 1989) located at the Jet Propulsion Laboratory (JPL) in Pasadena, California. The experimental method adopted for measuring sp^{ecta}_{λ} follows method of Salisbury *et al* (1988). The reflectance spectra were collected at $4cm^{-1}$ spectral resolution from 2.17 to 13.5 μm, using a gold coated integrating sphere attached to the external port. The integrating sphere creates spectra that are directional-hemispherical rather than bidirectional (pers. comm. G. Hoover (1990)). This is more representative of the scanner geometry, (Salisbury *et al* (1988)).

5.2.2.2 CONVOLUTION TO TIMS EQUIVALENT EMITTANCE SPECTRA

The TIR spectra are measured at $4cm^{-1}$ intervals. In order to produce spectra that are equivalent to the emittance spectra that the TIMS would produce it is necessary to convolve the spectra with the response functions of the TIMS for the flight campaign of October 1985. Assuming Kirchoff's law that;

$$\varepsilon + \rho = 1 \qquad [5.7]$$

where:

ε = Emittance.
ρ = Reflectance.

It is possible to directly relate the reflectance measured by the FTIR spectrometer to values of emittance. After this conversion to emittance the convolution to TIMS equivalent emittance spectra is derived from the function ;

$$\varepsilon_i = \frac{\int^{\lambda} \varepsilon(\lambda) \, . \, S(\lambda)_i \, d\lambda}{\int^{\lambda} S(\lambda)_i \, d\lambda} \qquad [5.8]$$

where:

ε_i = resultant TIMS equivalent emittance in band i.
$\varepsilon(\lambda)$ = continuous spectral emittance values from the FTIR spectrometer.
$S(\lambda)_i$ = spectral response of TIMS band i.

For discrete values of $S(\lambda)_i$ and emittance, $\varepsilon(\lambda)$ this becomes a numerical integration problem, solved using the trapezoidal rule. The algorithm used to convolve the FTIR data was kindly supplied by Dr. S. J. Hook of the JPL, Pasadena, California.

5.2.2.3 QUALITY OF SPECTRA COLLECTED

Each TIR spectrum is the average of 255 individual measurements. The quality of the spectra in the 8-12μm range is illustrated in figures 5.4 and 5.5. The FTIR emittance spectrum in Figure 5.4 is for green vegetation. This sample is from a eucalyptus species taken from trees within the grounds of the JPL. The reflectance is calculated by ratioing the response of the sample to that of a blackbody. Since the reflected signal is low for vegetation the resultant emittance contains noise of the order of 1% in emittance. For quartz, Figure 5.5, the reflected radiance response is stronger, thus the emittance spectrum appears less noisy. When the FTIR spectra are convolved to 6 points to create TIMS equivalent spectra the noise in each band will be reduced still further.

5.2.2.4 EFFECT OF CONVOLUTION ON SPECTRA

Lyon (1965) states;

"Rock and mineral types can be determined from the wavelength position of the minima of absorption and emission, or the maxima of reflectance, in their infrared spectra. Detailed study of the shape, intensity and position of individual secondary minima (or maxima) can reveal specific differences within mineral groups and between assemblages in rocks."

Convolution to 6 TIMS equivalent emittance values will destroy the information on the secondary minima. Only the general shape of the curve is maintained with the approximate position of the emittance minima being indicated. This in itself is not diagnostic. It is the specific wavelength that is. Only generic groupings of lithologies may be determined using these data.

The effect of the loss of resolution on TIR spectra is illustrated in Figure 5.5 and 5.6. The TIMS equivalent emittance spectra of a quartz sample follows the general shape of the FTIR emittance curve without exhibiting the finer features of the laboratory spectrum. The distinctive sharp emittance maximum at 8.66μm indicative of the presence of SiO_2 has been reduced as the value in band 2 is effectively averaged over a bandwidth of about 1.0μm. The spectrum from a calc-silicate sample shows a small emittance minimum at 11.22μm which is indicative of the presence of carbonate. The convolved TIMS equivalent spectra does not highlight this feature. The TIMS equivalent emittance spectra of a sample of the Bungle Bungle Dolomite however, clearly highlights the strong emittance minimum at 11.22μm, (Figure 5.7), although the strength of the minimum has been reduced. The convolution to TIMS equivalent spectra will tend to reduce fine spectral features and display only the general shape of the curve. Shallow, or narrow features such as carbonate absorptions in carbonate bearing rocks may not be apparent, depending upon the strength of the feature and the adjacent emittance values.

5.2.2.5 VARIABILITY WITHIN SAMPLES

The spectra obtained for each sample is usually from the weathered surface of a lithology measured over a 15.4mm area, (Salisbury *et al* (1988)). This is the beam size impinging upon the surface of a sample. For large grain-size samples, or unevenly weathered samples there may be a variable response of the spectra as there are changes in the proportions of mineralogies that are being measured. Figure 5.8 shows the variability of TIR spectra taken from rocks collected from the fine grained edge of the Sophie Downs Granite. Each of the samples was fine-grained, the surfaces measured were free from any visible variation and in hand specimen each sample was identical. The variability of the sample spectra is as much as 20% in samples that appear the same in hand specimen. TIMS equivalent laboratory spectra for several dolerite samples is given in Figure 5.9, these spectra show variation of the order of 6%.

This variability highlights a major problem inherent to remote sensing. It is assumed that the characteristics of a spectrum taken from a small area of the surface of a sample will be representative of the response of a pixel from the TIMS data: a measurement over 15mm is extrapolated to pixel sizes of 15m. The variability of laboratory TIR spectra for any one lithology will create a suite of spectra, any one, or combination of which, may be representative of the response of a particular pixel. In the natural environment it is likely that the TIR response from a particular pixel will comprise of the integrated responses from a range of spectrally distinct surface materials. Thus when attempting to match or compare spectra from the laboratory to TIMS emittance spectra it must be remembered that the laboratory spectra will have a genuine variability associated with it and the TIMS derived spectra will have an error associated with them due to the assumptions used to calculate the emittance from TIMS radiance data.

5.2.2.6 A COMPARISON OF THE EMITTANCE ESTIMATING TECHNIQUES USING LABORATORY DATA

Using the Thermal InfraRed (TIR) spectral library created from the Halls Creek samples, it is possible to estimate which of the previously described methods for extracting emittance will be most accurate. The three quantitative methods compared are the Model Emittance method and the Maximum Temperature method described in

Chapter 3, and the Alpha Derived Emittance method described in Chapter 4. The assumptions utilised to solve the underdetermined equation set are summarised below;

Model Emittance method: $\varepsilon_6 = 0.93$

Maximum Temperature method: $\varepsilon_{max} = 0.94$

Alpha Derived Emittance method: $\bar{x} = f(\sigma^2_{\alpha_i})$

where:

$$\bar{x} = \frac{1}{6}\sum_{i}^{6}\lambda_i \ln\varepsilon_i$$

The Halls Creek TIR lab spectra were analysed to find the frequency of distribution of εmax values, and also the distribution of ε6 values. The histograms in Figure 5.10 show this distribution. It can be seen that the commonest εmax values are between 0.93 and 0.95. Table 5.1 indicates the percentage of lithologies whose εmax values lie within 0.02 and 0.04 of emittance from the εmax = 0.94 value. For the Halls Creek suite of TIR spectra an assumption that εmax = 0.94 will mean that 65.4% of lithologies will have their emittance values calculated to within 0.02 of emittance compared to the assumption of ε6 = 0.93 which has 63.6% of its spectra within the 0.02 range. The most accurate of these methods is the assumption that εmax = 0.94.

In order to assess the validity of the assumption used in calculating emittance from alpha coefficients we need to calculate the change in mean value that will cause a change in emittance of 0.02, and 0.04. This may be expressed using Equation [5.9];

$$\Delta\varepsilon = \varepsilon - \hat{\varepsilon} \qquad [5.9]$$

where:
$\Delta\varepsilon$ = Change in emittance due to a change in mean from $\bar{x}$ to $\hat{x}$.

Therefore

$$\Delta\varepsilon = \exp\left[\frac{\alpha_i + \bar{x}}{\lambda_i}\right] - \exp\left[\frac{\alpha_i + \hat{x}}{\lambda_i}\right] \qquad [5.10]$$

Equation 5.10 may be rearranged;

$$\hat{x} = \lambda_i \ln\left[\exp\left[\frac{\bar{x}}{\lambda_i}\right] - \frac{\Delta\varepsilon}{\exp\left[\frac{\alpha_i}{\lambda_i}\right]}\right] \qquad [5.11]$$

and the change in mean value is:

$$\Delta x = \bar{x} - \hat{x} \qquad [5.12]$$

Table 5.2 shows the difference in mean values, Δx, for combinations of mean, wavelength and alpha values. Figure 5.11 shows the mean variance curve with Halls Creek data plotted with the error envelope for a change in emittance of 0.02 and 0.04 in emittance for the band 6 wavelength and $\alpha = 0.0$. These values are illustrated as they may be compared to the Model Emittance where the error is calculated for band 6. These error curves show that the calibration curve will predict 63.6% of lithologies to within 0.02 of emittance, and a further 27.1% to within 0.04 in emittance, (see Table 5.1). The equation of the mean variance curve was originally calculated for Salisbury *et al* (1988) spectra. Plotting the mean variance for Halls Creek spectra indicates that this curve still provides a good fit to the new data. However the distribution of the points above and below the 'Salisbury' best fit curve indicates that a slight improvement of fit may be possible. Improving the fit would increase still further the number of data points that could be estimated to within the 0.02 emittance intervals. It is possible to calculate mean variance curves that are specific to a particular set of TIR spectra from a particular terrain. Each curve may then have error envelopes generated using Equation 5.12, and the accuracy of this method may then be compared to the other methods.

Table 5.1 shows the percentage of those lithologies whose emittance estimations are within certain intervals of emittance for each method. Assuming the Halls Creek TIR spectra are representative of the lithologies present within the scene the most accurate method for the prediction of emittance will be the Maximum Temperature method.

These percentages indicate that no single method is significantly more accurate at emittance estimation than the other methods for the Halls Creek TIR emittance spectra library.

The most accurate method for predicting emittance values for a sample will depend upon individual pixel characteristics. In some cases one method will be more accurate than the others. Figure 5.12 is a Venn diagram to show the distribution of the accuracy of emittance estimates determined for each method for the 107 spectra from Halls Creek. The spectra are divided into fields where the emittance will be estimated to within 0.02, 0.04 and greater than 0.04 of emittance for each method. This diagram shows that in Field A, 34 of the 107 spectra will be estimated to within 0.02 of emittance whichever of the methods is used. For these spectra the algorithm used will not significantly change the emittance estimation. These spectra, well behaved according to each criterion, are generally schistose and silica rich rocks.

Field B contains four spectra for which the Alpha Derived method provides an accurate estimate of emittance whereas the other methods do not. The two vegetation spectra fall within this field, acting as approximate greybodies, having high εmax and ε6 values. Conversely there are fields, field C, containing five spectra which can be accurately estimated using the Model Emittance and Maximum Temperature methods but do not conform well to the Alpha Derived Emittance criterion. These tend to be spectra with low means and little variation, such as basaltic rocks types, Figure 5.13.

In order to achieve the most accurate estimate of emittance over the scene, the assumption used to calculate emittance could be changed according to the individual pixel characteristics. This hybrid image would be created where the assumption used to calculate emittance will be different for different parts of the scene. The major difficulty in using variable criteria is the need to have a criterion to decide which method to use. Each set of six radiances would need to be investigated to decide which method would be most accurate. Such a criterion has not been found.

For geological investigations the shape of the emittance curve is of critical importance. Since each method will select one of the potentially correct suite of emittance curves, each will have similar shape. The major improvement would come not in the improvement of the spectral information but in the temperature estimate, which is not the most important factor for lithological mapping. However for studies where the temperature is important, such as for environmental remote sensing or

volcanic studies, it may be necessary to have the ability to calculate temperature to a greater degree of accuracy that would be possible if the criterion used to calculate emittance was not varied over the scene.

5.2.3 AN EVALUATION OF THE SPATIAL INFORMATION CONTENT CONTAINED IN TIMS IMAGES DERIVED FROM EACH METHOD

5.2.3.1 THE DECORRELATION-STRETCH METHOD.

The Decorrelation stretch (D-stretch) technique and its variants were applied to the TIMS data for Halls Creek. The most useful combinations in terms of lithological discrimination proved to be 1, 3, 5 and 2, 3, 5 in RGB respectively. These were calculated following the methodology of Gillespie *et al* (1986). Other variations to the commonly described methods provide alternative renditions of the data but did not represent an improvement in the information content present. Plates 1 and 2 are example subscenes from the Halls Creek D-Stretch images. The D-stretch proved very useful in discriminating between individual lithologies. As stated in Chapter 2, the identification of lithologies was not possible using this technique, and it was only possible to broadly associate hues with relative emittance values. For instance, blue coloured areas have very low values in bands 1, and 3, and higher values in 5, which can be attributed to silica rich areas. Thus it is possible to identify quartz areas only because of their extreme spectral behaviour.

5.2.3.2. THE ALPHA COEFFICIENT METHOD

Upon scaling to byte for display any three band combination of alpha coefficients is found to be very similar to the TLR images for the reason is stated in Chapter 4.

Individual alpha bands are shown in Plate 3, and a 1, 3, 5 combination (for comparison with D-stretch) is given in Plate 4. This colour combination of alpha coefficients provides a useful colourful image that facilitates the delineation of lithological boundaries. The alpha coefficients provide an increment of discriminatory power over the D-stretch, as they contain only emittance information, rather than residual temperature information. This is illustrated by the apparent "flatness" of the images, as they contain no temperature information which is usually manifest as differences in topography. The alpha coefficients also have a quantitative use when considering the data in the spectral sense; an advantage over the D-stretch. The alpha algorithm needs only to be applied once and three band combinations may

subsequently be selected for display. The D-stretch, in contrast, requires the pre-selection of bands for the application of the method, a process which must be repeated for each band selection. In the spatial sense the alpha coefficients (or the equivalent TLR) provide alternative processing techniques to the D-stretch for TIR multispectral data.

5.2.3.3 THE MODEL EMITTANCE METHOD

The Model Emittance method, in setting $\varepsilon 6 = 0.93$ creates a univalued image in band 6 and an adjacent noisy image in band 5. This method reduces the number of useful bands to the first 4 bands, with band 5 being noisy, (Plate 5). Plate 6, shows a subscene of the area with bands 1, 3, and 5. Although not as colourful as previous images, it is still possible to discriminate the same boundaries as the D-stretch. The Model Emittance method contains spectrally useful information which will be discussed below in Section 5.2.5 with regard to specific examples.

The Model Emittance method also produces a temperature image, (band 6 in Plate 5). This temperature image highlights the topography which emphasises its control on temperature over the scene. This image shows that the algorithm has qualitatively separated the temperature component from emittance component.

5.2.3.4 THE MAXIMUM TEMPERATURE METHOD

The Maximum Temperature method sets the maximum emittance in a pixel to a constant value, which for the Halls Creek scene was set at $\varepsilon max = 0.94$. Although the band in which the maximum occurs may vary from pixel to pixel, it is evident from Plates 7 and 8 that band 6 contains most of the εmax values. This band exhibits very little variation and does not provide much useful information. Since band 6 is, for the majority of pixels, the εmax band, band 5 is noisy. Plate 9 shows the temperature image derived from the application of this method. This image is qualitatively very similar to the temperature image of the Model Emittance method. For the Halls Creek scene the assumptions used for both the Model Emittance and Maximum Temperature methods have tended to be very similar with the result that the images look alike. The scene statistics for both these methods are discussed below and further indicate the similarity between the methods.

5.2.3.5 ALPHA DERIVED EMITTANCE METHOD

This method has created 6 emittance images and a temperature image (Plate 10). A 3 band colour composite in bands 1, 3, 5 is shown in Plate 11. These emittance images are not equivalent to the alpha coefficients images as the use of the mean (of Equation 4.22) alters the alpha coefficients values and will tend to reorder emittance values.

In an image sense this method allows discrimination of lithologies, but its major use is in the spectral sense, described below. The temperature image, band 7 in Plate 10, qualitatively similar to Model Emittance and Maximum Temperature methods, also highlights the topography of the area showing that separation of temperature from emittance has occurred using this technique.

5.2.4 ANALYSIS OF SCENE STATISTICS FROM EMITTANCE ESTIMATING METHODS.

Scene statistics may be used as a further indication of the effectiveness of each technique. These statistics are summarised in Table 5.3. Figure 5.14 shows the mean vector calculated for each emittance method. These mean curves are all very similar to each other and show a minimum in band 3. Each has a general shape resembling schist spectra.

Table 5.3 shows that the scene average emittance value for band 6 is 0.939 for the Alpha Derived Emittance method, 0.93 for the Model Emittance method and 0.932 for the Maximum Temperature method. This can be compared to Figure 5.10 which shows the histogram of the distribution of emittance values in band 6 for laboratory spectra. Both the tables and figures show that the average $\varepsilon 6$ value calculated by each method for the Halls Creek TIMS scene occurs in the mode of the distribution of $\varepsilon 6$ laboratory values. This suggests that each of the algorithms has produced the sort of average spectra that might be expected from the scene.

The mean image temperature is 294.0K for the Alpha Derived Emittance method, 293.7K for the Model Emittance method, and 293.4K for the Maximum Temperature method, which are reasonable temperatures for the scene again suggesting that the temperature information is separated from the emittance by each method. The standard deviations for each method for each band are given in Table 5.3. These values show that the Alpha Derived Emittance method produces more widely varying

spectra than the other methods, having a standard deviation of 0.1 in bands 2 and 3 in comparison to 0.08 for the same bands in the other two methods. The standard deviations of the temperatures are all similar to each other. Thus the variation in temperature is equivalent but the variation in emittance is greater for the Alpha Derived Emittance method. This suggests that the Alpha Derived Emittance method allows a greater degree of variability in the spectral variation than the Model Emittance and Maximum Temperature methods.

If the methods for calculating emittance have been entirely accurate, the temperature information should be uncorrelated with the emittance information (correlation = 0.0). The correlation values of the emittance in each band with respect to temperature are given in Table 5.4 and have values between 0.11 and 0.63 for Alpha Derived Emittance, 0.35 to 0.71 for the Model Emittance, and 0.39 to 0.87 for the Maximum Temperature methods. These can be compared to the original radiance correlation values in Table 2.1 which are of the order of 0.97. Although the correlations are not zero and are all positive the magnitude of the reduction again shows that each of the algorithms has separated a large component of the emittance information from the temperature information, the most uncorrelated being for the Alpha Derived Emittance method.

An analysis of the laboratory data for Halls Creek (Section 5.2.2.6) indicated that each of the methods would be equally accurate. This would be the case if the 107 spectra were representative of the overall scene components. The scene statistics suggest that the Alpha Derived Emittance method separates the emittance from the temperature components more effectively than the Model Emittance and Maximum Temperature methods. If the library sp were to contain more vegetation spectra, thereby making the library more representative of the proportions of the scene components, then the Alpha Derived Emittance method would be found to be more accurate. This is because the vegetation can be more accurately estimated using the Alpha Derived Emittance criterion than the other methods.

Use of the above techniques permits the discrimination of various lithologies on the basis of their inherent spectral variation. The easiest to utilise are the alpha coefficients or D-stretch methods which provide the most colourful images. The alpha coefficients produce an increment of enhancement ability over the D-stretch as they consist of emittance variations only. This has been noted by other workers for example Hook *et al* (1990), with TIMS data from Cuprite, Nevada. The images highlight some problems associated with identifying lithologies. The granite area

(Figure 5.3) has within it a great deal of variation. Although geologically one unit, it contains varying amounts of surface cropping granites, soil development, quartz float, and vegetation. Identifying an area whose spectral response will be directly related to the typical underlying lithology will in some cases be difficult.

The area I (Figure 5.15 and evident in the Plates shown) has, in the D-stretch image, Plate 2, a central core of reds and yellows surrounded by green hues. The boundaries are not consistent with geological boundaries but with creek beds. This indicates that it is the result of a fire that died out at creek beds. Fieldwork has shown that firescars of similar dimensions and characteristics are common in this area. The firescar highlights the effect vegetation has in the TIR. Areas covered in spinifex exhibit a white/green hue in Plate 1, whilst bare, firescarred areas show the underlying geological units clearly, without the masking effect of vegetation.

5.2.5 EVALUATION OF SPECTRAL INFORMATION FROM EMITTANCE ESTIMATING ALGORITHMS

In this Section spectra derived from laboratory measurements of samples collected in the Halls Creek area are compared to estimates of emittance calculated from the TIMS data. The aim is to assess the utility and accuracy of the emittance producing methods when applied to TIMS data. Spectra from seven example sites within the image are examined in this context. Included amongst the sites are a range of lithologies and vegetation.

5.2.5.1 SAMPLE SITE A: VEGETATION

Sample site A is taken from an area of dense vegetation within the Halls Creek scene. This area is situated at the edge of a creek bed located in Figure 5.15. Fieldwork has shown that this area is covered by a dense stand of eucalyptus with an understorey of leaf litter. A laboratory spectrum was taken of eucalyptus leaves. This spectrum is shown in Figure 5.16a, It can be seen that it exhibits very little spectral variation, and is effectively a greybody where $\varepsilon = 0.98$. Vegetation generally shows a small amount of spectral variation in the Thermal Infrared (Elvidge 1988) but this is not evident for eucalyptus leaves.

Figure 5.16b shows the image derived spectra for the vegetated area using the three different emittance estimating methods. Assuming the eucalyptus leaf sample to be representative of the response of the vegetated area, the Alpha Derived Emittance

spectrum has the closest match to the laboratory spectrum, showing an approximate greybody response of 0.97. The vegetation spectrum, being an approximate greybody of 0.98 behaves well according to the criterion used in the calculation of alpha derived emittance spectrum. For a "Wien" blackbody, (a blackbody spectrum calculated using the Wien approximation), the resultant estimation of emittance would be exact. For approximate greybodies that are close to a blackbody response the criterion is still satisfied.

The spectra calculated using the Model Emittance and Maximum Temperature methods produce similar spectral shapes, but under-estimate the emittance by approximately 5% to 6% of emittance. This causes an overestimation in temperature (in comparison to the Alpha Derived Emittance temperature) of 3.2K. Thus for vegetation pixels the Alpha Derived Emittance method agrees most closely to the laboratory measurements.

5.2.5.2 SAMPLE SITE B: GRANITE

Sample site B is taken from a well exposed area within the Sophie Downs Granite, Figure 5.15. The laboratory data from samples within the granite area are shown in Figure 5.17a. The laboratory spectra show considerable variation, within which a granite spectral response obtained from the image might be expected. The general shapes of the curves are similar, the variation being in the depth of the minima of the curves. The emittance spectra exhibit a minimum in band 3 and then rise to values of about 0.91 at the longer wavelengths. The minimum in band 3 can be attributed to the fundamental Si-O stretching vibration bands of the component minerals, Salisbury *et al* (1988), which for felsic rock types will cause the emittance minimum to be at short wavelengths, band 3 for the TIMS.

TIMS-derived emittance spectra for the area (Figure 5.17b) show that each of the emittance estimation methods provides spectra of similar shape but each has slightly different mean values. The spectral shapes will remain similar whatever method is used because the methods only differ in determining which of the possible suite of spectra is most likely to be correct. For the granite each of the methods provides similar results because the granite spectra behave well according to each of the assumptions. The value in band 6 is approximately 0.93. Since the highest emittance is in band 6, the Maximum Temperature method therefore makes $\varepsilon 6 = 0.94$ which produces a spectrum similar to the Model Emittance method. The Alpha Derived Emittance criterion is also well satisfied by the laboratory spectrum.

The Model Emittance and Maximum Temperature methods provide parallel emittance spectra varying in mean value. The Alpha Derived Emittance spectrum is not parallel, being closer at longer wavelengths to the other spectra (Figure 5.17b). This non-parallel behaviour is due to the use of the Wien approximation employed in the Alpha Derived Emittance method, rather than using the Planck function as is the case with the other two methods.

5.2.5.3 SAMPLE SITE C: BASALT

Sample site C is located on a basaltic intrusion of the Woodward Dolerite that forms a hill over 60m high. Its location is shown in Figure 5.15. Samples were taken from both sides of the hill that consisted of the same lithology, and were identical in hand specimen. The laboratory TIMS equivalent emittance spectrum for the Woodward Dolerite at this location show a high general emittance, lowering to a shallow minimum in band 4, followed by a small rise in emittance values at longer wavelengths (Figure 5.18a). The minimum in band 4 is due to the combined effect of individual mineralogies. The bond length will lengthen as the silicates exhibit progressive depolymerisation of the SiO_4 silica ion, (Salisbury *et al* 1988). The basic mineral assemblage of the basaltic lithology causes the minimum to occur at longer wavelengths than the granite, (Salisbury *et al* 1988), as the Si-O bonds of the silicates become longer and weaker.

Image spectra were calculated from pixels on the slopes of the hill towards and away from the sun, Figures 5.18b and 5.18c respectively. These pixels have different radiance values as one is at a higher temperature than the other due to the uneven heating of the ground by the sun. The resulting emittance calculated from each area are all of similar values despite being calculated from radiances that were originally very different. This indicates that the temperature component of the radiance signal has been separated from the emittance. The similarity of emittance values for each of the emittance estimating methods suggests that they are all equally effective at separating emittance from temperature.

5.2.5.4 SAMPLE SITE D: BIOTITE SCHIST

Sample site D is located in an horizon of biotite schist found within the Biscay Formation, located to the NW of the Sophie Downs Granite, (Figure 5.15). The laboratory derived spectrum of the weathered surface of the biotite schist shows a decrease in emittance from 0.86 to a minimum of 0.8 in band 3, followed by a rise to 0.92 in band 6, Figure 519a. This broad minimum centred in band 3 is due to the combined effect of the dominant quartz feldspar and biotite components of the lithology.

The corresponding emittance estimates from the three methods again show similar results to each other, Figure 5.19b. This is because the schist spectrum behaves well according to each of the assumptions used in each of the methods. The TIMS image spectra were calculated from 4 pixels, the standard deviations for each of the spectra are of the order of 0.02 of emittance, for each band. The laboratory and TIMS image spectra show good numerical agreement falling within the variability exhibited by the TIMS sample area.

5.2.5.5 SAMPLE SITE E: QUARTZ FLOAT

Sample site E is taken from an area where the Woodward Dolerite is overlain by a thin development of soil and an almost complete cover of quartz float, Figure 5.15 indicates its location within the scene. The underlying dolerite is not apparent, as the superficial cover is complete. The quartz laboratory spectrum obtained from this area is shown in Figure 5.20a. Other quartz spectra from elsewhere in the scene show similar spectral shapes but vary in terms of the absolute value. The strong absorption features in the lower bands are due to the Si-O bonding minima (Salisbury *et al* 1987). The corresponding TIMS-derived spectra for this area (Figure 5.20b) show good general agreement in both shape and absolute values. For sample E, a quartz rich area, each of the methods provide similar resultant emittance values. This is attributed to the characteristic behaviour of the spectrum which fulfils each of the criteria to similar accuracies.

5.2.5.6 SAMPLE SITE F: BIOTITE-QUARTZ-FELDSPAR META-DIORITE

Sample site F is situated at the edge of the firescarred area shown in Figure 5.15. A spectral traverse was made across the image, starting within the firescarred area and moving across the firescar boundary into a vegetated area. The underlying lithology was the same, the variation being in the density of vegetation. Figure 5.21a shows the laboratory spectrum for the lithological sample, a biotite, quartz, feldspar meta-diorite. Figure 5.21b shows the variation in pixel emittance for the traverse calculated using the Alpha Derived Emittance method. The spectra are numbered 1 to 8, spectrum 1 being from the well exposed end, and spectrum 8 being in the vegetated area. Spectra 1 to 3 show a close agreement to the laboratory spectrum for the meta-diorite. Spectra 4 onwards have gradually higher and flatter spectra as the traverse moves into the area where the lithology is overlain by vegetation. Spectra 6 and 7 exhibit a typical flat vegetation response (compare to Figure 5.16a) rather than that of the underlying lithology. The traverse highlights the masking effect of vegetation on the lithological component of the scene for the Thermal Infrared.

5.2.5.7 SAMPLE SITE G: DOLOMITE

Sample site G is taken from the Bungle Bungle Dolomite Formation of the Proterozoic sediments in the SE of the scene. The Bungle Bungle Dolomite has a pure dolomite lithology. Figure 5.15 indicates the sample site location. Figure 5.22a shows the laboratory spectrum taken from the weathered surface of the sample. The spectrum, convolved to TIMS wavelength response functions, maintains the minimum in band 6 (as discussed in Section 5.2.2.4). This minimum is due to the bending modes of C-O bonds within the dolomite crystal lattice (Salisbury *et al* 1988).

TIMS image derived emittance spectra calculated from each of the three methods, for the dolomite area again are similar in shape to each other but vary in mean value, Figure 5.22b. The Alpha Derived Emittance and Model Emittance methods both over-estimate the emittance response in comparison to the laboratory spectrum, whereas the Maximum Temperature method under-estimates the emittance by a similar amount. Despite errors in the absolute values, the shape displayed by each method is similar, such that it is possible to identify the spectra as having a dolomite response.

5.2.5.8 SUMMARY

Results from the analysis of seven sample sites given above, indicate that the TIMS image data can be related directly to laboratory data for various characteristic lithologies within the Halls Creek scene. It is possible however, to find many pixels whose TIMS emittance spectra do not bear a close resemblance to the laboratory spectra measured from samples taken from that point, whichever method is used. The apparent disagreement between these spectra can be assigned to several factors.

The difference between laboratory and image spectra is most likely to be due to the assumption that the spectral response from a laboratory sample of a lithology can be extrapolated to cover a TIMS pixel, or group of pixels. For Halls Creek the lithologies are tightly folded and vary in composition over small distances. Therefore there is a high possibility of mixed lithology pixels within the scene. In addition, variable amounts of vegetation cover, soil, quartz float and iron staining will affect the overall response from an area from which the laboratory sample was taken. It is only in homogeneous areas where the laboratory sample may be considered to be representative of the pixel response that it is possible to directly relate the data from the laboratory to the image.

Other reasons for the disagreement of pixel response could be attributed to errors in the atmospheric correction which would leave residual atmospheric artifacts in the data. Another source of error would be noise inherent in the TIMS data which would affect each of the algorithms.

The primary reason for the non agreement, in some cases, between laboratory and TIMS image spectra is attributed to the errors arising from the assumption that a small laboratory sample response can be extrapolated to TIMS pixel sizes. The failure of image data to match the laboratory data can therefore be assigned to the mixing of several individual responses from vegetation, soil, different lithological components as well as the variation in response exhibited by a single sample. Unmixing algorithms are needed to separate each of these responses. The problem of unmixing is the subject of current research, for example Gillespie *et al* (1990) who have attempted unmixing TIMS data from Death Valley with some success.

5.3 SUMMARY

The Halls Creek TIMS data were calibrated according to the method given in Palluconi and Meeks (1985), and subsequently atmospherically corrected using the LOWTRAN6 atmospheric model (Kneizys *et al* (1983)) installed on JPL VICAR software. The atmospheric correction was made using radiosonde data and modified to account for residual artifacts by flat field correction to a known vegetated response area. The atmospheric correction is a source of error. It is unlikely that all the parameters used will be exactly correct. However a study of the TIMS spectra reveals no obvious atmospheric component. The error due to the atmospheric correction is believed to be small.

A study of the Halls Creek laboratory spectra collected during the fieldwork season reveal that for any single sample, a range of emittance spectra can be found that are all of similar shape but vary in the absolute emittance values. The variability of the laboratory samples creates a range of emittance values with which it is possible to match TIMS image derived spectra. This variation of the weathered surfaces of samples from Halls Creek leads to spectral responses that may be similar for different rock types. For example, the TIMS-equivalent spectra for granite and basalt (Sections 5.2.5.2 and 5.2.5.3) both have minima in band 3 rather than the response that may be expected from the fresh surfaces of these rock types as for example see Figure 1.3. The Halls Creek data were analysed to determine which of the emittance estimation techniques would be most accurate over the scene. The distribution of emittance values and their characteristic behaviour show that for the 107 spectra, the Model Emittance and the Maximum Temperature methods provide similar accuracies in emittance estimations. The Alpha Derived Emittance method, using the mean variance curve fitted to Salisbury *et al* (1988) data, also shows the same order of accuracy in emittance estimations for Halls Creek data. Plotting the mean and variance values for the Halls Creek laboratory data (Figure 5.11) indicates that an improvement in fit is possible but this would not significantly improve the accuracy of the method.

Figure 5.12 shows the distribution of accuracies for Halls Creek laboratory spectra and indicates that certain spectra will be better approximated using different criteria. Vegetation spectra are best estimated using the Alpha Derived Emittance method, schists and granitic spectra can be equally well estimated using any of the three methods, and certain basic lithologies are best estimated using the Model Emittance or Maximum Temperature methods.

Of the many image enhancement techniques applied to the Halls Creek data, the D-Stretch of bands 1, 3, 5 and 2, 3, 5 proved highly discriminating for delineating boundaries. The same band combinations of alpha coefficient data were also highly discriminating. The alpha coefficients have the advantage of creating temperature independent coefficients, rather than merely enhancing the emittance information and maintaining the subdued temperature component of the signal. The alpha coefficients also need only be calculated once and three chosen bands selected for display, rather than choosing a three band combination and performing the D-stretch transformation on each.

5.4 CONCLUSIONS

1. The TIMS equivalent laboratory spectra have noise associated with them of less than 1% in emittance.

2. Thermal laboratory spectra vary in spectral response over the surface of single samples by as much as 20%. This variation is chiefly exhibited in changes in magnitude of minima rather than the spectral shape.

3. The variation within samples may be assigned to variations in the exact degree of weathering. The weathering may alter the position of the minimum away from that which may be expected from certain rock types. For example the basalt of section 5.2.5.3 exhibits a minimum in band 3 whereas the fresh surfaces of basaltic rocks have a mimimum in band 5.

4. Convolution of the laboratory data to 6 point emittance spectra reduces the spectrum to display overall curve shape and not the fine spectral features.

5. Analysis of the Halls Creek laboratory spectra indicate that, if the library is representative of the scene, the emittance estimating methods produce equally accurate results.

6. Improved estimates of emittance using the Alpha Derived Emittance method for the Halls Creek scene could be achieved by fitting the mean variance curve to the Halls Creek laboratory data set.

7. The weighting of the spectral library to include more vegetation spectra to make the library more representative of the scene proportions, would preferentially increase the estimated accuracy of the Alpha Derived Emittance method because the Alpha Derived Emittance method is the most accurate estimation method for vegetation.

8. The Model Emittance and Maximum Temperature methods provide similar images for the Halls Creek data because the εmax band tends to be in band 6.

9. Scene statistics from each of the emittance estimating methods show similar average emittance curves resembling schistose spectra.

10. The Alpha Derived Emittance method exhibits the least correlation between the estimated emittance and the temperature for the Halls Creek scene.

11. Example sample spectra show that the laboratory data can be directly compared to the TIMS image data.

12. Vegetation will mask the underlying lithological signal.

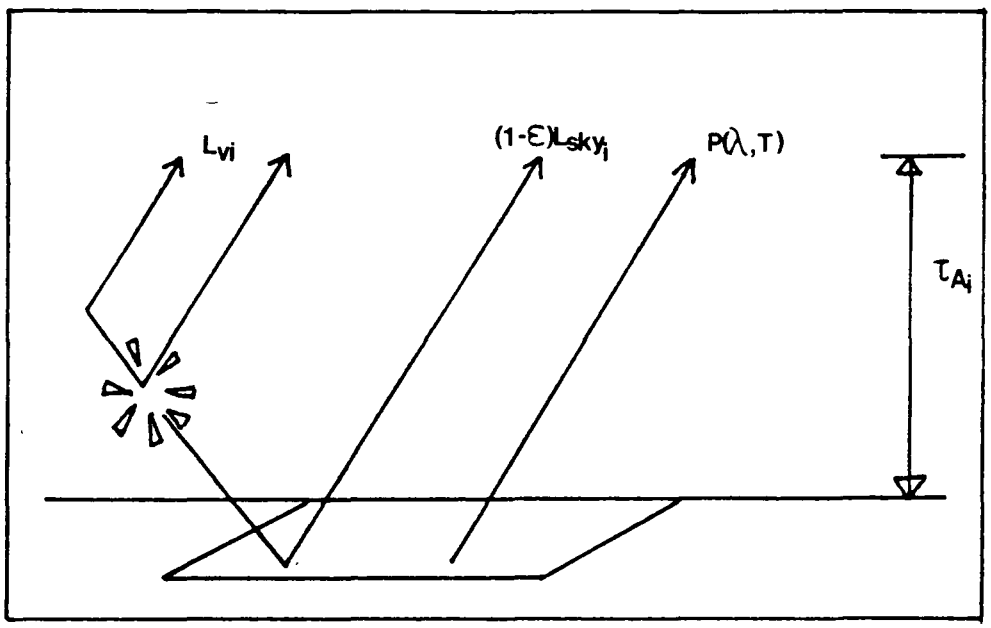

Figure 5.1 Sketch to show the origin of components of the signal received by a Thermal Scanner according to the model of Kahle et al (1980).

L_i = Radiance received by the scanner in band i from the following components:

ε_i = Surface emittance in band i.

$P(\lambda, T)$ = Planck function for a blackbody.

L_{skyi} = Spectral radiance incident upon the surface from the atmosphere in band i.

τ_{Ai} = Spectral atmospheric transmissivity for band i.

L_{Vi} = Spectral radiance from atmospheric emission and scattering that reaches the sensor in band i.

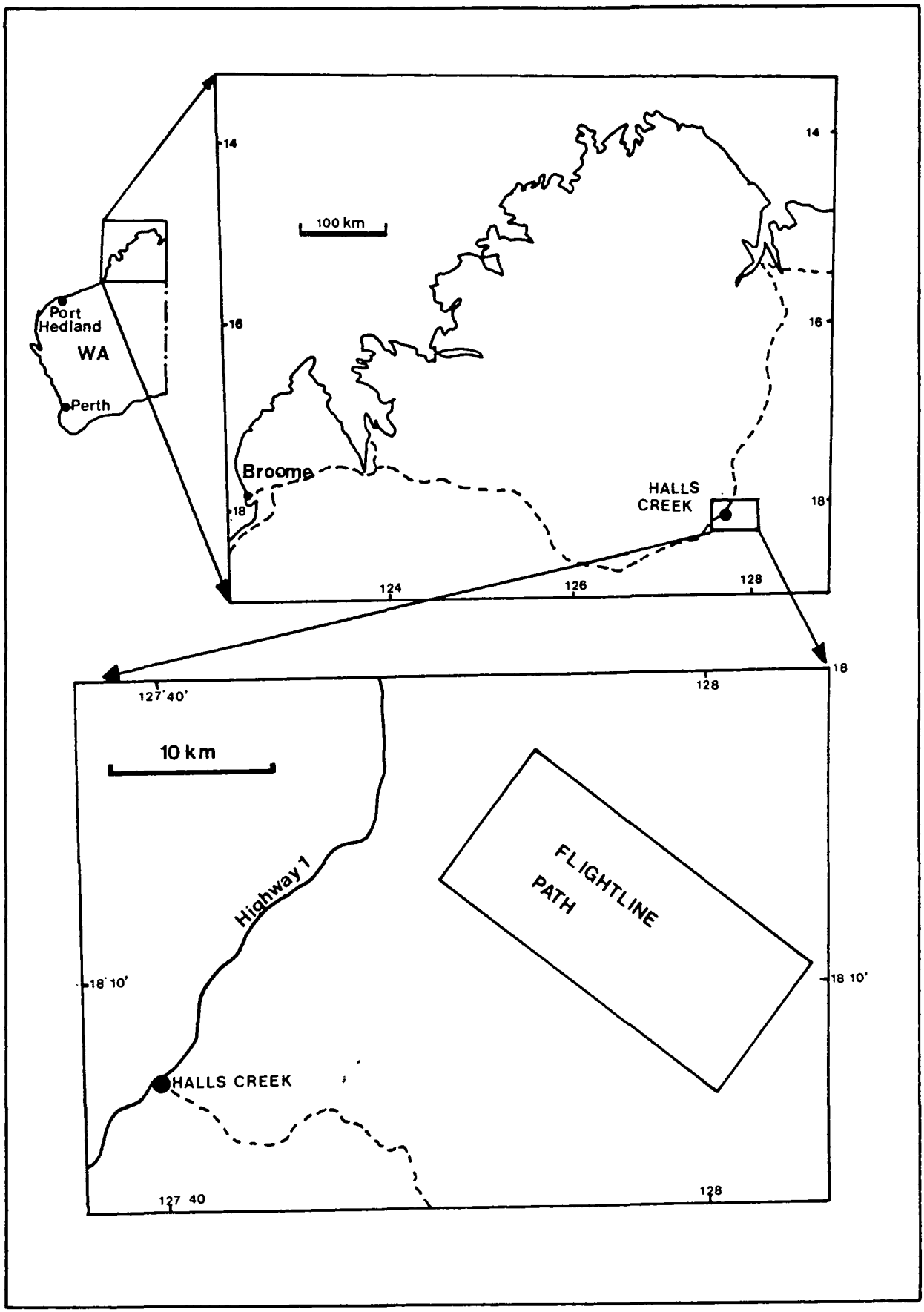

Figure 5.2 Location of the Halls Creek test area.

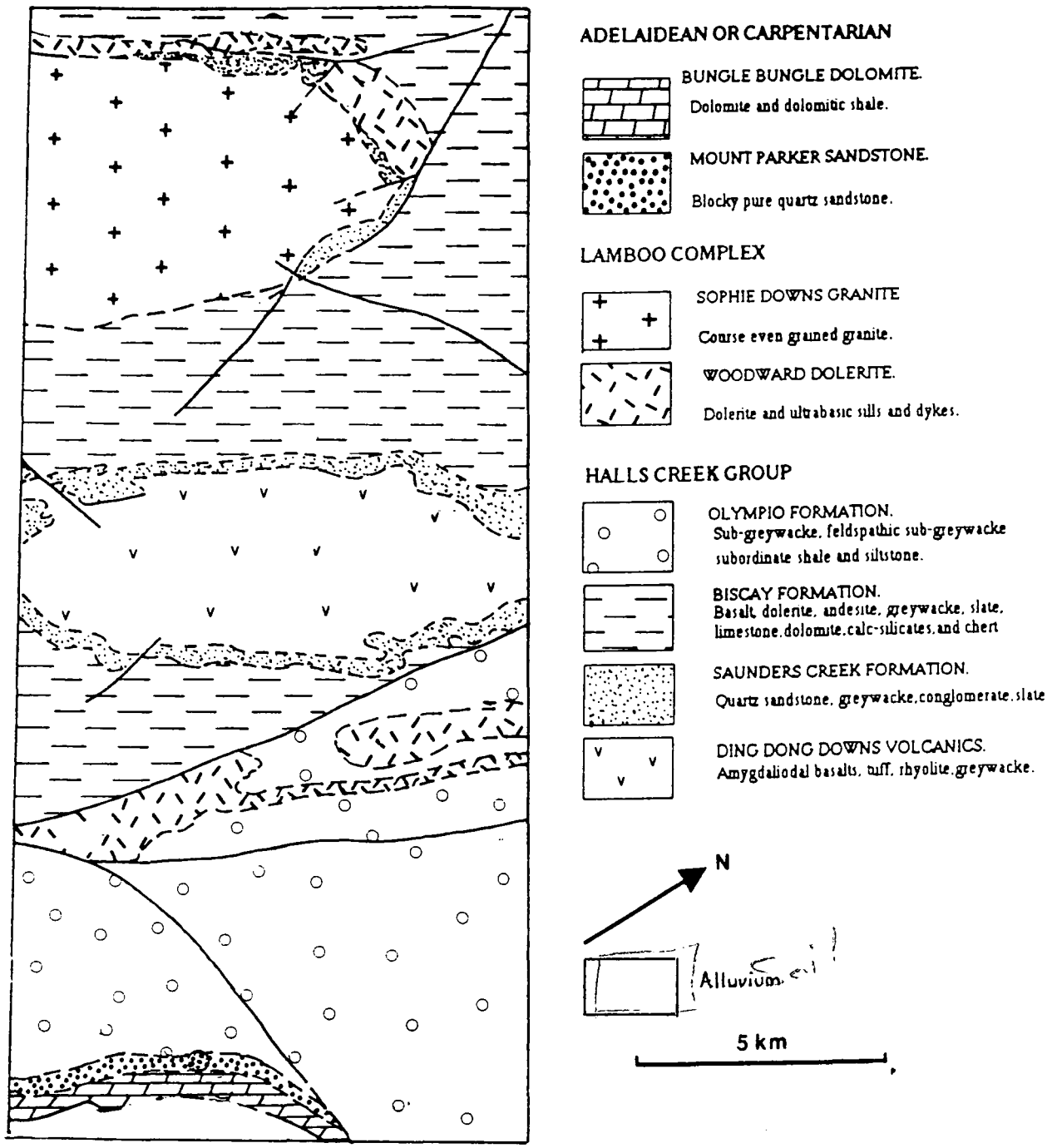

Figure 5.3 Simplified geological map of the Halls Creek flightline, (redrawn from Gemuts 1968).

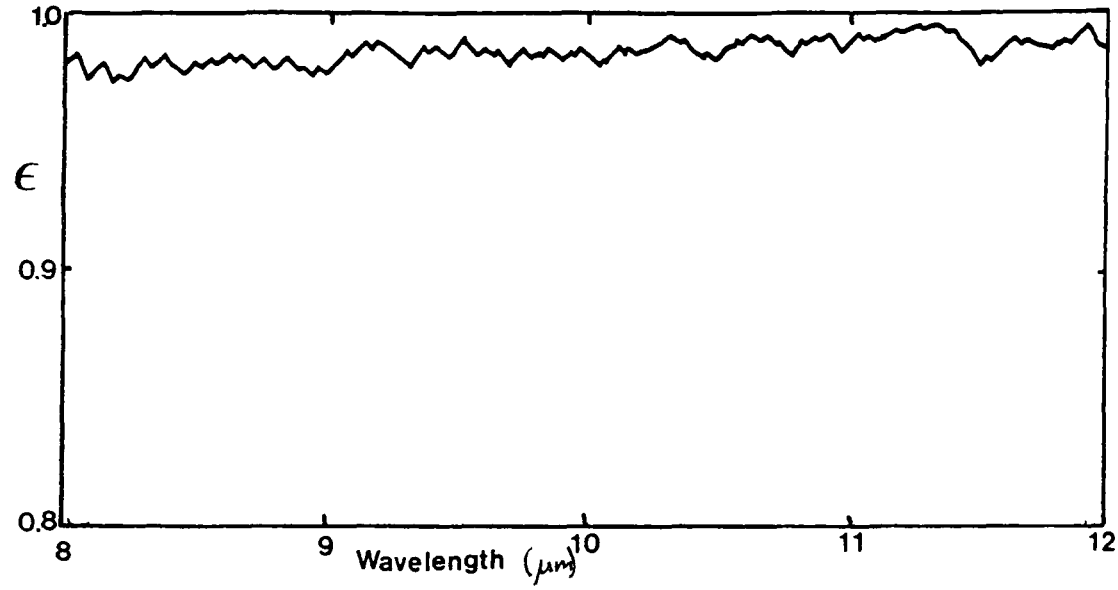

Figure 5.4. FTIR spectrum for green eucalyptus leaves.

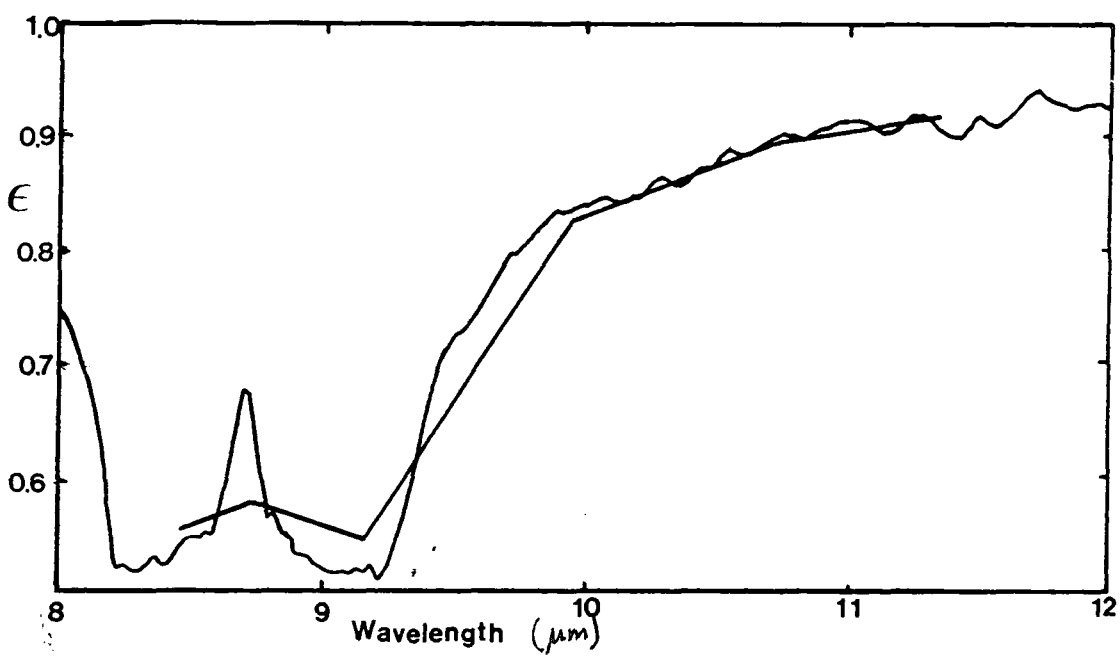

Figure 5.5. FTIR and corresponding TIMS equivalent spectrum for a quartz sample.

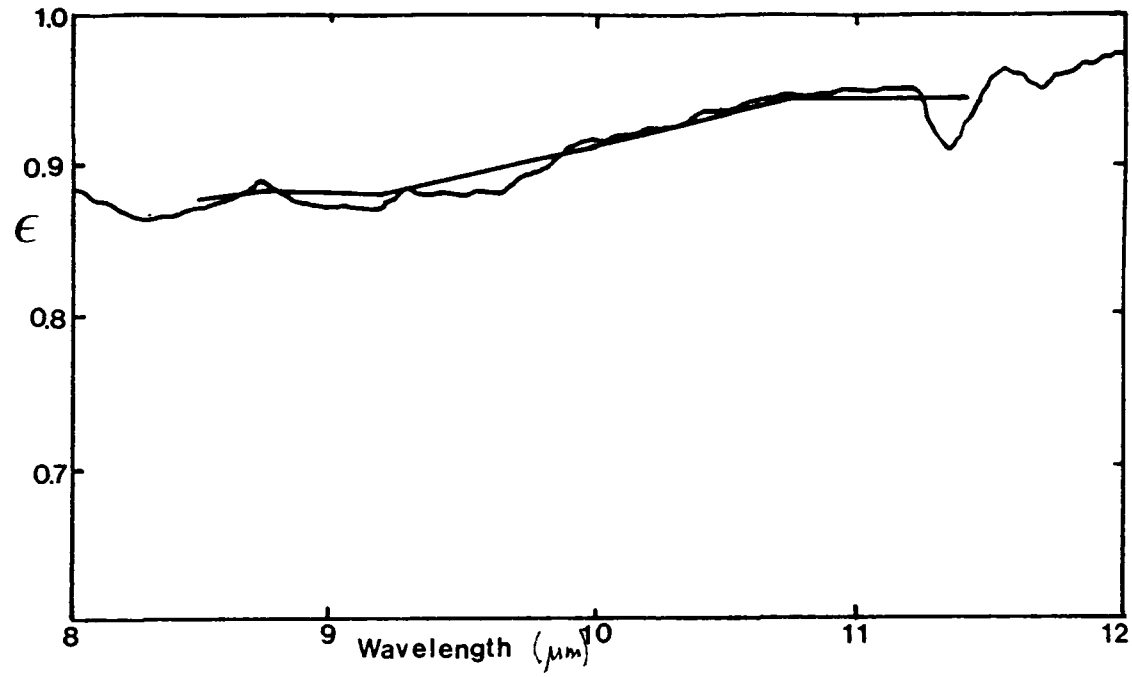

Figure 5.6. FTIR and corresponding TIMS equivalent spectrum for a calc-silicate sample.

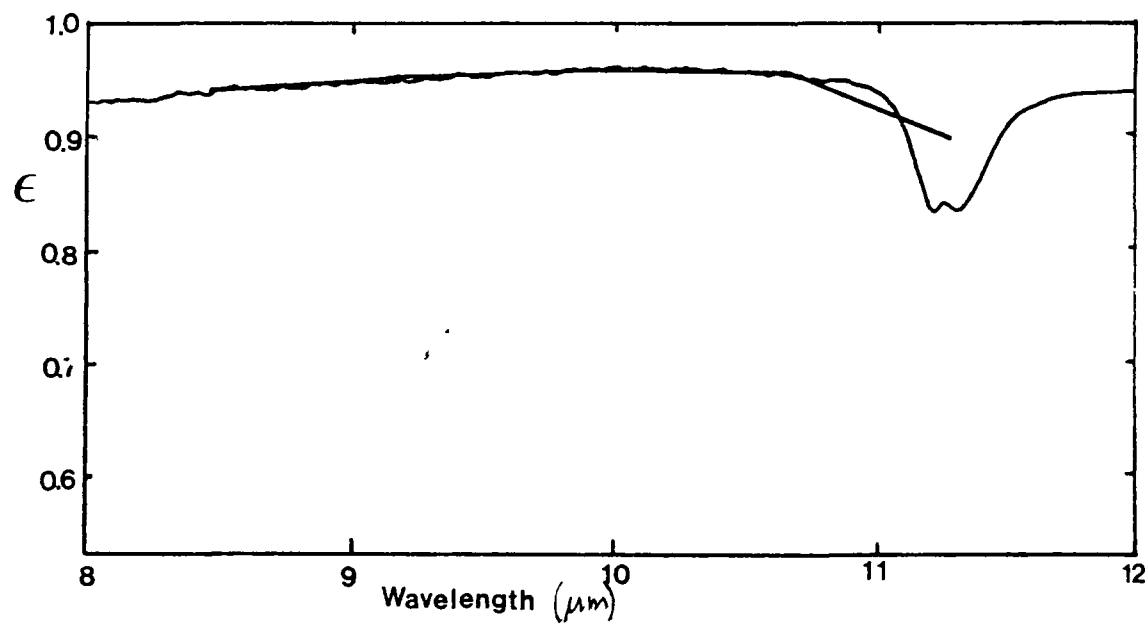

Figure 5.7 FTIR and corresponding TIMS equivalent spectrum for a dolomite sample from the Bungle Bungle Dolomite.

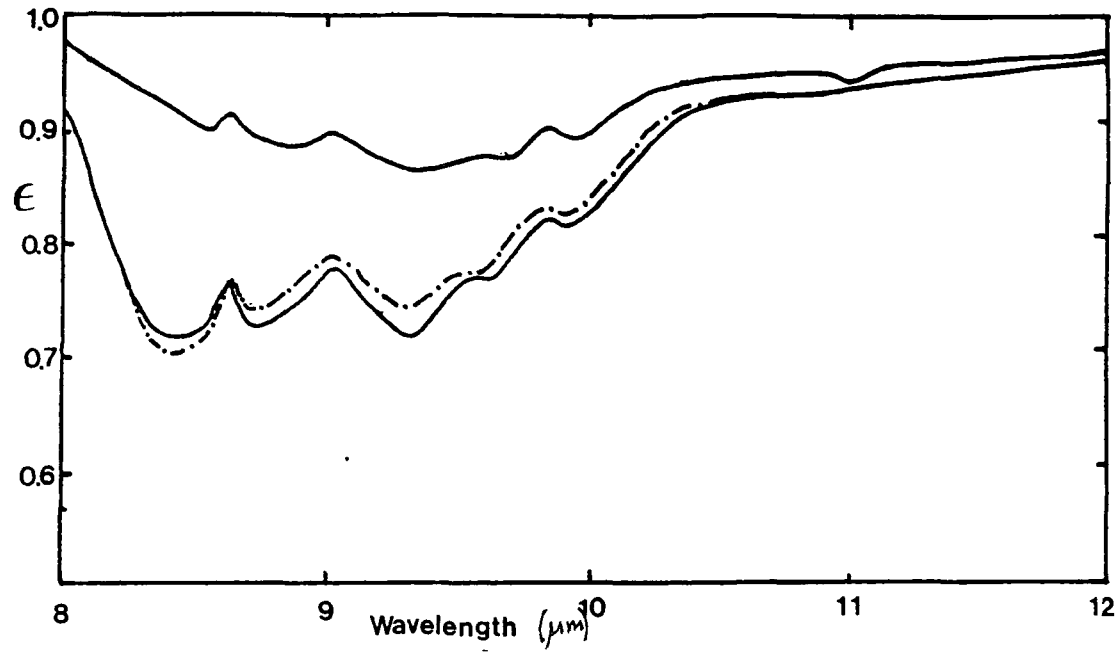

Figure 5.8 FTIR spectra from the weathered surface of a single sample of the Sophie Downs Granite.

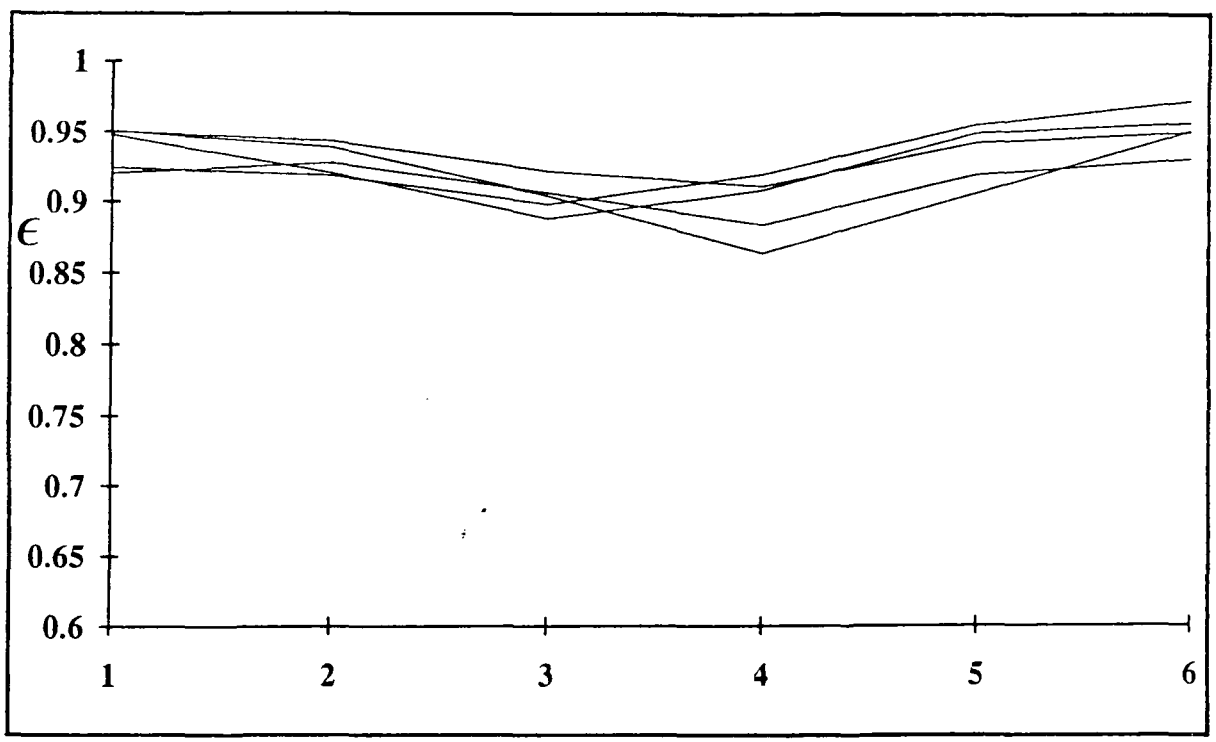

Figure 5.9 TIMS equivalent emittance spectra for dolerite samples from the Halls Creek scene.

Figure 5.10 Histograms of the distribution of emittance values for 107 Halls Creek laboratory spectra.

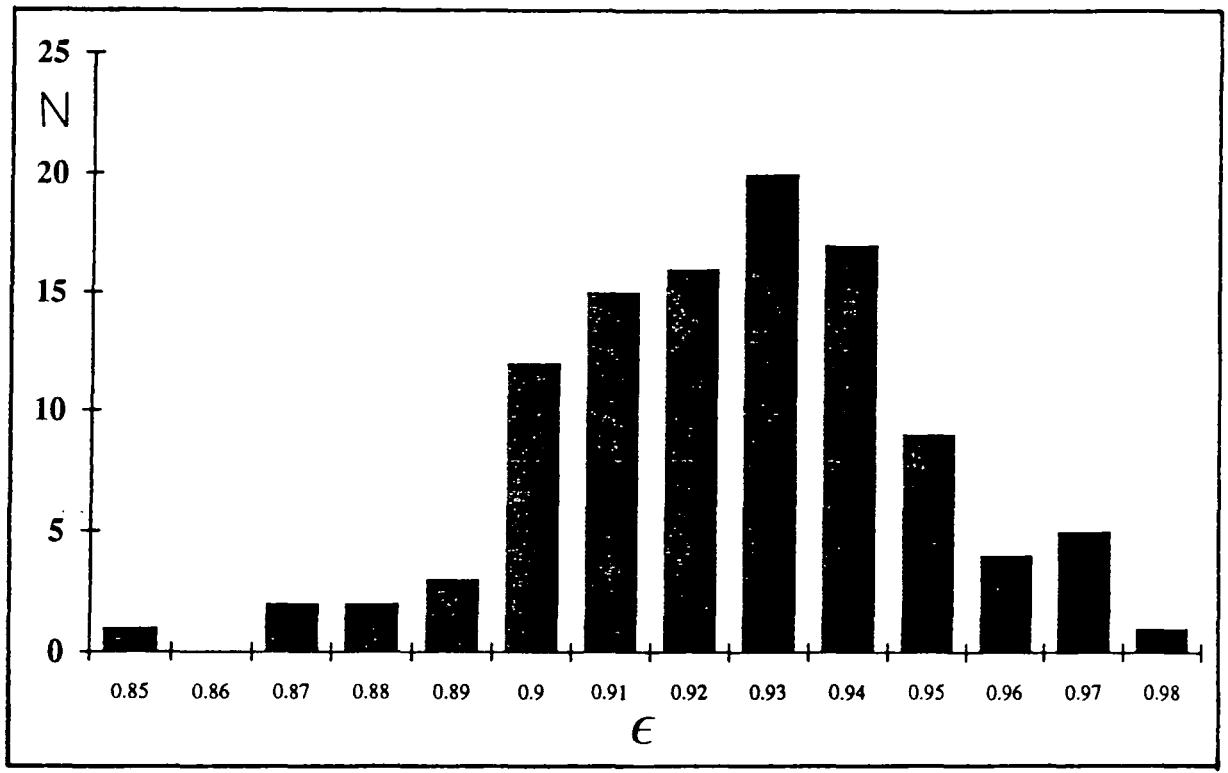

5.10a. Distribution of emittance values in band 6.

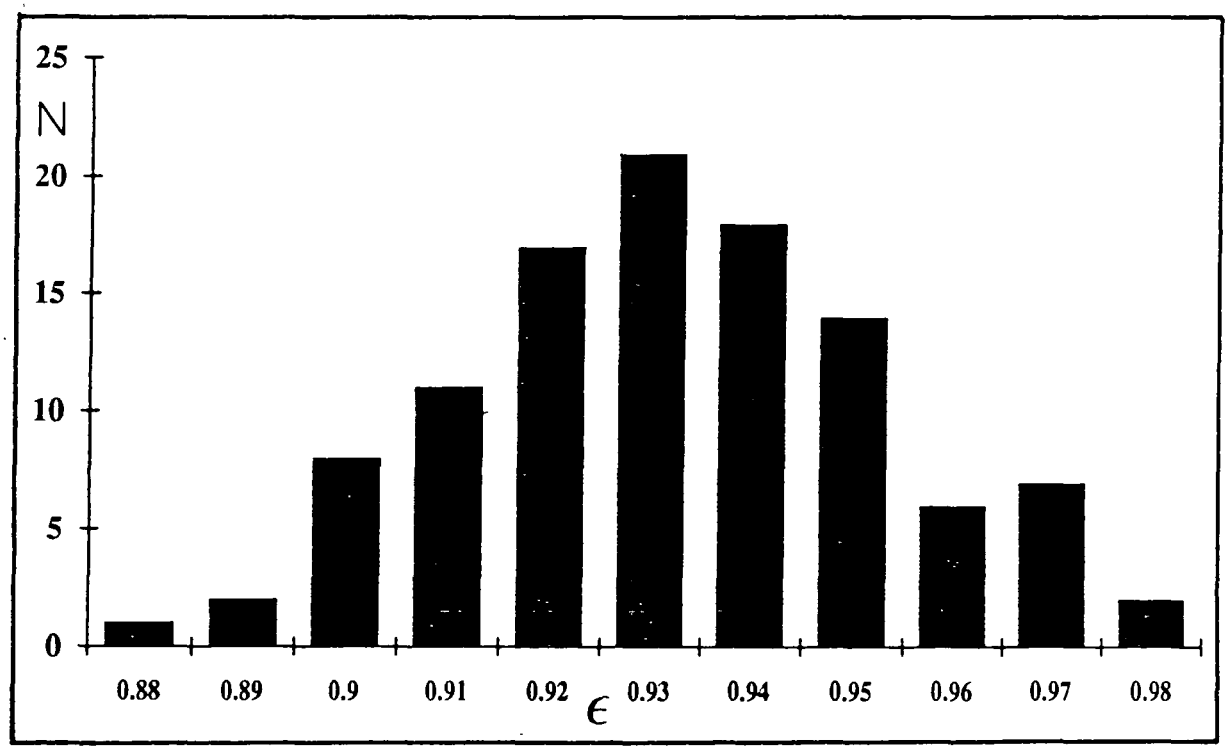

5.10b. Distribution of the maximum emittance value for each spectrum.

ACCURACY	EMAX = 0.94	E6 = 0.93	ALPHA
< 0.02 OF E	65.42%	63.55%	63.55%
< 0.04 OF E	29.90%	26.17%	27.10%
> 0.04 OF E	4.68%	10.28%	9.35%

Table 5.1 Table showing the percentages of lithologies for the Halls Creek laboratory data which fall within accuracies of +/- 0.02 and +/- 0.04 of emittance for each of the emittance estimating methods.

VARIANCE	MEAN	MEAN +0.02	MEAN -0.02	MEAN +0.04	MEAN-0.04
5.25	-3	-3.3	-2.71	-3.61	-2.42
1.78	-2.5	-2.79	-2.22	-3.08	-1.94
0.58	-2	-2.28	-1.73	-2.56	-1.47
0.36	-1.7	-1.97	-1.44	-2.24	-1.18
0.28	-1.5	-1.76	-1.24	-2.03	-0.99
0.21	-1.3	-1.56	-1.05	-1.82	-0.8
0.14	-1	-1.25	-0.75	-1.51	-0.51
0.09	-0.7	-0.946	-0.46	-1.2	-0.22
0.06	-0.5	-0.74	-0.26	-0.99	-0.03
0.03	-0.3	-0.54		-0.78	
0.01	-0.1	-0.33		-0.57	
0	0	-0.23		-0.47	

Table 5.2 Table showing error envelopes for the best fit curve for Salisbury *et al* (1988) data, for $\lambda = 11.424$, and $\alpha = 0.0$. The envelopes are lines within which emittance may be calculated to accuracies of +/- 0.02 and +/- 0.04 of emittance. These envelopes are plotted in Figure 5.11.

	MEAN OF E6 = 0.93 METHOD	MEAN OF EMAX = 0.94 METHOD	MEAN OF ALPHA METHOD	S. D. E6 = 0.93 METHOD	S. D. EMAX = 0.94 METHOD	S. D. ALPHA METHOD
E1	0.841	0.848	0.845	0.077	0.073	0.098
E2	0.817	0.823	0.822	0.08	0.077	0.102
E3	0.812	0.818	0.817	0.083	0.08	0.104
E4	0.871	0.877	0.878	0.065	0.062	0.08
E5	0.916	0.922	0.924	0.058	0.057	0.068
E6	0.93	0.932	0.939	0	0.056	0.062
T	293.742	293.407	293.957	19.805	18.922	19.564

Table 5.3 Table of scene mean and scene standard deviations for emittance values calculated over the Halls Creek scene using the emittance estimating methods.

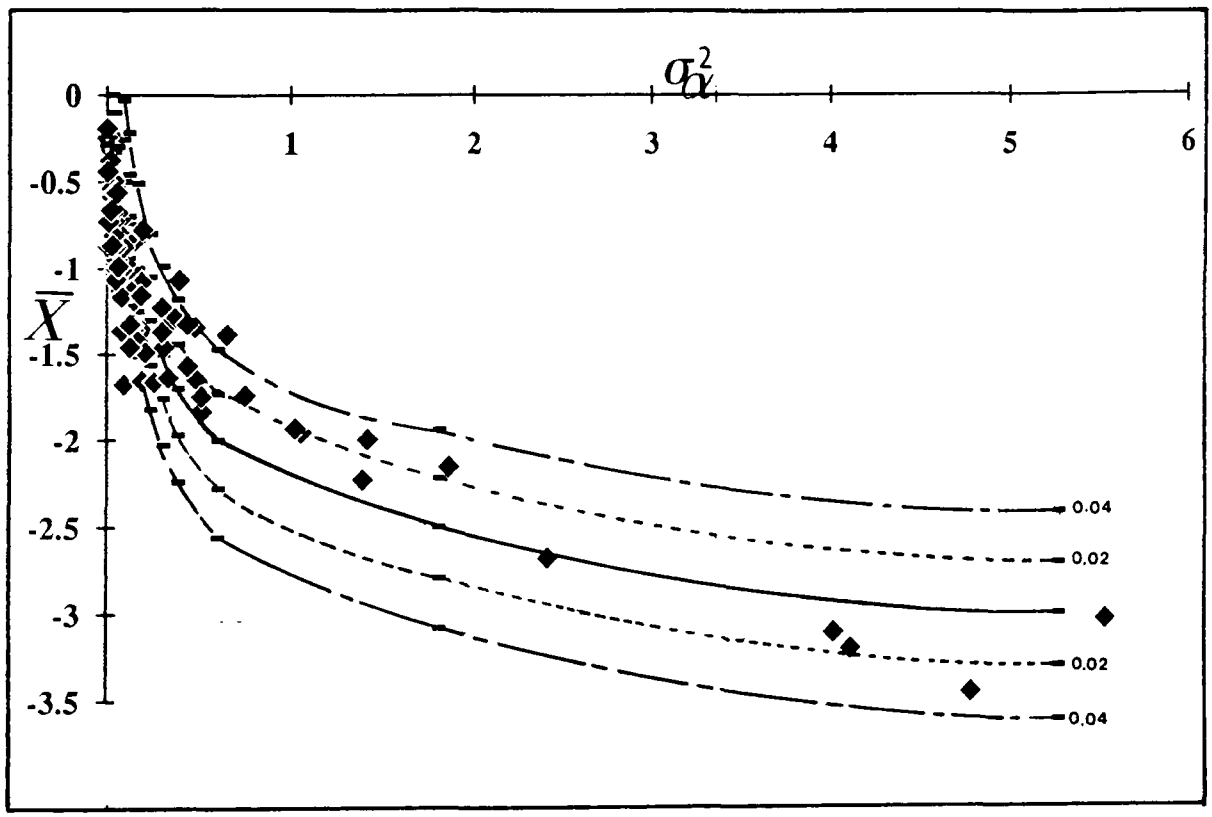

Figure 5.11 Plot of Halls Creek laboratory data with the best fit curve for Salisbury *et al* (1988) data. Also shown are the error envelopes indicating the accuracy to which the curve will estimate the emittances.

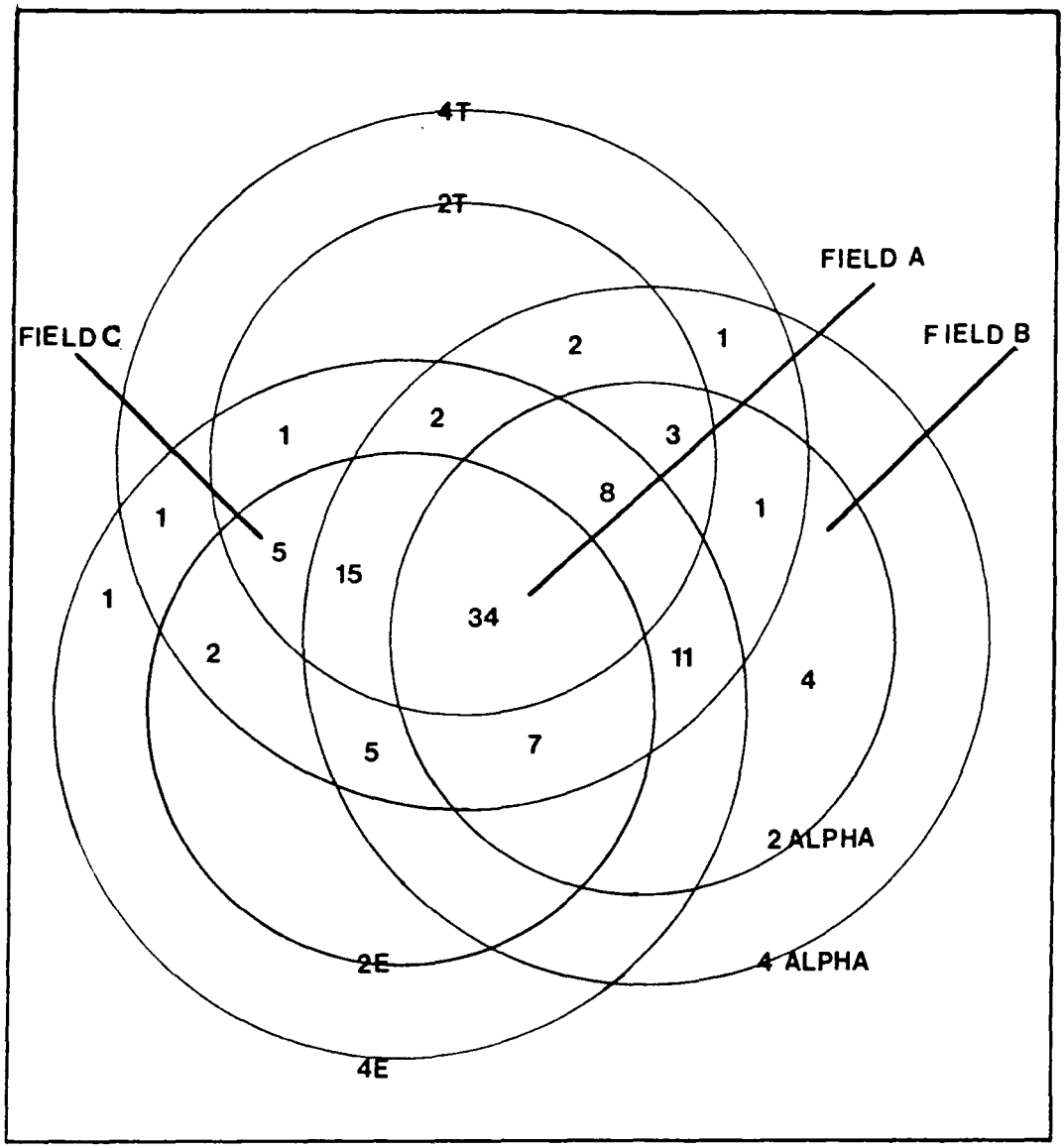

Figure 5.12 Venn diagram showing the distribution of the number of emittance spectra that may be calculated to within +/-0.02 and +/-0.04 of emittance for each emittance estimating method.

Spectra that can be estimated to within +/- 0.02 of emittance using the Model Emittance method fall inside the 2E circle.
Spectra that can be estimated to within +/- 0.02 of emittance using the Maximum Temperature method fall inside the 2T circle.
Spectra that can be estimated to within +/- 0.02 of emittance using the Alpha Derived Emittance method fall inside the 2ALPHA circle.
Not shown in the venn diagram for reasons of geometry are four spectra that can be estimated to within +/-0.04 of emittance for each of the three methods.

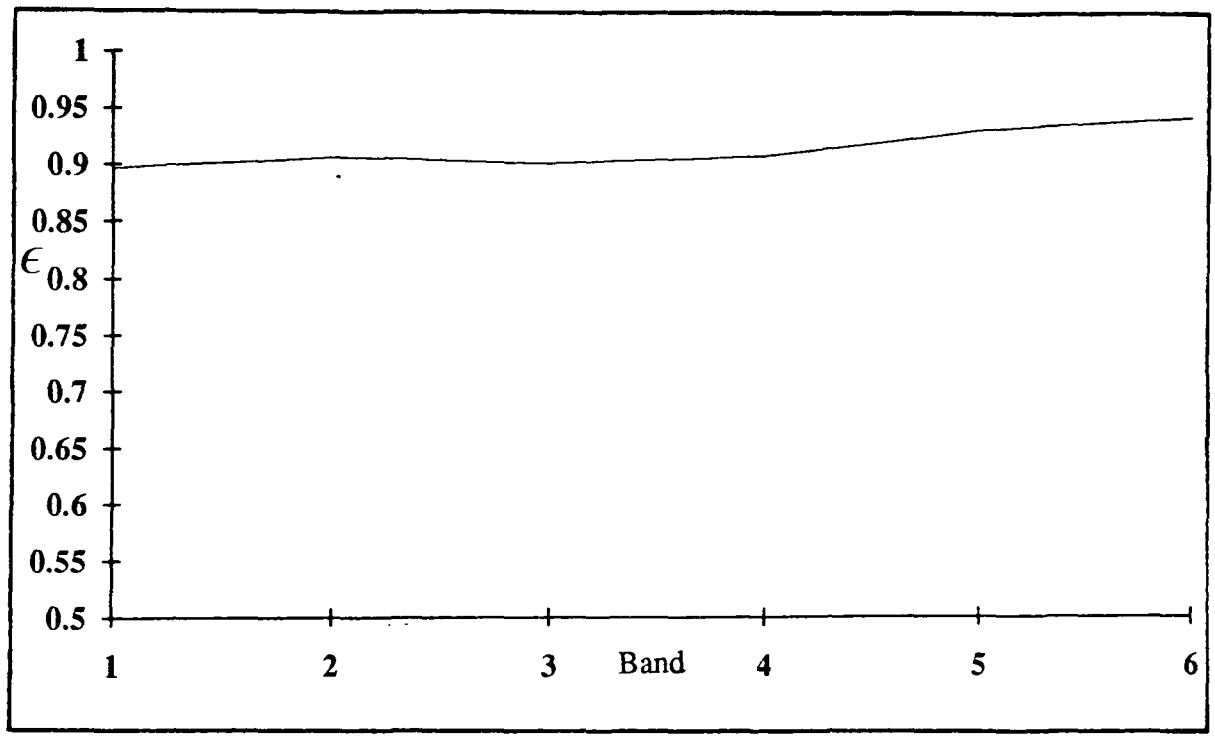

Figure 5.13 TIMS equivalent laboratory spectrum of a basalt from the Halls Creek area. This basalt does not behave well according to the Alpha Derived Emittance criterion, but can be estimated well using the Model Emittance and Maximum Temperature methods.

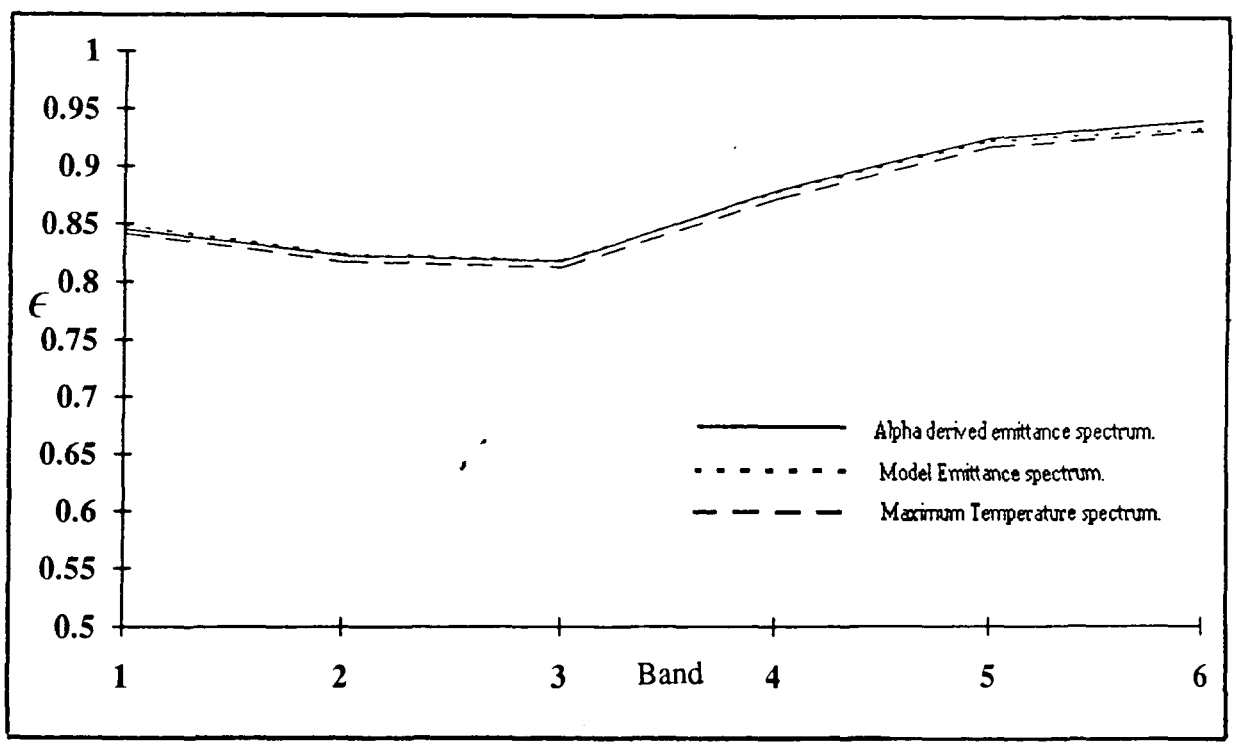

Figure 5.14 Diagram to illustrate the scene mean emittance spectra calculated from each emittance estimating method.

CORRELATION COEFFICIENTS WITH RESPECT TO TEMPERATURE			
BAND	E6 = 0.93	EMAX = 0.94	ALPHA
1	0.345	0.386	0.11
2	0.334	0.371	0.108
3	0.315	0.349	0.099
4	0.475	0.522	0.231
5	0.705	0.741	0.443
6		0.868	0.625

Table 5.4 Correlation coefficients for each emittance band with respect to temperature derived from the three emittance estimating methods for the Halls Creek data.

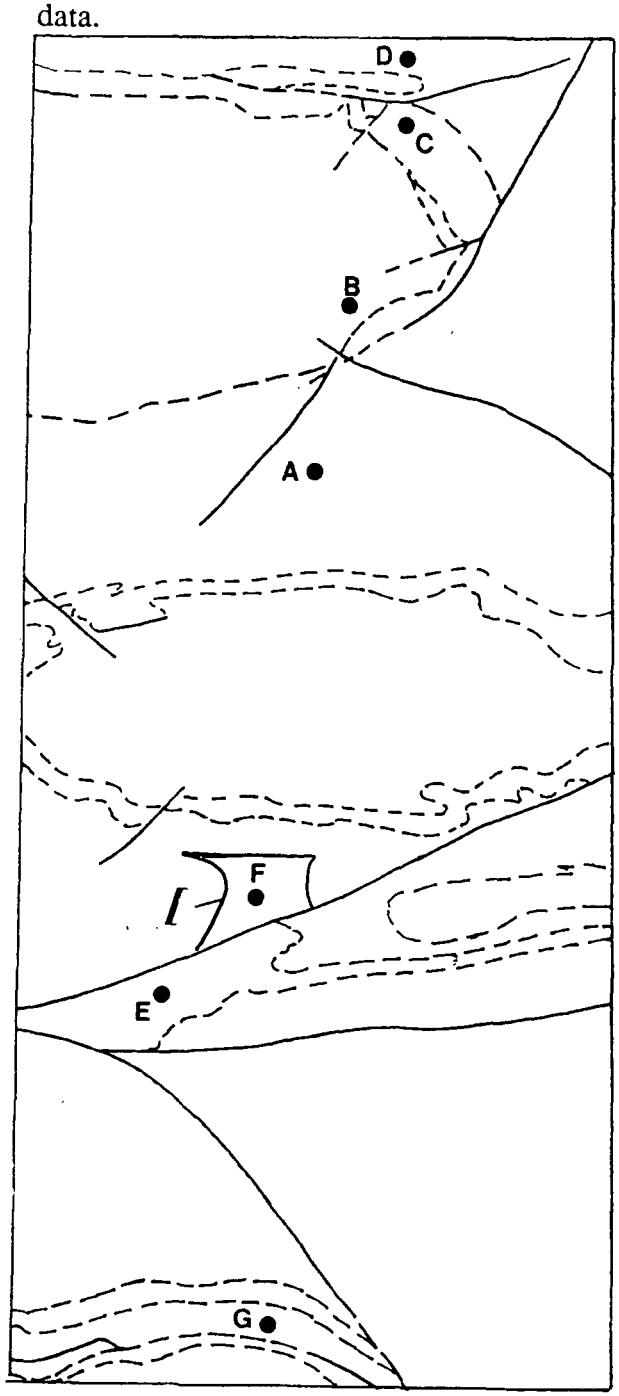

Figure 5.15 Location map for example spectra, showing the outline geology of Halls Creek.

Figure 5.16 Spectra from Sample site A: Vegetation.

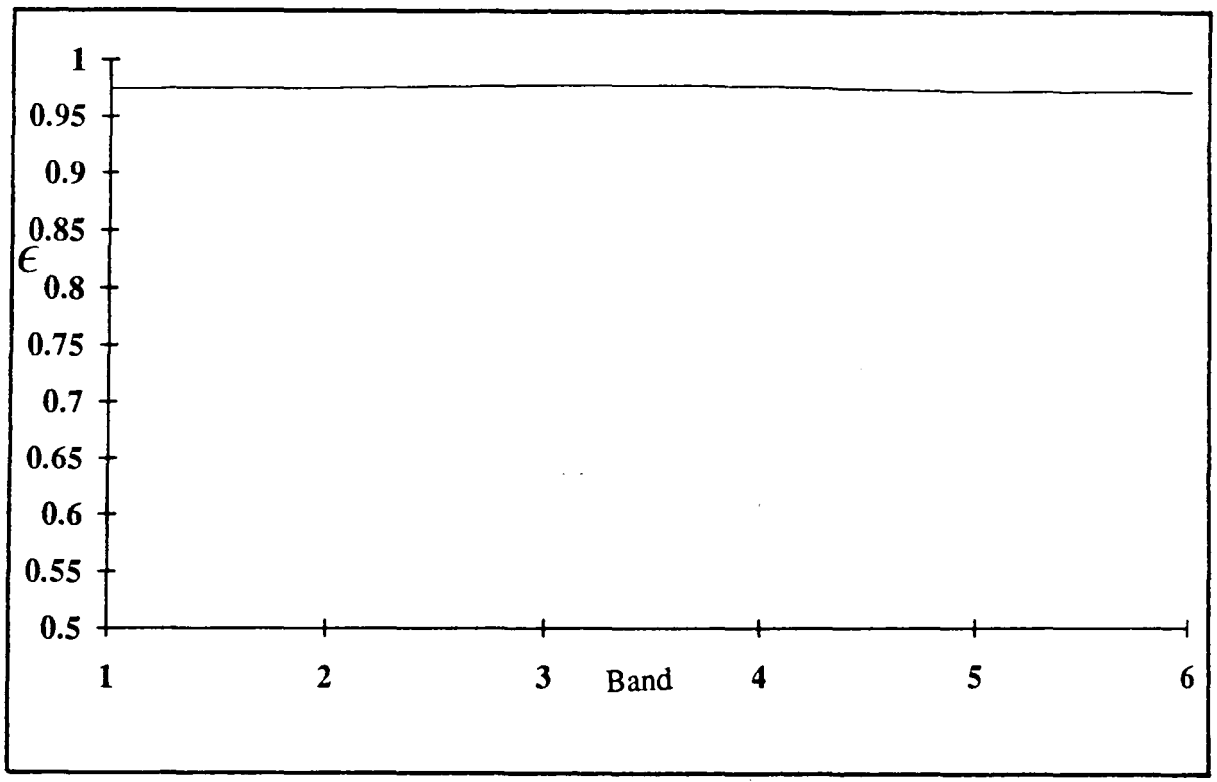

5.16a. Laboratory spectrum of green eucalypt leaves.

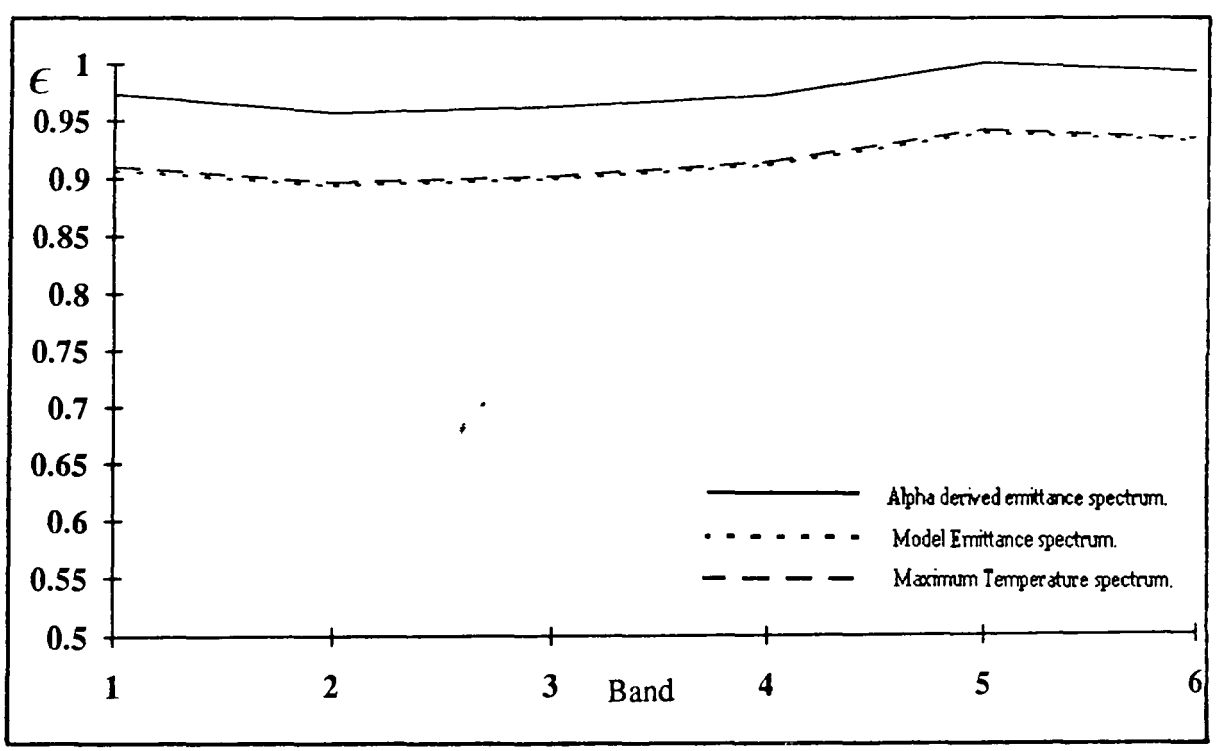

5.16b. TIMS derived emittance spectra for a vegetated area.

Figure 5.17 Spectra from sample site B: Granite.

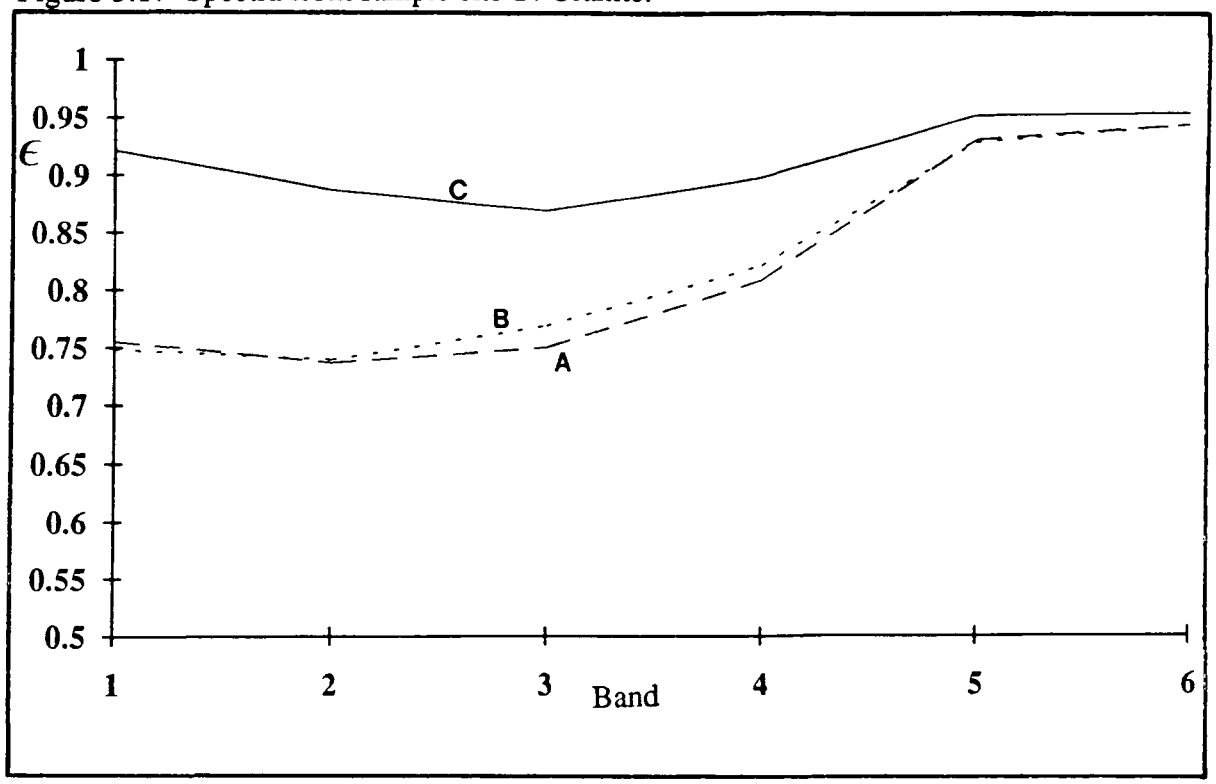

5.17a. Laboratory spectra for granite sample showing the variation in emittance response from a single sample.
Spectrum A is from the fresh surface.
Spectra B and C are from the weathered surfaces.

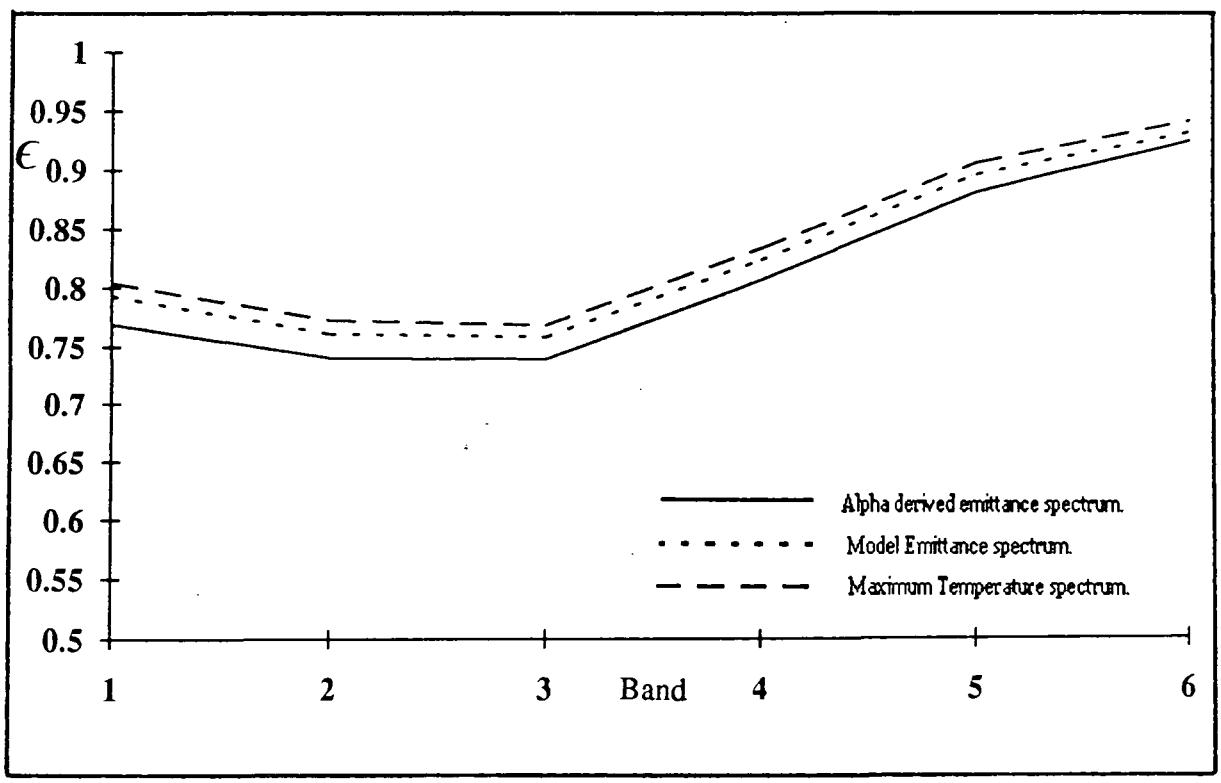

5.17b. TIMS derived emittance spectra from the granite area.

Figure 5.18 Spectra from Sample site C: Basalt.

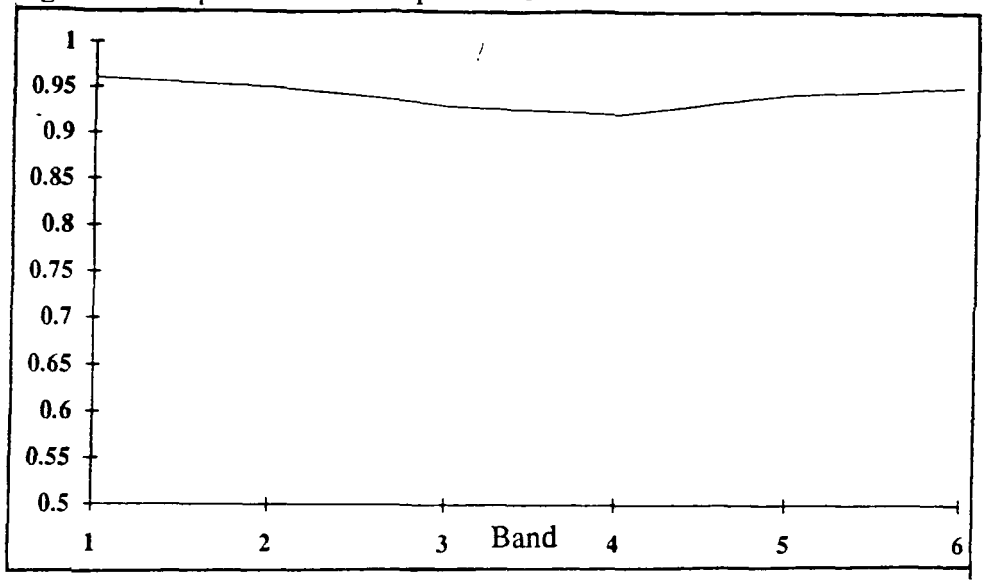

5.18a. Laboratory spectrum from the basalt area.

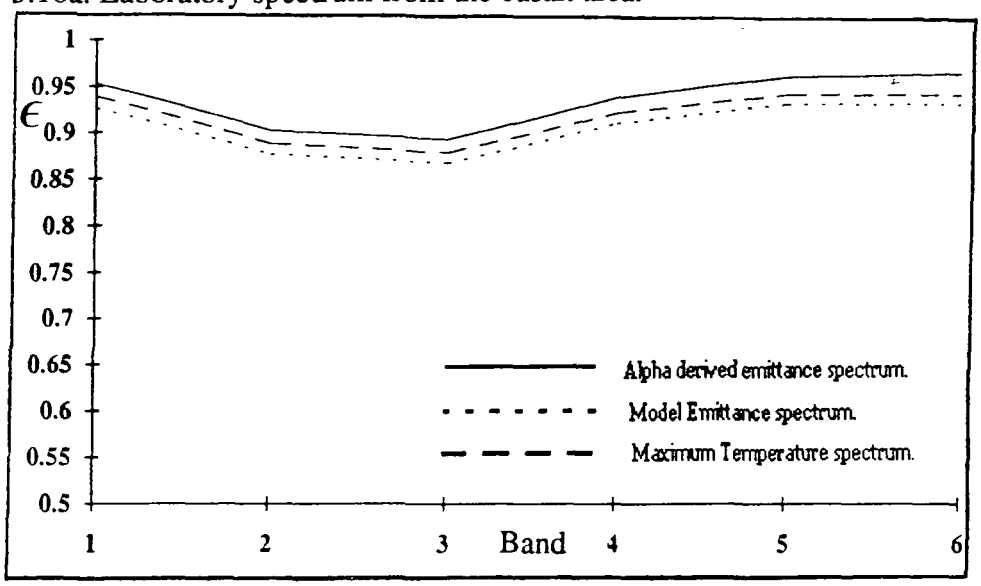

5.18b. TIMS spectra from the sun facing side of the basaltic hill.

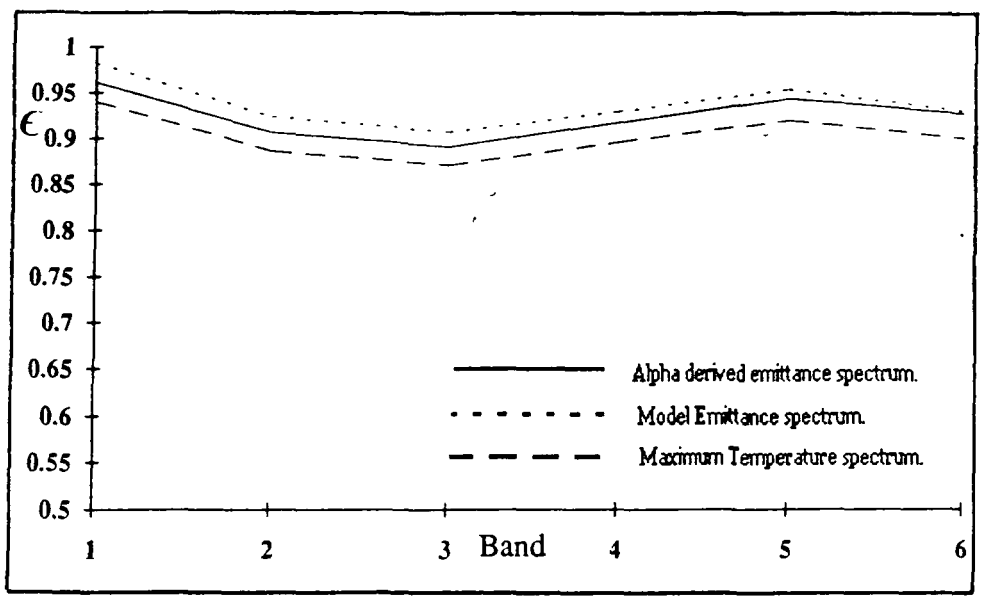

5.18c. TIMS spectra from the shadier side of the basaltic hill.

Figure 5.19 Spectra from Sample site D: Biotite schist.

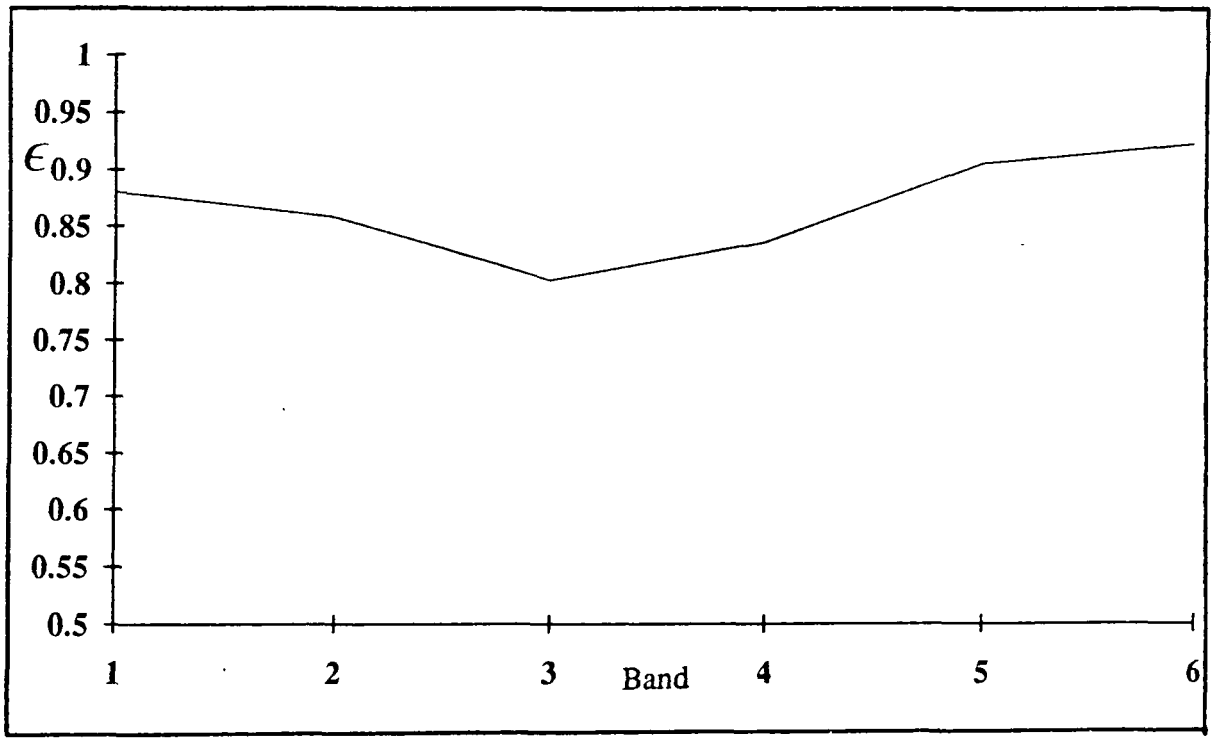

5.19a. Laboratory spectrum of biotite schist.

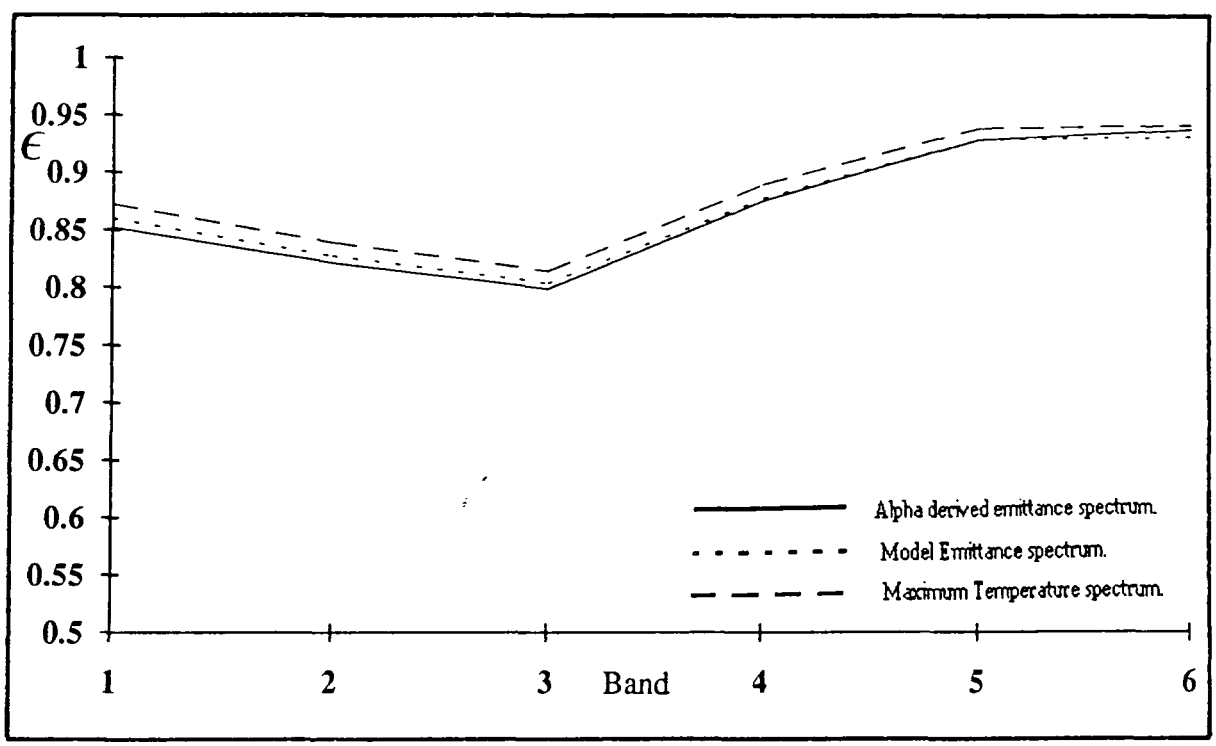

5.19b. TIMS spectra from the area of biotite schist.

Figure 5.20 Spectra of from Sample site E: quartz float.

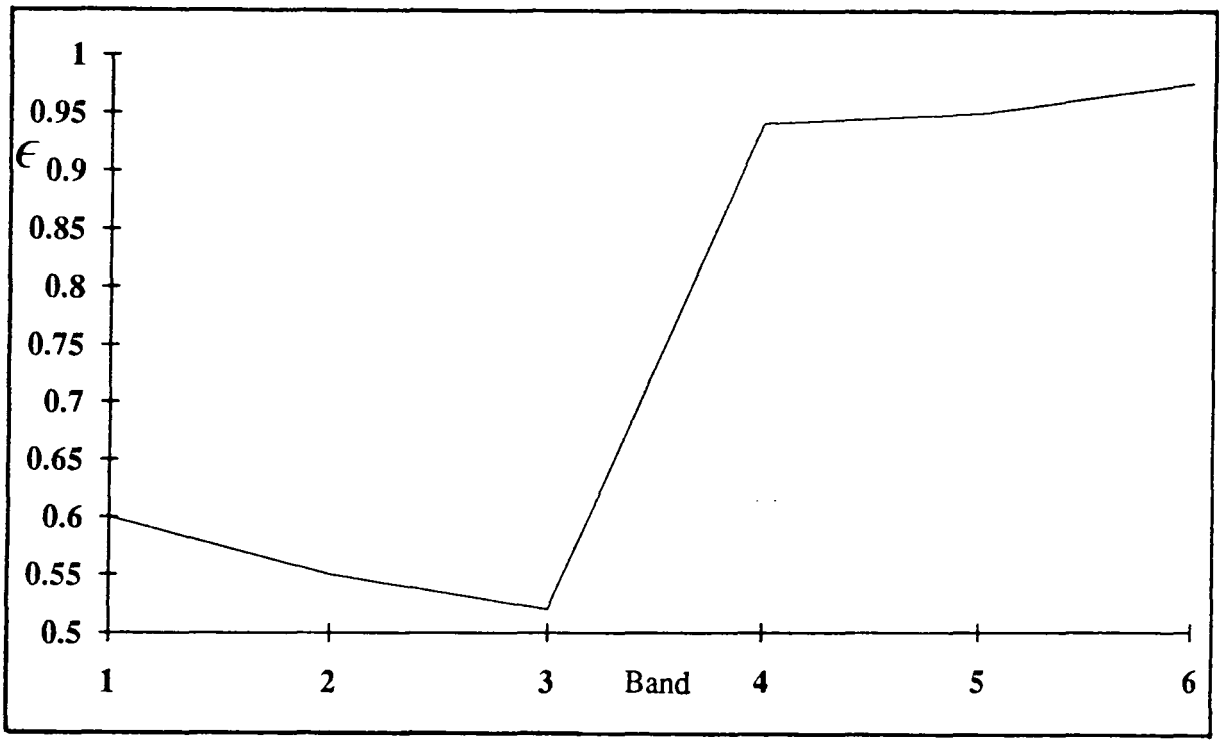

5.20a. Laboratory spectrum of quartz float.

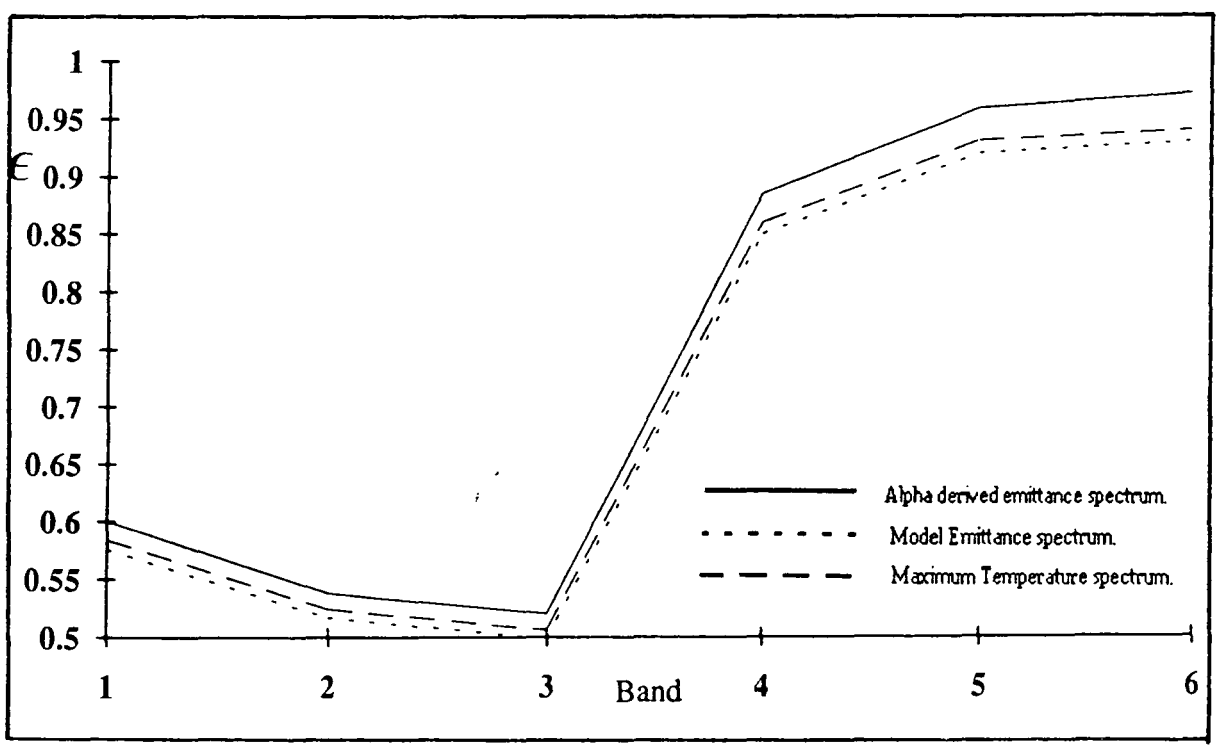

5.20b. TIMS spectra from an area of the Woodward Dolerite overlain by quartz float.

Figure 5.21 Spectra from Sample site F: Biotite-quartz-feldspar meta-diorite.

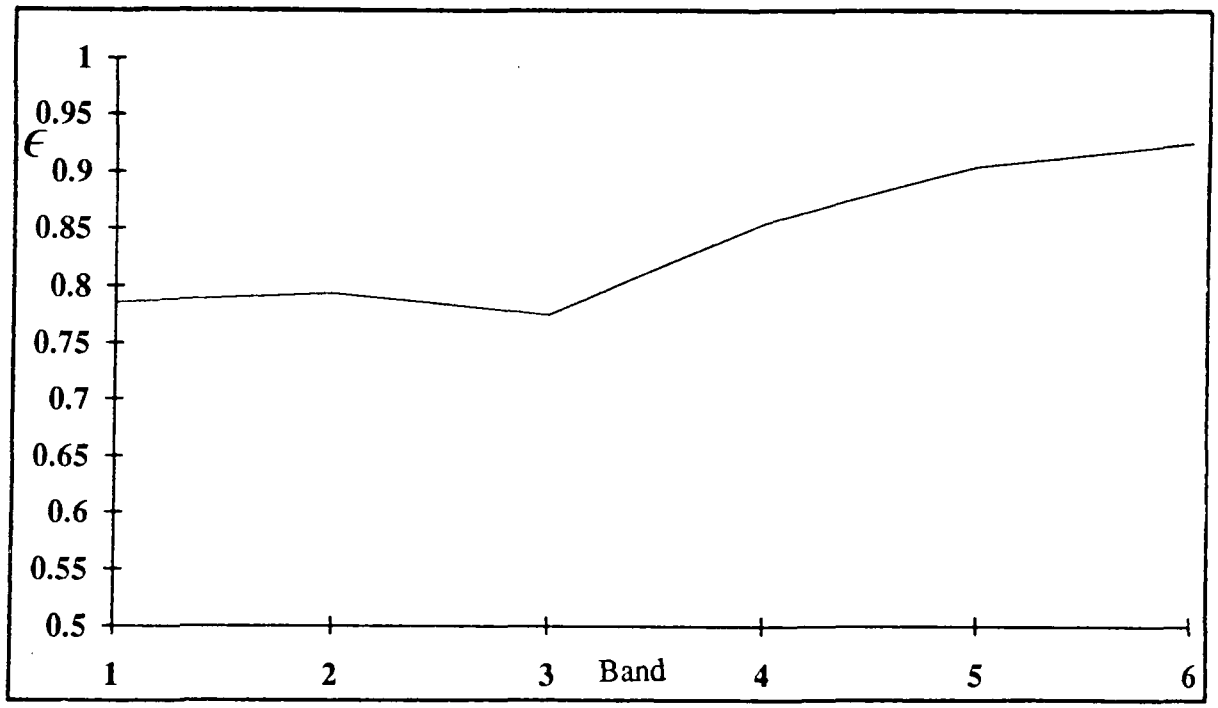

5.21a. Laboratory spectrum of meta-diorite.

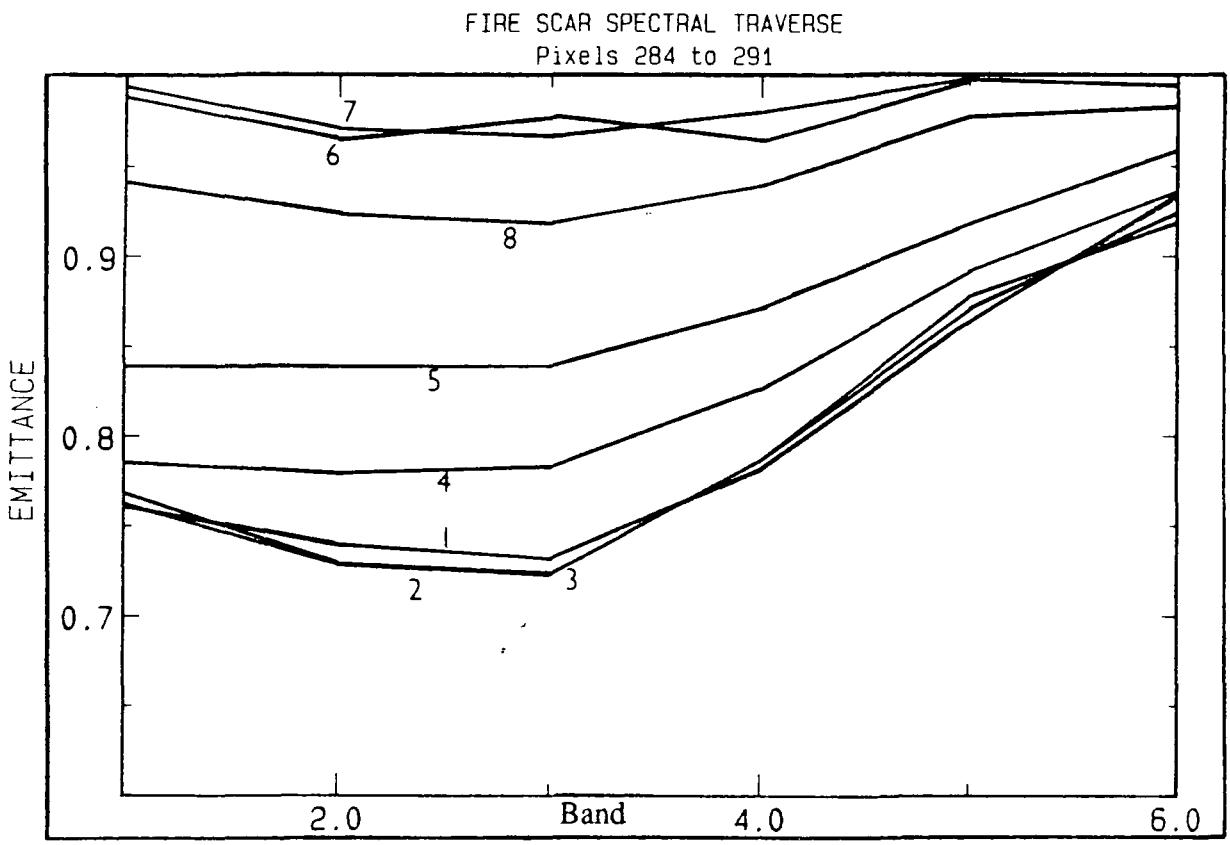

5.21b. Pixel traverse across the meta-diorite lithology from the TIMS scene from an unvegetated area to a vegetation covered area.

Pixel 1 is situated in the firescarred area.

Pixel 8 is in the vegetated area.

Figure 5.22 Spectra from Sample site G: Dolomite.

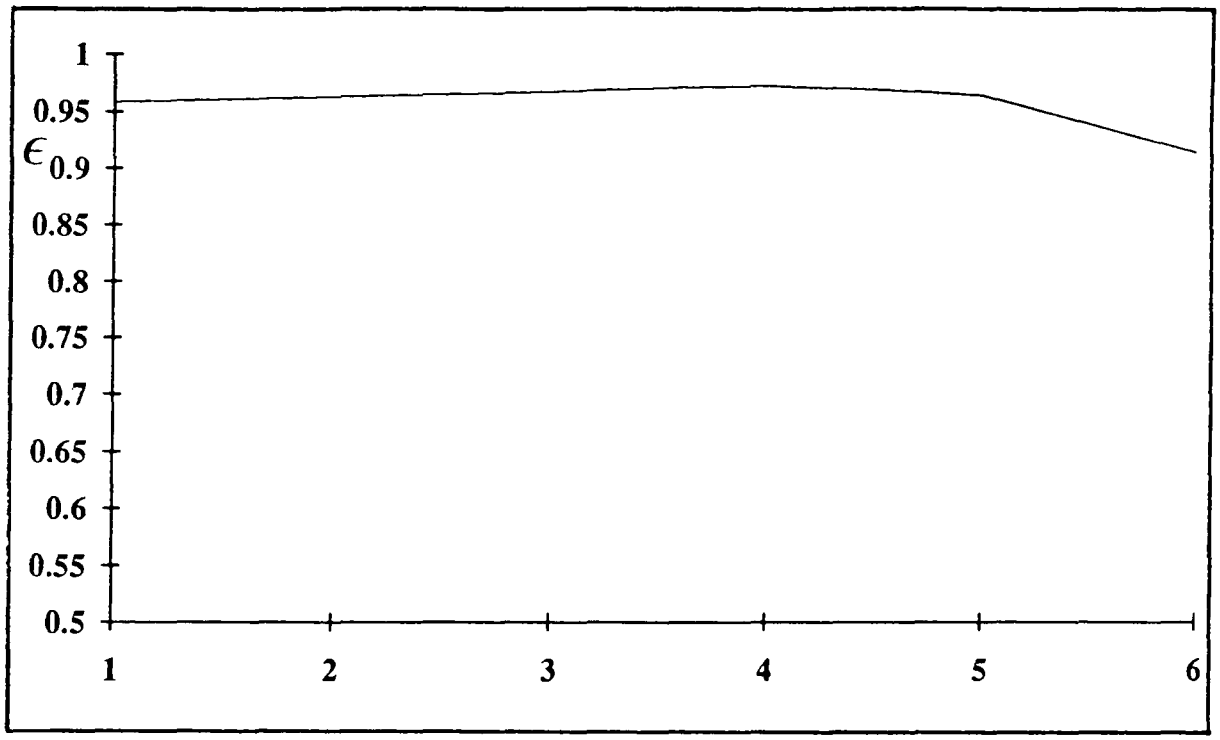

5.22a. Laboratory spectrum from the Bungle Bungle Dolomite.

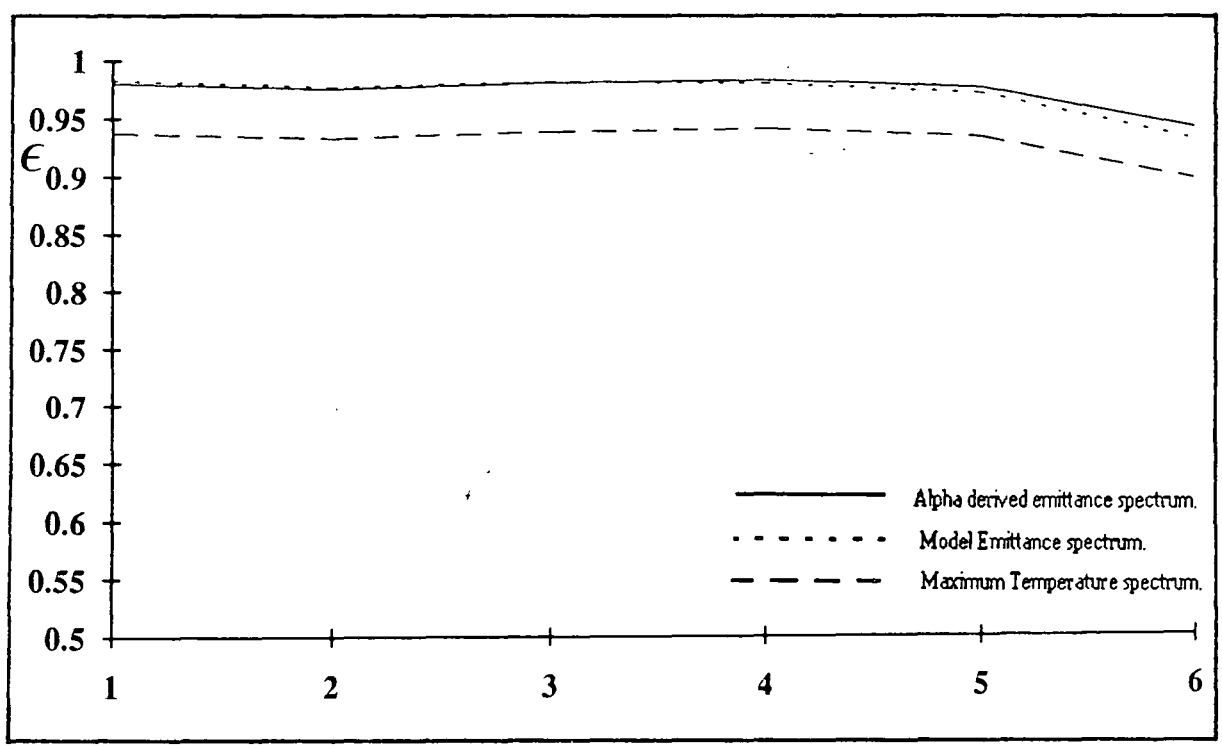

5.22b. TIMS spectra from an area of the Bungle Bungle Dolomite.

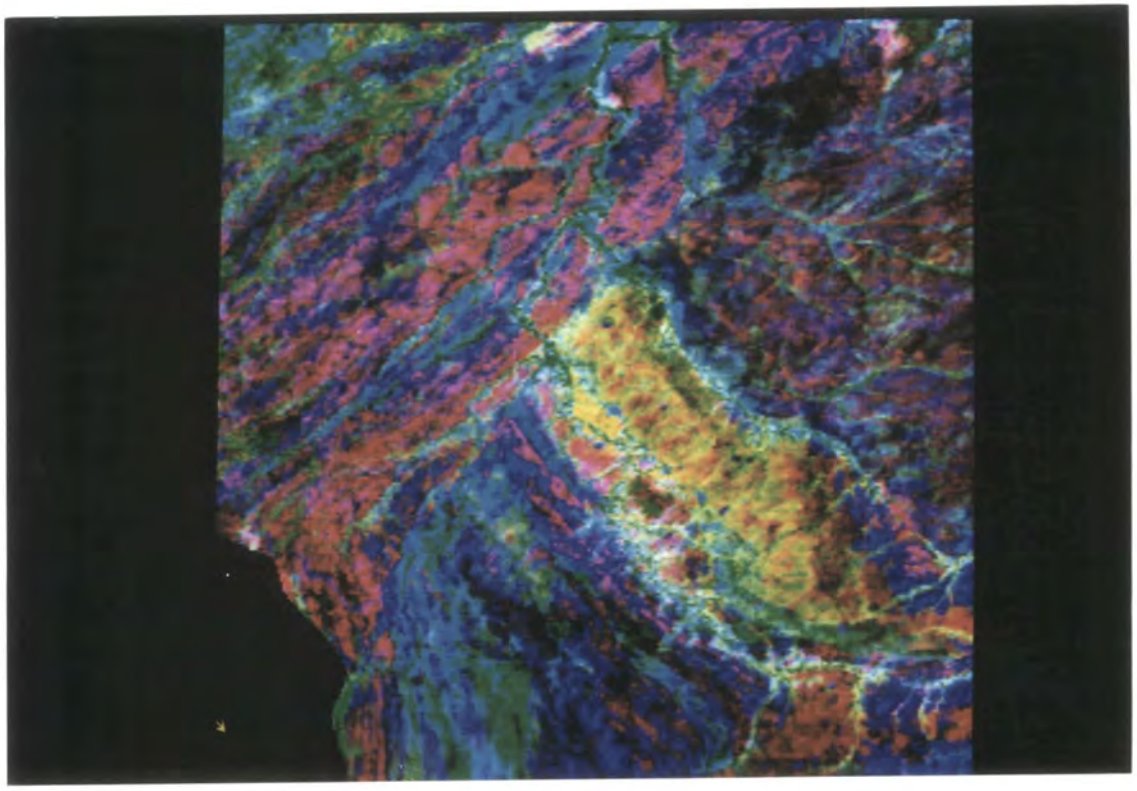

Plate 1. Decorrelation Stretch from the area of the Basaltic hill of Sample site C. Bands 1, 3, 5 are displayed in red, green, blue.

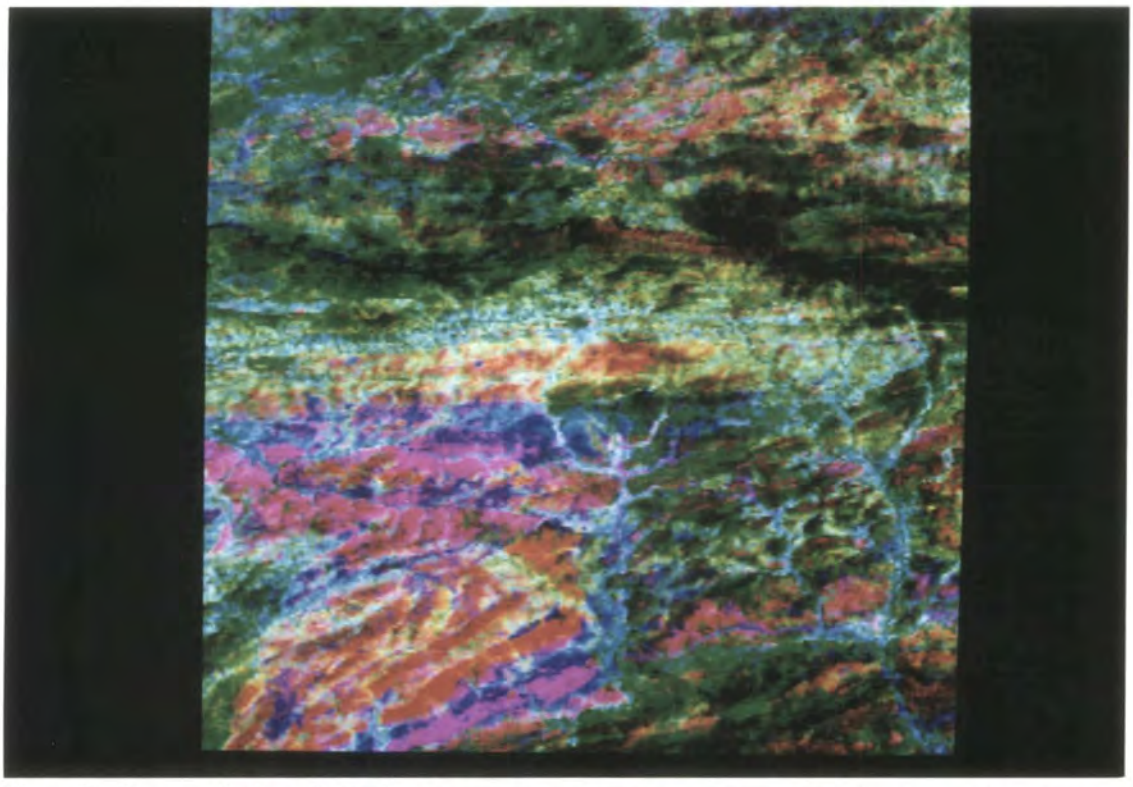

Plate 2. Decorrelation Stretch from the firescarred area, containing Sample site F. Bands 1, 3, 5 are displayed in red, green, blue.

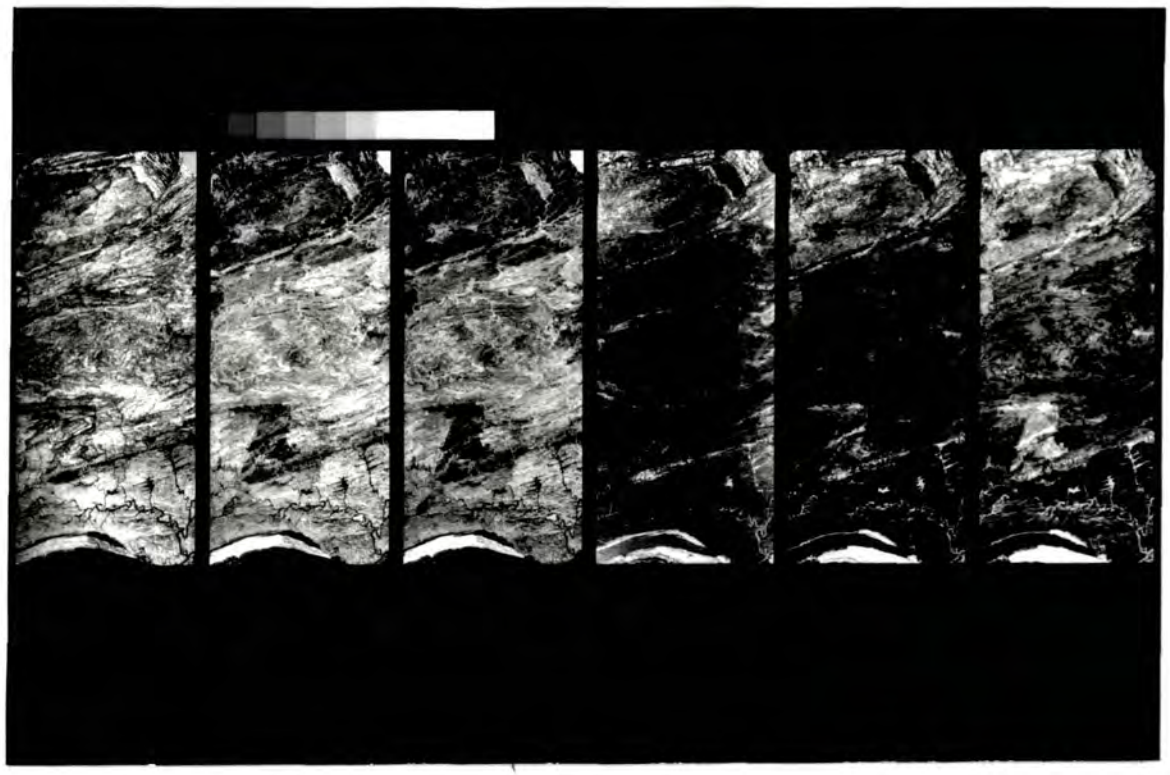

Plate 3. Alpha coefficients bands 1 to 6 displayed from left to right.

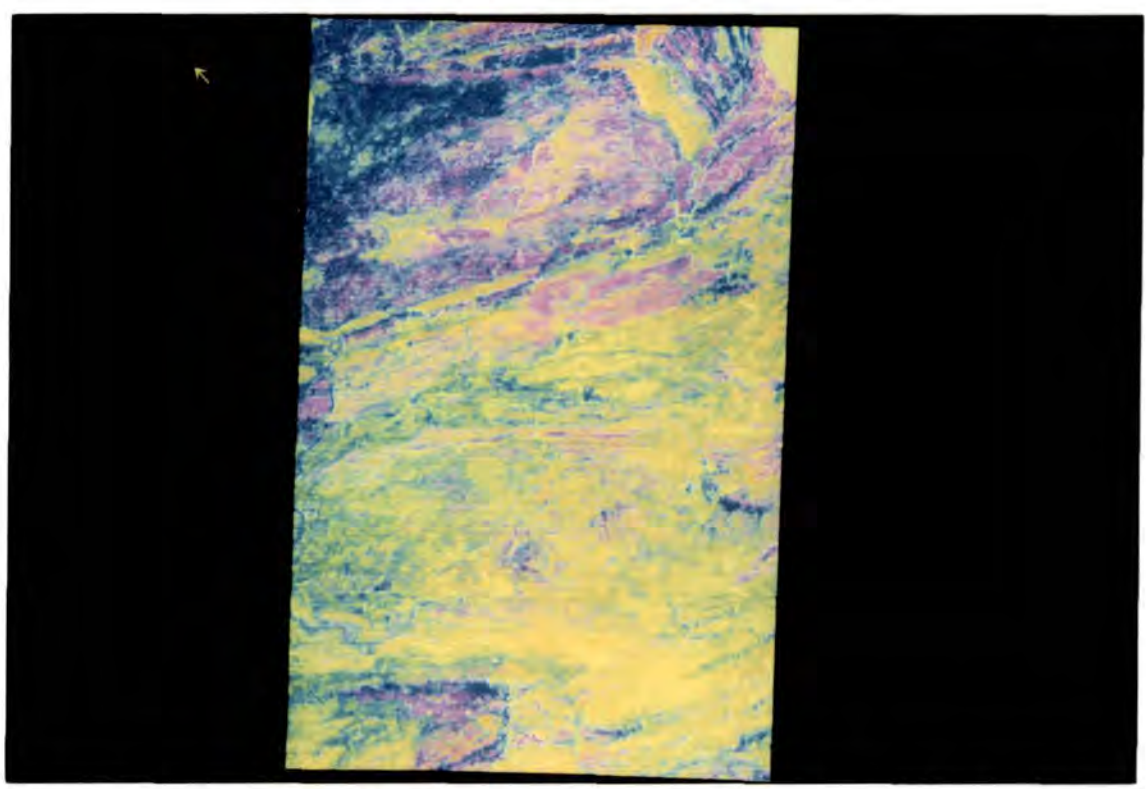

Plate 4. Three band combination of Alpha coefficients from the upper part of the Halls Creek scene. Alpha coefficients bands 1, 3, 5 are displayed in red, green, blue.

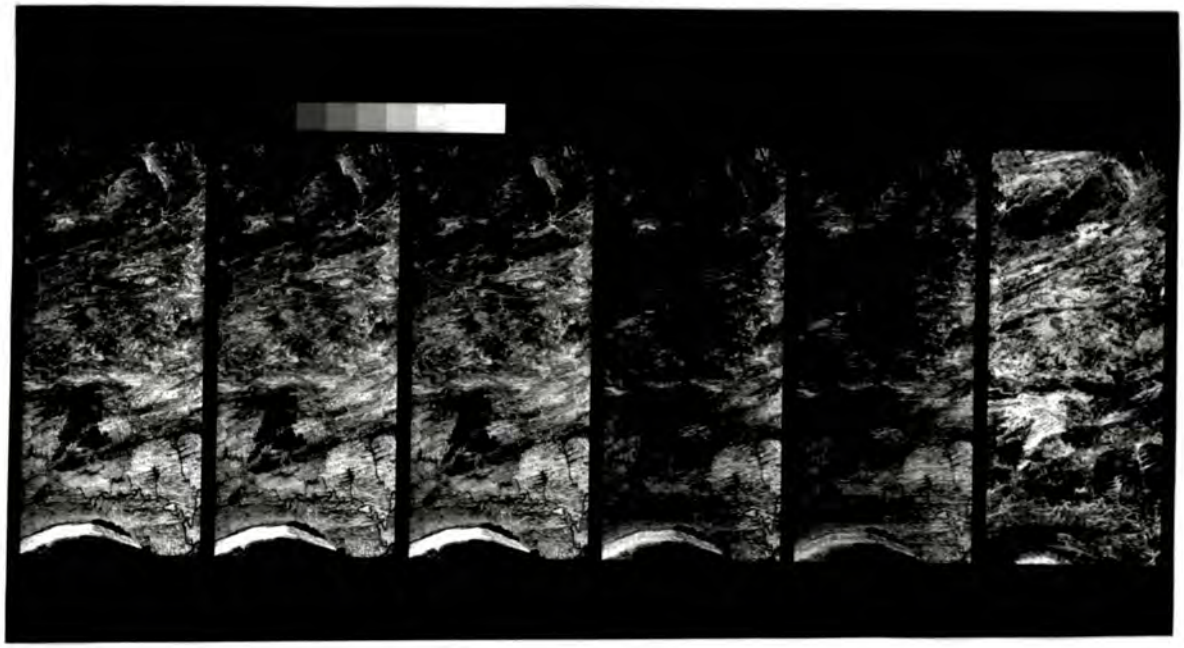

Plate 5. Emittance and temperature images calculated using the Model Emittance method. Emittance bands 1 to 5 are displayed from left to right. The rightmost band displays temperature.

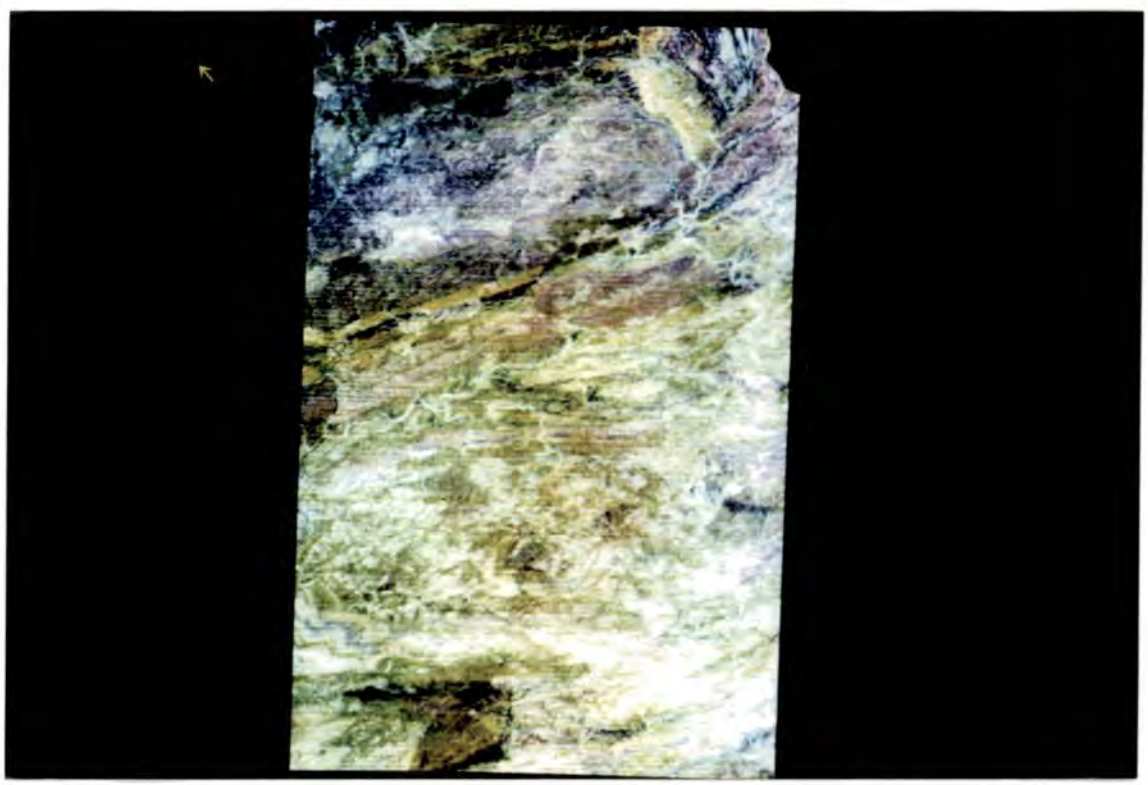

Plate 6. Three band combination of Model Emittance images from the upper part of the Halls Creek scene. Model Emittance bands 1, 3, and 5 are displayed in red, green, blue.

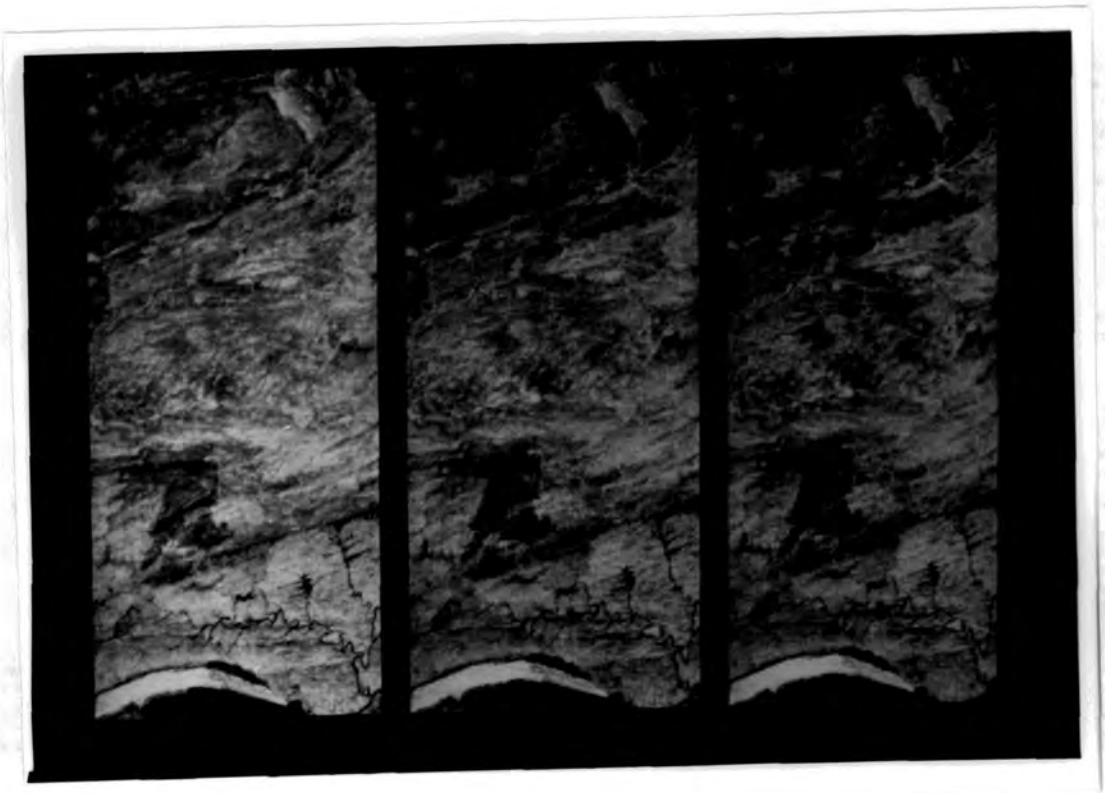

Plate 7. Emittance images calculated using the Maximum Temperature method. Emittance bands 1, 2, and 3 displayed from left to right.

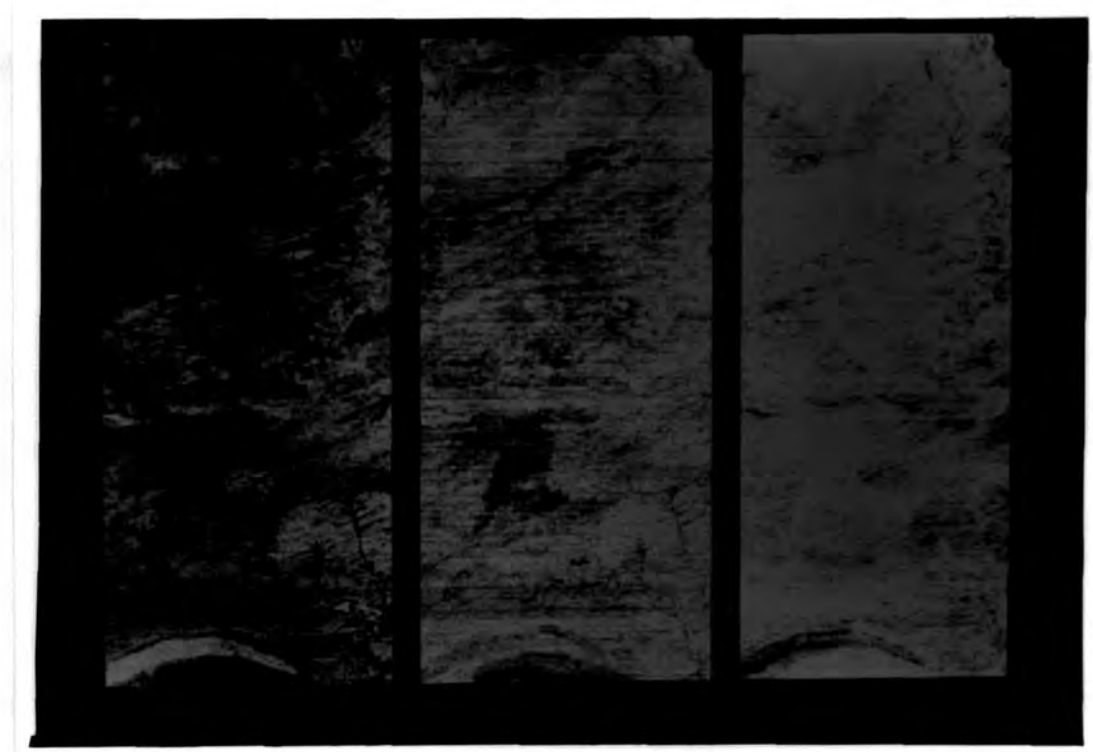

Plate 8. Emittance images calculated using the Maximum Temperature method. Emittance bands 4, 5, and 6 displayed from left to right.

Plate 9. Temperature image derived from the Maximum Temperature method.

Plate 10. Emittance and temperature images calculated using the Alpha Derived Emittance method. Emittance bands 1 to 6 are displayed from left to right. Rightmost band is the temperature estimate.

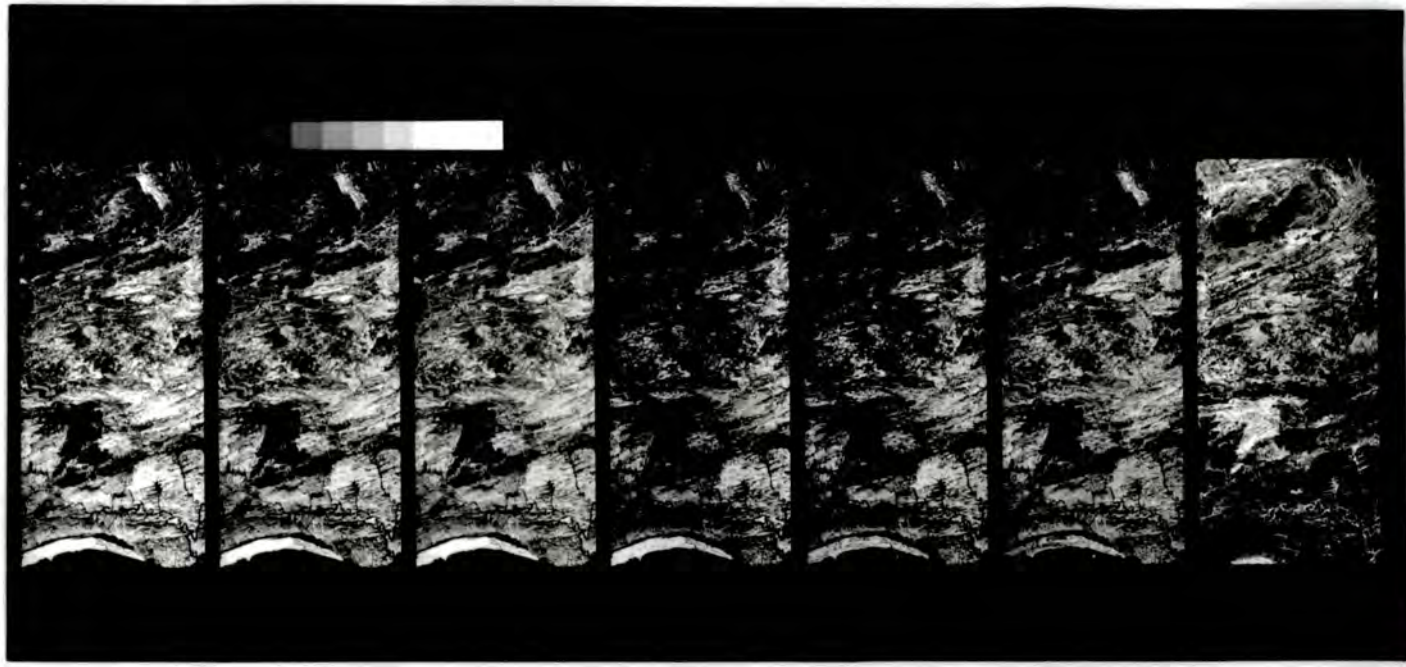

Plate 11. Three band combination of Alpha Derived Emittance images from the upper part of the scene. Bands 1, 3, 5 are displayed in red, green, blue.

CHAPTER 6

SUMMARY AND CONCLUSIONS

6.1 SUMMARY

The principal aims of this study were to assess existing and develop new techniques for extracting the geologically significant parameter spectral emittance from passive Thermal InfraRed (TIR) multispectral data. The thermal spectral radiance measured remotely is related to both temperature and emittance of the surface. Calculation of emittance from radiance data is a non trivial task due to the underdetermined nature of the Planck function which relates the radiance received by the scanner to the emittance and temperature of the sensed body. For the TIMS instrument this results in six equations containing seven unknowns. The atmosphere presents a further problem that needs to be overcome before a quantitative numerical solution may be applied. The radiance received by the scanner is due, not only to the signal emitted by the ground area under investigation, but also to components related to the attenuation and emittance properties of the atmospheric column. These effects need to be modelled for quantitative analysis to be possible. If an accurate atmospheric correction is not possible then only qualitative image enhancement and analysis techniques can be applied. Since the TIMS is the only passive TIR scanner that can be calibrated to physical units, and has been widely used, the quantitative emittance extraction techniques have been designed specifically with respect to the TIMS. However these methods can be modified to be used with other multispectral TIR scanners.

In Chapter 2 the Decorrelation Stretch (D-stretch) and its variants were discussed. This algorithm enhances the emittance component of the signal, displaying it as variations in colour. The temperature component of the signal is still apparent however as brightness variations in the image. The main drawback is that a complete separation of emittance and temperature has not been achieved. In addition this manipulation produces qualitative differences in emittance that are scene dependant, as is the case with all scaled images, such that the colour exhibited by one lithology in one scene is not necessarily related to the same colour in another. The D-stretch is a widely used method producing colourful variations throughout the scene, but in not separating emittance from temperature it does not permit quantitative analysis, particularly in spectral terms.

Other techniques that produce highly discriminatory and colourful images are the Thermal Log Residual (TLR) and alpha coefficient methods. The alpha coefficients, developed during this study represents a simplification of the TLR method. The TLR method, in calculating temperature independent values, incorporates scene dependant parameters, whereas the alpha coefficients produce temperature independent and scene-independent coefficients of emittance, whose overall shape is similar to emittance spectra. When scaled the alpha coefficients become scene dependant due to the imposed scaling factors and are very similar to the TLR images. The alpha images, being temperature independent, permit the generation of any three band combination image which will exhibit variations due entirely to the emittance. A further advantage of the alpha coefficients images over the D-Stretch technique is that the process need only be applied once to the data. The D-Stretch needs a subset of three bands to be chosen and then the manipulation is applied for each set independently.

There are three emittance estimation techniques examined and compared in this thesis; the Model Emittance calculation of Kahle *et al* (1980), the Maximum Temperature method originally suggested by Gillespie (1986), and the Alpha Derived Emittance method developed during this study. The Model Emittance method reduces the underdetermined system of equations by setting the emittance values in one band to a constant value. This assumption allows quantitative estimates of emittance and temperature to be made. For the Halls Creek TIMS data the band and value were $\varepsilon 6 = 0.93$. The Maximum Temperature method set the maximum emittance in any of the bands to a constant value. For the Halls Creek data this was $\varepsilon max = 0.94$. This method also allows quantitative estimates of emittance and temperature to be calculated. The Alpha Derived Emittance method reduces the underdeterminacy by imposing upon an individual spectrum the condition that the mean emittance value of the emittance spectrum is related to its variability. The exact relationship is determined by an analysis of the behaviour of TIR laboratory spectra.

The assumptions used in each of the above mentioned methods imposes certain characteristics on the estimated emittance images. The Model Emittance method, in setting $\varepsilon 6$ to a constant, prevents any variation in that band from being apparent, and reduces the variability in the adjacent band, thus only four bands show any great emittance variations. The Maximum Temperature method allows the $\varepsilon max = 0.94$ value to vary from band to band, and so produces six emittance images, within which some areas will be set to $\varepsilon = 0.94$. Although six emittance bands are calculated, the constant value (band six for the Model Emittance method), is spread amongst each

band. For the Halls Creek image the εmax band is generally found in band 6, and so these images become very similar to the Model Emittance method derived images. In contrast, the Alpha Derived Emittance, in utilising the empirical relation between mean and variation of emittance, produces six emittance bands, none of which suffer from the obvious handicaps of the other methods. The Alpha Derived Emittance method therefore provides six emittance images that can be combined to display emittance variations.

The use of other simple approximations to reduce the number of variables were investigated but proved to be generally inaccurate for the majority of cases. An attempt to model the emittance component of the Planck function as polynomial and gaussian approximations failed to yield stable results.

A comparison of the various approaches to processing TIMS data for isolating the emittance from the temperature was conducted on a TIMS flightline from the Halls Creek area of the Kimberley of Western Australia. The TIMS data were calibrated and atmospherically corrected using the LOWTRAN atmospheric modelling program with user-specified atmospheric parameters. These corrections permitted the application of quantitative numerical techniques to the data.

The D-stretch technique was performed on the data, the most discriminating images were found to be combinations of bands 1, 3, 5 and 2, 3, 5 calculated according to the method outlined in Gillespie *et al* (1986). Three band combinations of alpha coefficients also proved highly discriminating and allowed the discrimination of lithological boundaries to a comparable degree as the D-stretch.

In order to assess the relative merit and accuracy of each of the emittance estimation methods, a laboratory library of 107 emittance spectra were measured from a representative sample of materials from within the Halls Creek scene. These spectra were collected using the Analect Fourier Transform InfraRed (FTIR) spectrometer and subsequently convolved to TIMS equivalent emittance spectra. Histograms of the distribution of ε6 values and εmax values indicate that the Model Emittance method will estimate 63.6% of lithologies to within 0.02 of emittance and 26.2% to within 0.04 of emittance. This is similar to the accuracy of the Maximum Temperature method where 65.4% are accurate to 0.02 and 29.9% are accurate to 0.04 of emittance. The accuracy of the Alpha Derived Emittance method was assessed by investigating the fit of Halls Creek data to the mean variance function calculated for the Salisbury *et al* (1988) data. If the function was recalculated for the

Halls Creek data the resulting accuracy would be improved. The Halls Creek data maintain a good fit to the 'Salisbury' derived function and consequently estimates 63.6% of lithologies to within 0.02 of emittance and 27.1% to within 0.04 of emittance. The percentages obtained from the application of each method are of a similar order of accuracy for this data set. This suggests that for the Halls Creek scene, as represented by the 107 spectra, the emittance estimating methods produce similarly accurate results.

The spectral library however, contains only two vegetation spectra. Increasing the number of vegetation spectra in the samples, to allow for a more accurate representation of the proportions of vegetation in the scene, will preferentially make the Alpha Derived Emittance method more accurate, since this method predicts vegetation more accurately than the Model Emittance and Maximum Temperature methods. This fact coupled with the increment of accuracy that would be obtained if the mean variance curve was recalculated for Halls Creek data suggest that the Alpha Derived Emittance method represents the best technique for separating emittance from temperature. It must be remembered however that the Alpha Derived Emittance method uses the Wien approximation in its calculation which causes an error of the order of 1% of emittance for the wavelength and temperature ranges under consideration. The Wien approximation will thus cause the Alpha Derived Emittance method to be slightly less accurate than the analysis might suggest. The assertion that the Alpha Derived Emittance method separates the emittance from the temperature component more accurately than the other methods is further substantiated when the correlation statistics from the various methods are compared. The emittance component of the radiance in each band should be uncorrelated to the temperature information. The Alpha Derived Emittance method has the lowest correlation coefficients of any of the methods used. Thus although the Halls Creek laboratory data suggest that each emittance estimating method is equally as accurate, the Halls Creek TIMS data suggest that the Alpha Derived Emittance method has best separated the emittance and temperature from the radiance signal.

Several example spectra are given in section 5.2.5 for different geologic materials found in the Halls Creek scene. These show that the laboratory data can be related to emittance values calculated from the TIMS scene. Inaccuracies in the estimation of emittance for each of the methods used are manifest primarily as differences in the mean value for emittance, rather than in the shape of the spectral curve. Thus the errors that may be introduced by the assumptions adopted have only a limited effect on the shape of the curve which is important for lithological mapping. Errors in

emittance estimation do not prevent the emittance spectra from being interpreted in a geological sense. Rather, errors in the mean value will alter the temperature calculated by each method. For the purposes of lithological mapping, temperature differences are not of critical importance. If it were necessary for certain applications to know the temperature more accurately, then the method used to calculate emittance should be varied such that the method applied to each pixel will be the most accurate. The task of defining a criterion which would indicate which of the methods is most likely to prove most accurate on a per pixel basis has not been achieved.

6.2 PROPOSED PROCESSING METHODOLOGY FOR ENHANCING EMITTANCE INFORMATION IN THE THERMAL INFRARED USING TIMS DATA.

To extract emittance by any of the methods given above, it is necessary to accurately atmospherically correct the TIR data. For TIMS data, correction to ground radiance is possible. If however it were not possible to completely model out the atmospheric effects only image enhancement techniques can be used.

The calculation of alpha coefficients and subsequent three band combinations will provide highly discriminating images, exhibiting only emittance variations. On radiance data containing atmospheric effects the relative values of the alpha coefficients within a band will not change. Thus the alpha coefficients may still be applied to atmospherically uncorrected data in order to create images. Similarly the D-stretch can still be utilised on uncorrected data. Either of these methods will provide colourful images with which to delineate boundaries.

For corrected data it is necessary to decide which of the emittance estimating methods is most accurate over the scene under investigation. For most scenes the gross components of the scene will be known from geological maps. Assuming *a priori* knowledge of the likely components of the scene will enable a suite of laboratory spectra to be chosen to be representative of the composition of the scene. These spectra can be analysed to calculate the variation in εmax and $\varepsilon 6$ values (i.e. for the application of the Model Emittance and Maximum Temperature methods). The laboratory spectra may also be used to calculate means and variances which can in turn be used to derive a function that best fits the relation of the means and variances of the spectra. This terrain specific curve can then be analysed to assess its accuracy. Whichever of the Model Emittance, Maximum Temperature or Alpha Derived

Emittance methods proves the most accurate for these spectra should then be applied to the data.

If no *a priori* knowledge of the surface lithologies is available then the Alpha Derived Emittance method should be used because it is as likely to be as accurate as the other methods and will create six emittance images that do not suffer from the obvious noise characteristics of the emittance images of the Model Emittance and Maximum temperature methods.

6.3 FUTURE RESEARCH.

There are two main areas of study that remain to be researched in the context of lithological mapping by extracting emittance information from passive radiance scanners in the Thermal Infrared.

The processes responsible for the observed variation in spectral emittance responses from the weathered surfaces of lithologies are not fully known. Research should be directed at attempting to characterise the effect that weathered surfaces and coatings have on emittance signals so that the received signal can more easily be related to the underlying geological composition.

The Alpha Derived Emittance method, developed during this research, has been applied to Halls Creek data. The accuracy of this method proved to be equally, if not slightly better than, the accuracy of the other emittance estimating methods for this terrain. For an exhaustive appraisal of this technique, the analysis of these methods should be applied to other terrains containing different lithologies, weathering conditions, and vegetation characteristics. Application of the Alpha Derived Emittance method to other TIMS scenes with complementary laboratory spectra will yield terrain specific mean variance curves that can then be applied to similar terrains elsewhere.

6.4 FINAL CONCLUSIONS

1. It is possible to extract quantitative estimates of emittance for lithological mapping from calibrated passive Thermal Infrared multispectral scanners using the Model Emittance, Maximum Temperature, and Alpha Derived Emittance methods.

2. For the Halls Creek laboratory data set each of these methods proved to be of approximately equal accuracy in estimating emittance, estimating approximately 65% of lithologies to within 0.02 of emittance.

REFERENCES

Bartholomew, M. J.; Kahle, A. B., and Hoover, G. 1989. Infrared spectroscopy (2.3 - 20μm) for the Geological Interpretation of Remotely Sensed Multispectral Thermal Infrared Data.*Int. J. Remote Sensing* 10. 529-544.

Carroll, J. E., and Doyle, W. M. 1981. Quantitative Diffuse Reflectance Fourier Transform Infrared (FTIR) spectroscopy. *SPIE* 289 111-113.

Doyle, W. M.; McIntosh, B. C., and Clarke, W.L., 1980. Refractively Scanned Interferometers for Fourier Transform Infrared Spectroscopy. *Applied Spectrometry.* 34. 599-603.

Drury, S. A., and Hunt, G. A. 1989. Reflected and Emitted Airborne Remote Sensing Data from Archean Granite-Greenstone Terrains, W.A. *Int. J. Remote Sensing* 10.

Elvidge, C. D. 1988. Thermal Infraraed Reflectance of Dry Plant Materials: *Rem. Sen. Env.* 26. 265-286.

EOSAT 1986. Putnam, E. S. ed. Commercial Applications and Scientific Research Requirements for Thermal Infrared Observations of Terrestrial Surfaces. A Report of the Joint EOSAT/NASA Thermal Infrared Working Group: Lanham, Maryland.

Farmer V. C. ed. 1974. The Infrared spectra of Minerals. London, Eng.: Mineral. Soc.

Gemuts, I. 1968. 1:250,000 Geological Series, Gordon Downs, W. A. BMR Sheet SE/52-10.

Gillespie, A. R. 1986. Lithologic Mapping of Silicate Rocks Using TIMS: TIMS Data Users Workshop, June 1986. JPL Publication 86-38.

Gillespie, A. R.; Smith M.O.; Adams, J. B., and Willis, S. C. 1990. Spectral Mixing Analysis of Multispectral Thermal Infrared Images: Two Test Cases. Proceedings of the 5th Australasian Remote Sensing Conference, Perth, W.A.

Gillespie, A. R.: Kahle, A. B.: and Palluconi, F. D. 1984. Mapping alluvial fans in Death Valley, California, using multichannel infrared images. *Geophys. Res. Lett.* 11: 1153-56.

Gillespie, A. R.: Kahle, A. B.; and Walker, R. E. 1986. Colour Enhancement of Highly Correlated Images. I Decorrelation and HSI Contrast Stretches. *Rem. Sen. Env.* 20 209-235.

Green, A. A., and Craig, M. D. 1985. Analysis of Aircraft Spectrometer Data with Logarithmic Residuals: *Proceedings of the First Airborne Imaging Spectrometer Data Analysis Workshop:* JPL 85-41.

Gonzales, R. C., and Wintz, P. 1977. Digital Image Processing,Addison Wesley, Reading MA. pp 103-112 and 309-317.

Hook, S. J. 1989. An Evaluation of NS-001 and TIMS Data Lithological Mapping and Mineral Exploration in Weathered Vegetated Terrain. Ph. D. Thesis, Durham.

Hook, S. J.; Gabell, A. R.; Green, A. A.; Kealy, P. S., and Kahle, A. B. 1990. Comparison of Model Emittance, Thermal Log Residuals and Alpha Residuals Techniques Using TIMS data over Cuprite NV. TIMS Data Users Workshop, June 1990.

Hovis, W. A., Jr.: Blaine, L. R.; and Callahan, W. R. 1968. Infrared reflectance aircraft spectra over desert terrain, 8.5 to 16μm. *Appl. Opt.* 7:1137-40.

Hunt, G. R. 1980. Electromagnetic Radiation: The Communication Link in Remote Sensing. In Remote Sensing in Geology, eds B. S. Siegal, and A. R. Gillespie. New York, NY: John Wiley.

Hunt, G. R., and Salisbury, J. W. 1974. Mid infrared spectral behaviour of igneous rocks. Environ. Res. Paper 496-AFCRL-TR-74-0625, AD/A007 680. Washington, DC: NTIS.

Hunt, G. R., and Salisbury, J. W. 1975. Mid infrared spectral behaviour of sedimentary rocks. Environ. Res. Paper 510-AFCRL-TR-75-0356, AD/A016 427. Washington, DC: NTIS.

Hunt, G. R., and Salisbury, J. W. 1976. Mid infrared spectral behaviour of metamorphic rocks. Environ. Res. Paper 543-AFCRL-TR-76-0003, Hanscom AFB, MA; Air Force Cambridge Res. Lab.

Kahle, A. B. 1983. Mineralogic information from a new airborne thermal infrared multispectral scanner. *Science* 222: 24-27.

Kahle, A. B. 1987. Surface Emittance, Temperature and Thermal Inertia derived from Thermal Infraraed Multispectral Scanner (TIMS) Data for Death Valley, CA. *Geophysics* 52 858-874.

Kahle, A. B.; Madura D. P., and Soha, J. M. 1980. Middle infrared multispectral aircraft scanner data Analysis for geological applications. *Appl. Opt.*19:2279-90.

Kahle, A. B., and Rowan, L. C. 1980. Evaluation of multispectral thermal infrared images for lithological mapping in the East Tintic Mountains, UT. *Geology* 8:234-39.

Kahle, A. B., and Goetz, A.F. H. 1983. Mineralogic Information from a New Airborne Thermal Infrared Multispectral Scanner. *Science* 222. 24-27.

Kahle, A. B.: Gillespie, A. R.; Abbott, A. E.; Abrams, M. J.; Walker, R. E.; Hoover, G. and Lockwood, J. P. 1988. Relative Dating of Hawaiian Lava Flows Using Multispectral Thermal Infraraed Images: A New Tool for Geologic Mapping of Young Volcanic Terranes. *J. G. R.* Vol 93, 15,239-15,251.

Karr, C., Jr., ed 1975. Infrared and Raman spectroscopy of Lunar and Terrestrial Minerals. New York, NY; Academic Press.

Kneizys, F. X.; Settle, E. P.; Gallery, W. O.; Chetwynd, J. H., Jr.; Abreu, L.W.; Selby, J. E. A.; Clough, S. A.; and Fenn, R. W. 1983. Atmospheric transmittance/radiance: computer code LOWTRAN-6. Report AFGL-TR-83-0187. Bedford, MA: Air Force Geophysics Lab.

Lahren, M. M.; Schweickert, R. A., and Taranik, J. V. 1988. Analysis of the Northern Sierra accreted Terrane, CA, with airborne Thermal Infrared Multispectral Scanner Data. *Geology* 19 525-528.

Lazerev, A. N. 1972. Vibrational Spectra and Structure of Silicates. New York, NY; Consultants Bureau.

Lyon, R. J. P.,1962. Evaluation of infrared spectroscopy for compositional analysis of lunar and planetary soils. Final Report, contract NASA 49(04), Palo Alto CA; Stanford Research Institute.

Lyon, R. J. P. 1965. Analysis of rocks by spectral infrared emission (8 to 25μm). *Econ. Geol.* 60:715-36.

Lyon, R. J. P. 1972. Infrared Spectral Emittance in Geologic mapping: Airborne spectrometer data from Pisgah Crater, CA. *Science* 175:983-85.

Macias, L. F.; Simpson, C. J.; Moore, R. F., and Needham, R. S. 1987. Diffeetiation of Sedimentary and Mafic volcanic rock types using NS-001 and TIMS Data, Eastern Creek Volcanics, Mount Isa. Proceedings of the Fourth Australasian Remote Sensing Conference. 1 352-363.

Palluconi, F. D., and Meeks, G. R. 1985. Thermal Infrared Multispectral Scanner (TIMS): An Investigators Guide to TIMS Data. JPL Pub. 85-32. Pasadena CA: JPL.

PNC Exp Aust. Pty Ltd. 1986. Sophie Downs Uranium Exploration. Mines Department of W. A. Geological Survey Division WAMEX Open File Register.

Press, W.H.; Flannery, B. P.; Tenkolsky, S. A., and Vetterling, W. T., 1986. Numerical Recipes. Cambridge University Press.

Realmuto, V. 1989. Airborne Optical Pyrometry. Seventh Thematic Conference on Remote Sensing for Exploration Geology. Calgary, Canada.

Realmuto, V. 1990. Emittance Calculation using the Thermal Infrared Multispectral Scanner, (TIMS) over Hawaii. Proc. of the First JPL Airborne Geoscience Workshop, JPL, Pasadena, CA.

Rothery, D.A., and Hunt, G. A., 1989. Technical Note. A Simple Way to Perform Decorrelation Stretch and Related Techniques on a Menu-Driven Image Processing System. *Int. J. Remote Sensing*. 11:133-138.

Salisbury, J. W.; Walter, L. S., and Vergo, N. 1987. Mid-Infrared (2.1 to 25μm) Spectra of minerals: U. S. Geological Survey Open File Report 87-263.

Salisbury, J. W.; Walter, L. S., and D'Aria, D. 1988. Thermal Infrared (2.5 to 13.5μm) Spectra of Igneous Rocks. U.S. Geological Survey Open File Report 88-686.

Siegal B. S.,and Gillespie, A. R. 1980. Remote Sensing in Geology. Wiley, New York, NY.

Slater, P. N., 1980. Remote Sensing. Optics And Optical systems. Addison-Welsley Publishing Company. Reading MA.

Soha, J. M.,and Schwartz, A. A. 1978. Multispectral Histogram Normalisation Contrast Enhancement. Proceedings of Fifth Canadian Symposium on Remote Sensing, Victoria, B. C., Commonwealth of Canada.

Swain, P. H., and Davis, S. M., 1981. Remote Sensing : The Quantitative Approach. McGraw-Hill, New York, NY.

Vickers, R. S., and Lyon, R. J. P. 1967. Infraraed sensing from spacecraft: A geological interpretation. In Thermophysics of Spacecraft and Planetary Bodies-Radiation Properties of Solids and the Electromagnetic Radiation Environment in Space, ed O. B. Heller. New York,NY; Academic Press.

Vincent, R. K. 1975. The potential role of thermal infrared multispectral scanners in geologic remote sensing. *Proc IEEE* 64:137-47.

Vincent, R. K., and Thompson, F. J. 1972. Spectral compositional imaging of silicate rocks. *J. Geophys. Res.* 77:2465-71.

Vincent, R. K.; Thompson, F. J.; and Watson, K. 1972. Recognition of exposed quartz sand and sandstone by two-channel infraraed imagery. *J. Geophys. Res.* 77:2473-84.

Watson, K.: Kruse, F., and Hummer-Miller, S. 1990. Thermal Infrared Exploration of the Carlin Trend Northern Nevada. *Geophysics* 55.

Wolfe, W. L., and Zissis, G,. 1979. The Thermal Infrared Handbook. U. S. Government Printing Office, Washington D. C.

ANNEX A

ANNEX A TO SECTION 5.1.3.1

INPUT AND OUTPUT PARAMETERS FROM LOWTRAN MODEL FOR HALLS CREEK DATA USING THE JPL 'TIMSCAL2' PROGRAM.

1) ATMOSPHERIC DATA FOR HALLS CREEK 1

```
Beginning VICAR task TIMSCAL2
Using the 7/8/85 calibration data
      ***LOWTRAN PARAMETERS***
USER SPECIFIED ATMOSPHERIC MODEL
MIDLATITUDE SUMMER OZONE PROFILE
  ALTITUDE  PRESSURE    TEMP     HUMIDITY
    (KM.)     (MB.)   (DEG. C)     (%)
    0.400   1030.00     35.00      13.00
    1.450    900.00     27.50      17.00
    1.900    850.00     22.50      22.00
    2.400    800.00     18.00      28.00
    3.450    700.00     11.00      25.00
    4.650    600.00      4.00      15.00
    6.210    500.00     -6.70       0.00
    7.920    400.00    -16.80       0.00
   10.010    300.00    -32.00       0.00
   12.760    200.00    -53.60       0.00
   14.540    150.00    -67.80       0.00
   16.900    100.00    -78.80       0.00
   18.100     80.00    -75.60       0.00
   18.950     70.00    -70.90       0.00
   19.880     60.00    -65.00       0.00
   21.010     50.00    -58.90       0.00
   22.410     40.00    -58.00       0.00
WATER RESCALING FACTOR = 1.000
OZONE RESCALING FACTOR = 1.000
RURAL AEROSOLS, VISIBILITY - 23 KM.
SENSOR ALTITUDE =     6.800 KM
TARGET ALTITUDE =     0.400 KM
ANGLE = 180.00 DEGREES
SPECTRAL RANGE =   800 TO  1325 cm-1, WITH    5 cm-1 STEP SIZE
```

	Transmittance		Radiance (mW/m**2/sr)	
Band	Nadir	Off-nadir	Nadir	Off-nadir
1	0.65666	0.60638	9524.9	9292.6
2	0.77665	0.73583	10304.6	10121.0
3	0.78322	0.74198	10462.2	10281.1
4	0.73002	0.68049	10216.7	9998.0
5	0.80052	0.75777	10211.9	10045.4
6	0.76637	0.71782	9622.3	9448.8

Sky Radiance

Band	Down	E	Up
1	2197.74	0.930	48.97
2	1632.01	0.930	36.36
3	1661.17	0.930	37.01
4	2099.32	0.930	46.78
5	1872.58	0.930	41.72
6	2114.35	0.930	47.11

.....and there you go.